Electronic Supplementary Material (ESI) for New Journal of Chemistry.

Binding study on 1-adamantylalkyl(benz)imidazolium salts towards cyclodextrins and cucurbit[*n*]urils

Kristýna Jelínková, Jelica Kovačević, Eva Wrzecionková, Zdeňka Prucková, Michal Rouchal, Lenka Dastychová, and Robert Vícha*

Department of Chemistry, Faculty of Technology, Tomas Bata University in Zlín, Vavrečkova 275, 760 01 Zlín, Czech Republic

SUPPLEMENTARY INFORMATION

Table of Contents

Synthetic procedures

*3-(1-adamantyl)prop-2-enal (**4**)*

(1,3-Dioxolane-2-methyl)-triphenylphosphonium bromide (1.6017 g, 3.71 mmol) was dissolved in dry THF (10 cm^3) under nitrogen atmosphere. NaH (60% dispersion in mineral oil, 0.2971 g, 7.42 mmol) was added in small portions over a period of 10 min and the reaction mixture was vigorously stirred at room temperature for 30 min. Subsequently, a solution of **2** (0.4692 g, 2.86 mmol) in dry THF (5 cm^3) was slowly added portion-wise. The colourless mixture became dark orange. The reaction mixture was stirred at room temperature for 3 h and progress was monitored by GC-MS. When the reaction was completed, the mixture was diluted with 5 cm^3 of water and extracted with CH_2Cl_2 (3×10 cm^3). Collected organic portions were dried over anhydrous Na_2SO_4 and evaporated using rotary evaporator. Crude dioxolane **3** (0.5556 g, 2.371 mmol) was dissolved in acetone (15 cm^3) and *p*-TSA·H_2O (0.3897 g, 2.05 mmol) was added in one portion. The reaction mixture was stirred overnight at room temperature and progress was monitored by GC-MS. After disappearing of **3**, saturated solution of $NaHCO_3$ (5 cm^3) was added and water layer was extracted with toluene (3×20 cm^3). Collected toluene portions were washed with brine (3×5 cm^3) and dried over anhydrous Na_2SO_4. Solvent was removed in vacuo to get **4** (0.3609 g, 66 % in respect to **2**) as a pale yellow solid. M.p.: 132–135 °C. Calcd. for $C_{13}H_{18}O$ (190.28) C 82.06, H 9.53 (%). Found C 82.10, H 9.47 (%). ^{1}H NMR (500 MHz, $CDCl_3$): δ 9.51 (d, 1H, *J*=8.0 Hz), 6.63 (d, 1H, *J*=16.0 Hz), 6.02 (dd, 1H, *J*=8.0 Hz, *J*=16.0 Hz), 1.84 (m, 3H), 1.77–1.68 (m, 12H) ppm. ^{13}C NMR ($CDCl_3$): δ 193.3, 145.5, 130.5, 41.9, 38.2, 28.9 ppm. IR: 2906 (s), 2849 (s), 1688 (s), 1675 (m), 1452 (m), 1124 (m), 731 (w), 575 (w) cm^{-1}. MS (EI: 200 °C, 70 eV) 40(7), 41(61), 43(8), 51(10), 52(6), 53(23), 55(31), 57(12), 65(22), 66(12), 67(36), 68(6), 69(8), 70(7), 77(46), 78(18), 79(77), 80(25), 81(30), 82(5), 83(8), 91(79), 92(40), 93(56), 94(23), 95(27), 96(13), 97(13), 103(9), 104(8), 105(45), 106(19), 107(21), 108(10), 110(11), 111(15), 115(9), 117(16), 118(6), 119(25), 120(15), 121(10), 129(11), 130(5), 131(14), 133(48), 17), 135(11), 147(22), 148(8), 161(11), 162(6), 175(20), 189(8), 190(100), 191(14) m/z (%).

*2-(1-adamantyl)-1-bromoethane (**7a**)*

Alcohol **6a** (0.3550 g, 1.97 mmol) was dissolved in dry CH_2Cl_2 (30 cm^3) under inert atmosphere and cooled down to 0 °C in ice bath. CBr_4 (1.0090 g, 3.04 mmol) was added followed by addition of triphenylphosphine (1.2600 g, 4.81 mmol) in small portions. The mixture was stirred for 3 h at 0 °C and then poured into cold pentane and stirred for 20 min. The liquid phase was evaporated to dryness and the solid was washed with cold pentane. Pentane fractions were evaporated and obtaining colourless oil which was purified by column chromatography on silica gel using petroleum ether as a mobile phase to get colourless solid **7a** (0.3460 g, 72%). M.p.: 135–138 °C. Calcd. for $C_{12}H_{19}Br$ (243.18) C 59.27, H 7.88 (%). Found C 59.50, H 7.85 (%). ^{1}H NMR (500 MHz, $CDCl_3$): δ 1.51 (d, 6H, *J*=14.5 Hz), 1.60–1.73 (m, 8H), 1.95 (s, 3H), 3.40 (m, 2H) ppm. ^{13}C NMR ($CDCl_3$): δ 28.5, 29.0, 34.0, 37.0, 42.1. 48.1 ppm. IR: 2902 (s), 2844 (s), 1452 (m), 560 (b) cm^{-1}. MS (EI: 200 °C, 70 eV) 41(7), 67(6), 77(5), 79(15), 91(5), 93(12), 107(8), 135(100), 136(11), 242(1), 244(1) m/z (%).

*3-(1-adamantyl)-1-bromopropane (**7b**)*

Compound **7b** was prepared according the same procedure as described above for **7a** using **6b** (0.2400 g, 1.24 mmol) to get 0.2477 g (78%) of **7b** as a viscous oil. ^{1}H NMR (500 MHz, $CDCl_3$): δ 1.60 (m, 2H), 1.91 (m, 6H), 2.04–2.16 (m, 6H), 2.22–2.30 (m, 2H), 3.82 (t, 2H, *J*=14.0 Hz) ppm. ^{13}C NMR ($CDCl_3$): δ 26.5, 28.7, 32.1, 35.0, 37.2, 42.4, 43.1 ppm. IR: 2902 (s), 2846 (s), 1451 (w), 1271 (w), 1241 (w), 1099 (w), 670 (m) cm^{-1}. MS (EI: 200 °C, 70 eV) 41(8), 67(6), 79(12), 91(7), 93(12), 107(7), 135(100), 136(11), 256(1), 258(1) m/z (%).

^{1}H, ^{13}C NMR and MS spectra of new guests

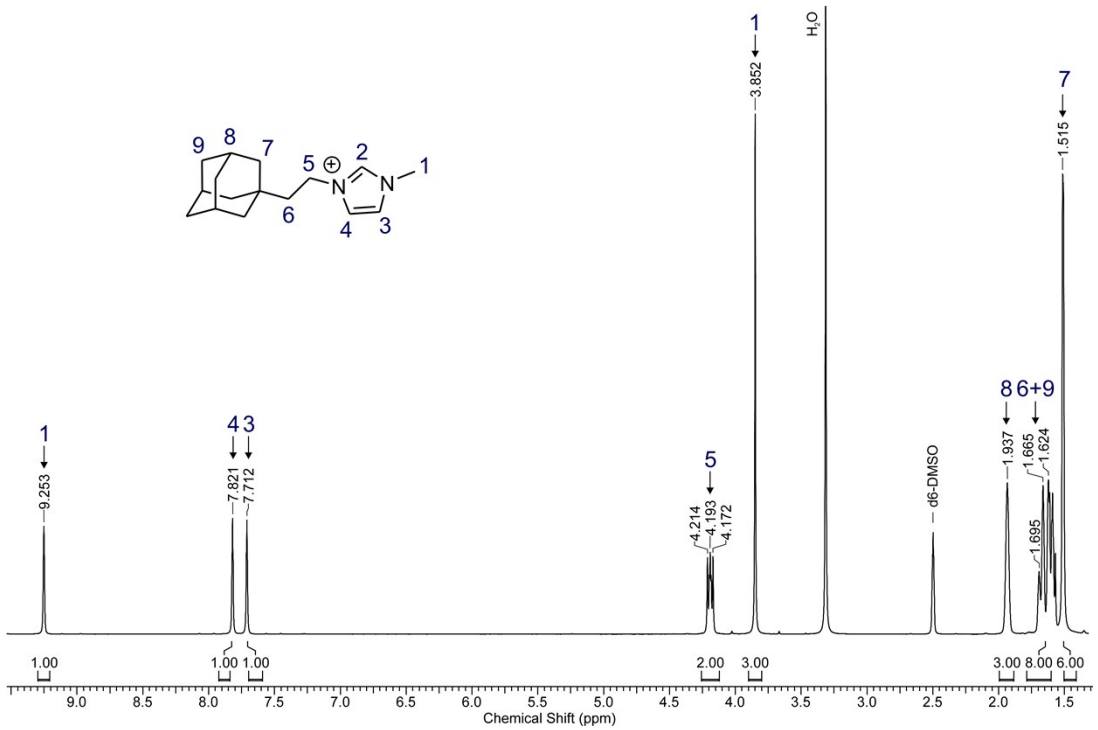

Figure S1: The ^{1}H NMR (DMSO-d_6, 400 MHz) spectrum of compound **9b**.

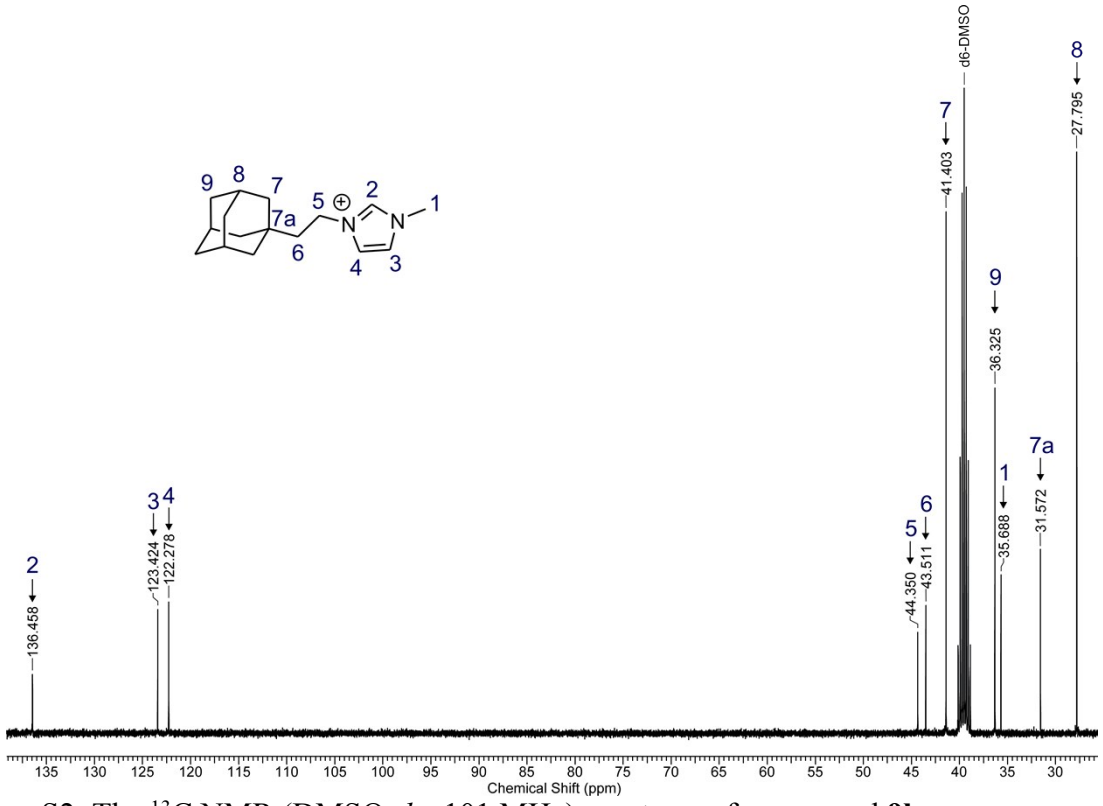

Figure S2: The ^{13}C NMR (DMSO-d_6 , 101 MHz) spectrum of compound **9b.**

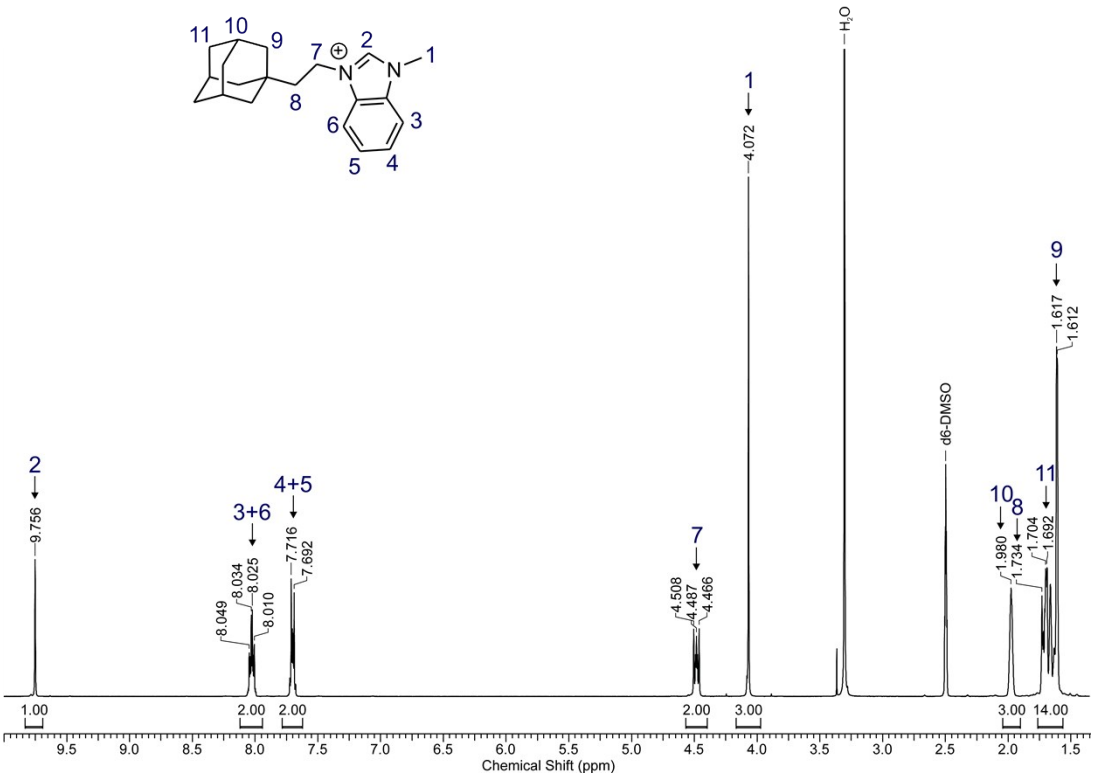

Figure S3: The ^{1}H NMR (DMSO-d_6, 400 MHz) spectrum of compound **10b.**

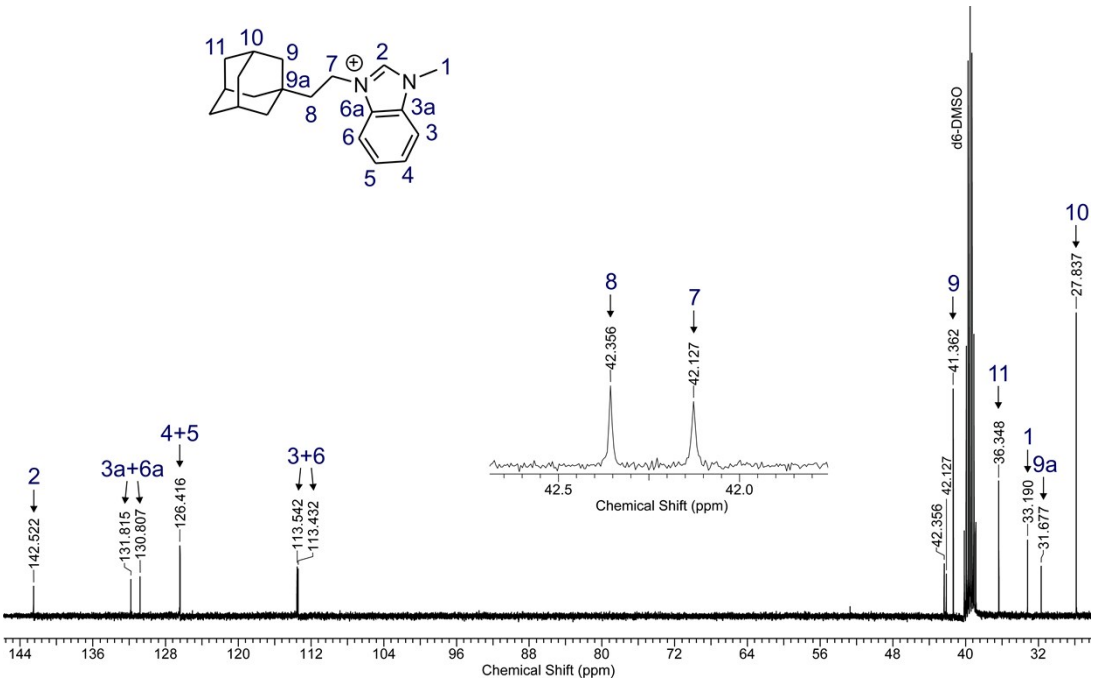

Figure S4: The ^{13}C NMR (DMSO-d_6, 101 MHz) spectrum of compound **10b.**

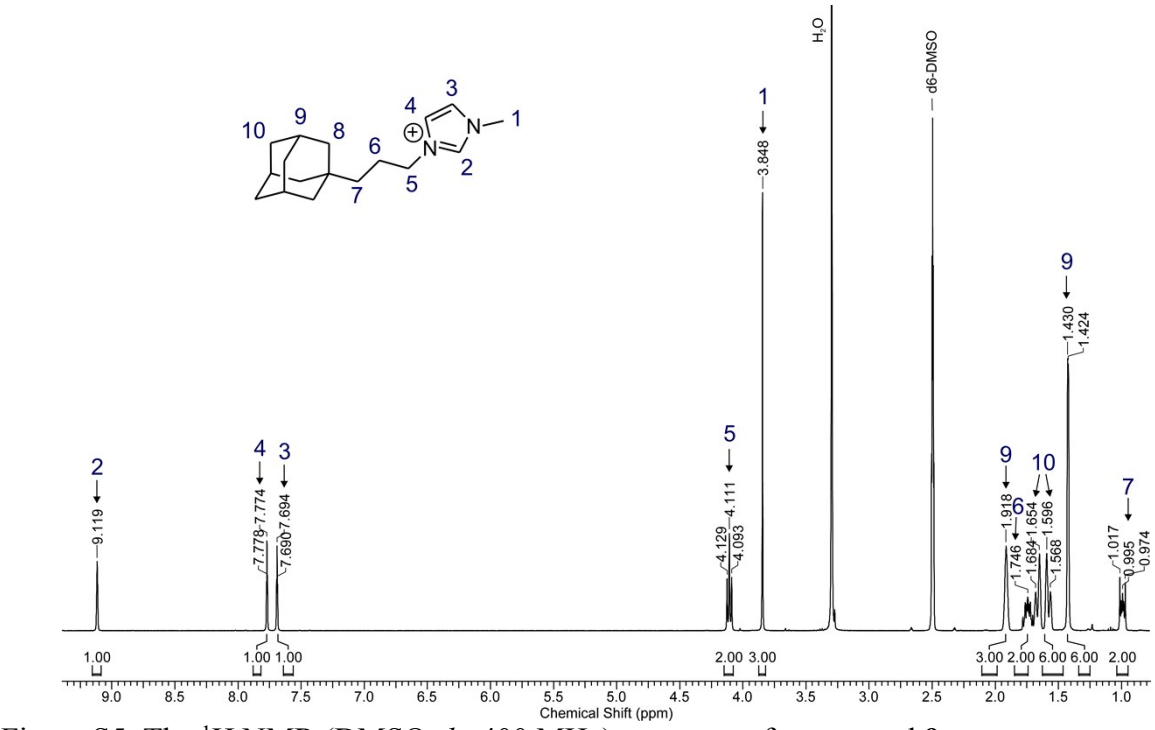

Figure S5: The ^{1}H NMR (DMSO-d_6, 400 MHz) spectrum of compound **9c.**

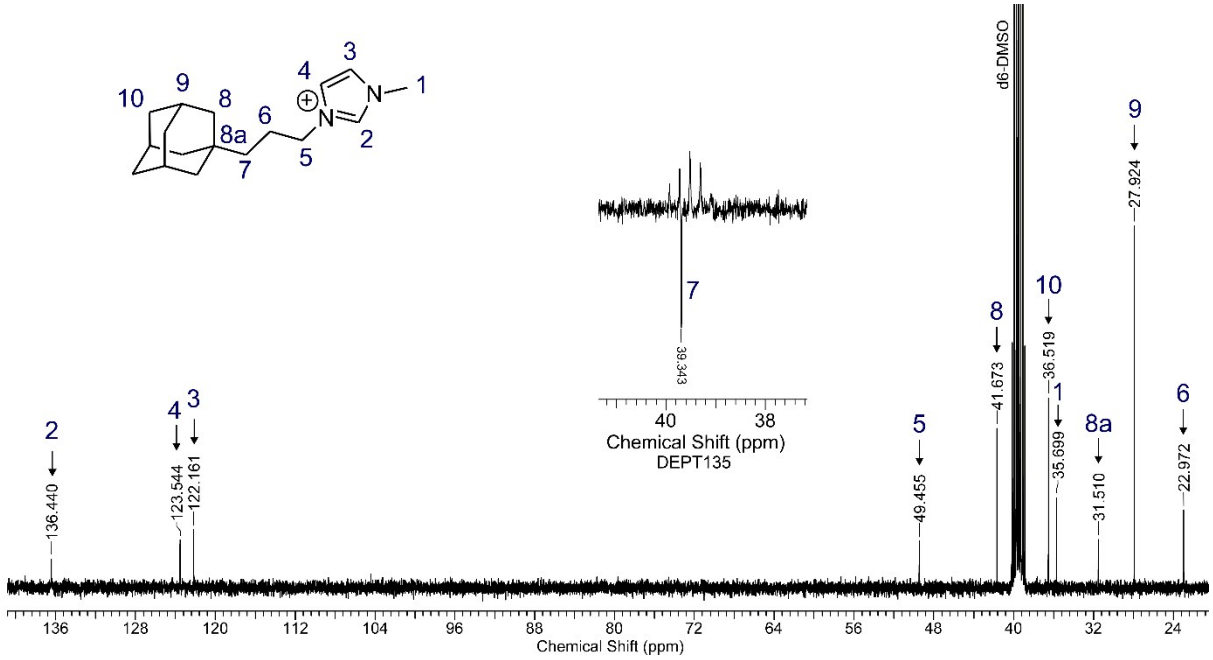

Figure S6: The ^{13}C NMR (DMSO-d_6 , 101 MHz) spectrum of compound **9c.**

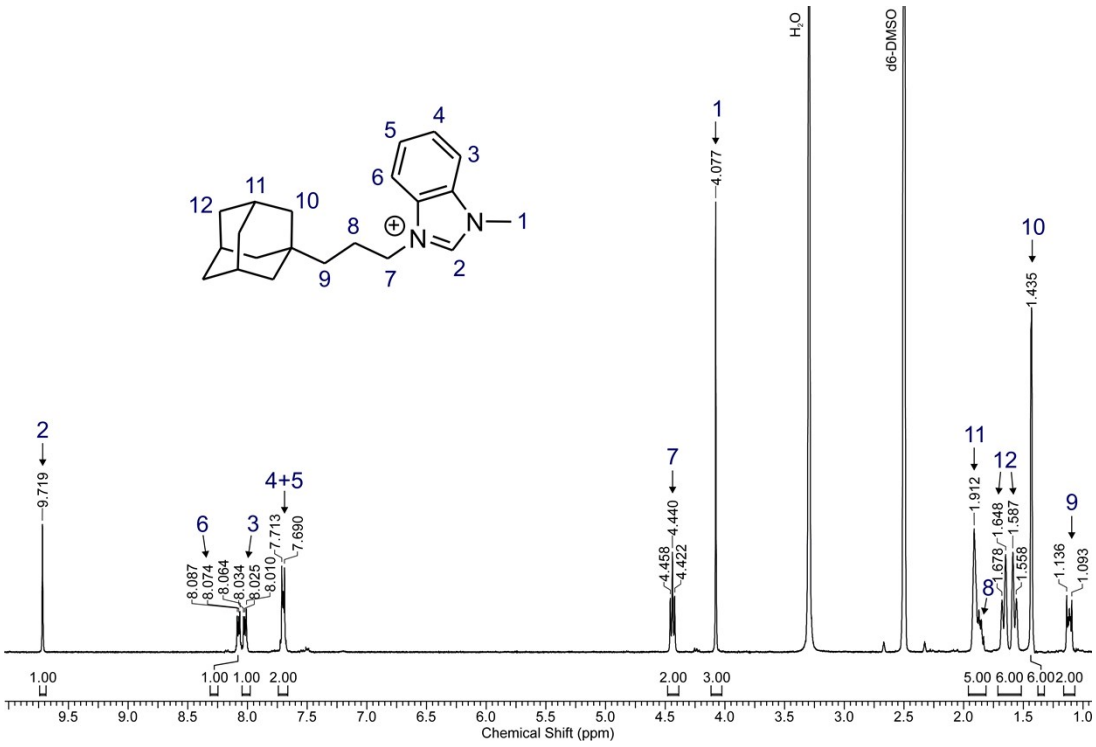

Figure S7: The ^{1}H NMR (DMSO-d_6, 400 MHz) spectrum of compound **10c**.

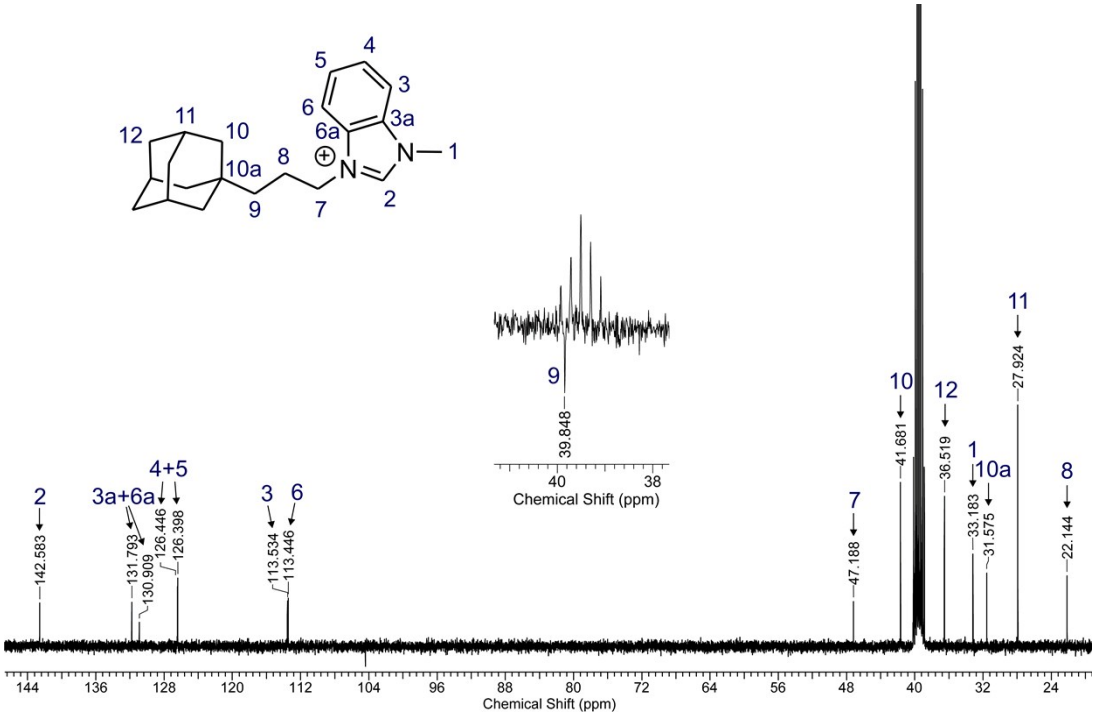

Figure S8: The ^{13}C NMR (DMSO-d_6, 101 MHz) spectrum of compound **10c**.

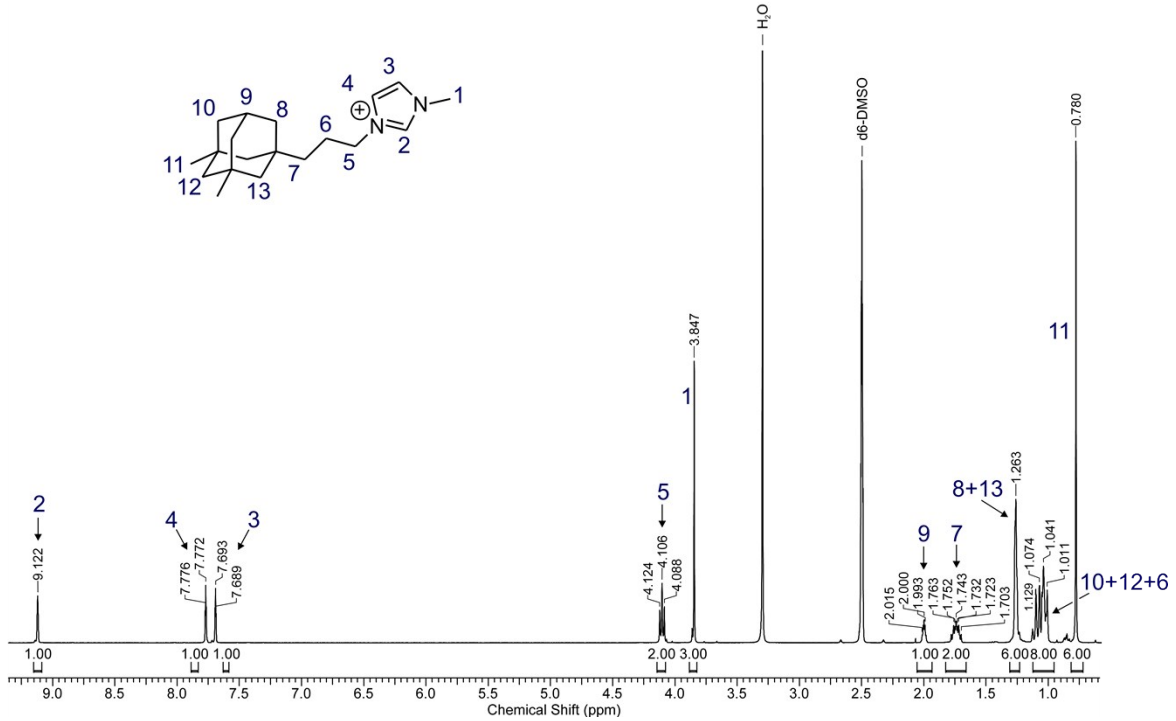

Figure S9: The ^{1}H NMR (DMSO-d_6, 400 MHz) spectrum of compound **9d**.

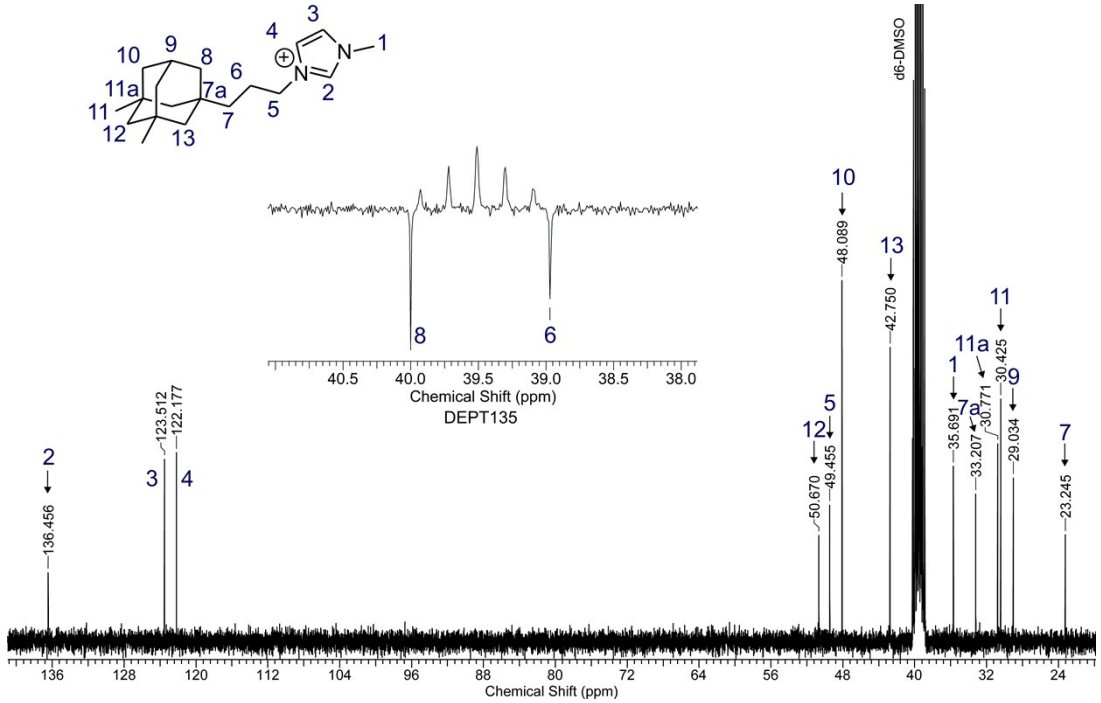

Figure S10: The ^{13}C NMR (DMSO-d_6, 101 MHz) spectrum of compound **9d**.

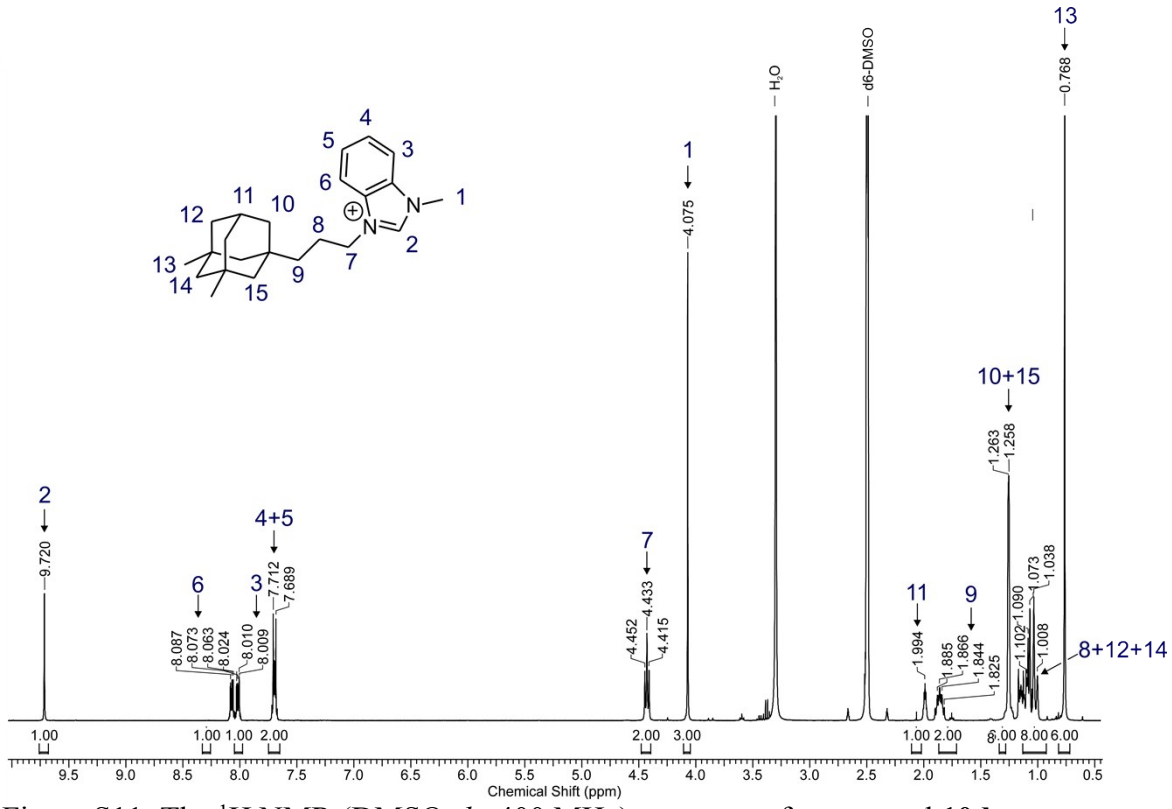

Figure S11: The ^{1}H NMR (DMSO-d_6, 400 MHz) spectrum of compound **10d**.

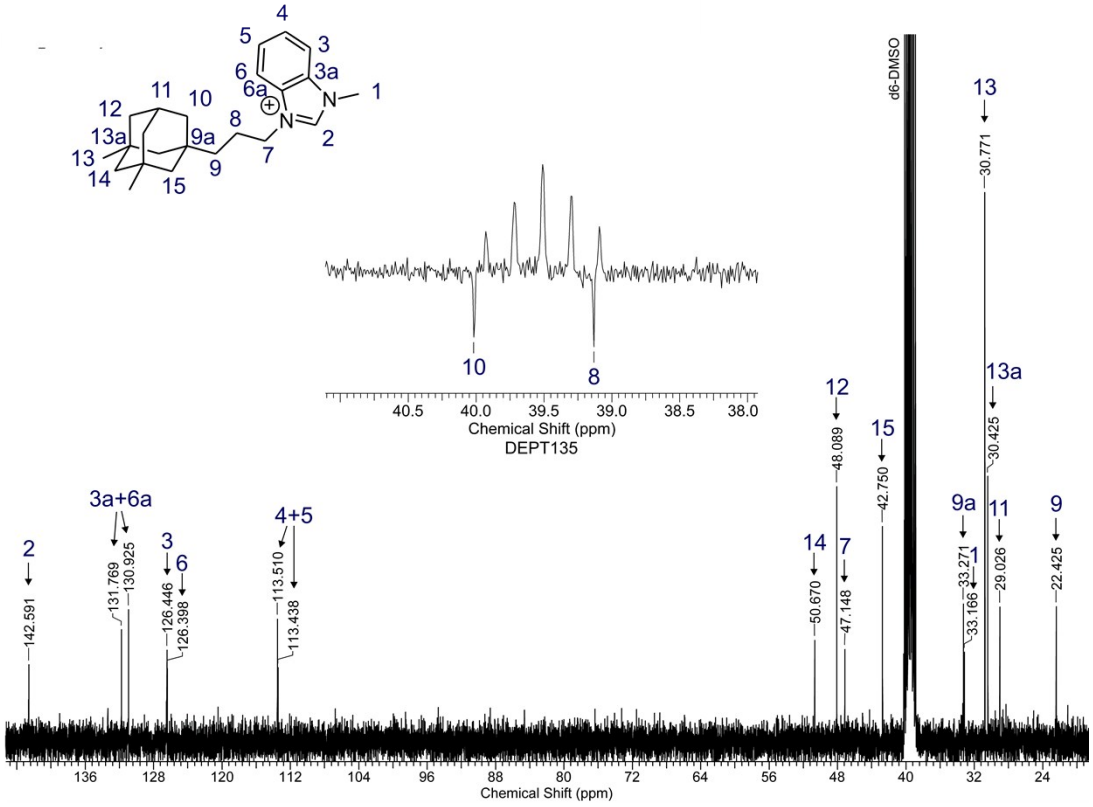

Figure S12: The ^{13}C NMR (DMSO-d_6, 101 MHz) spectrum of compound **10d**.

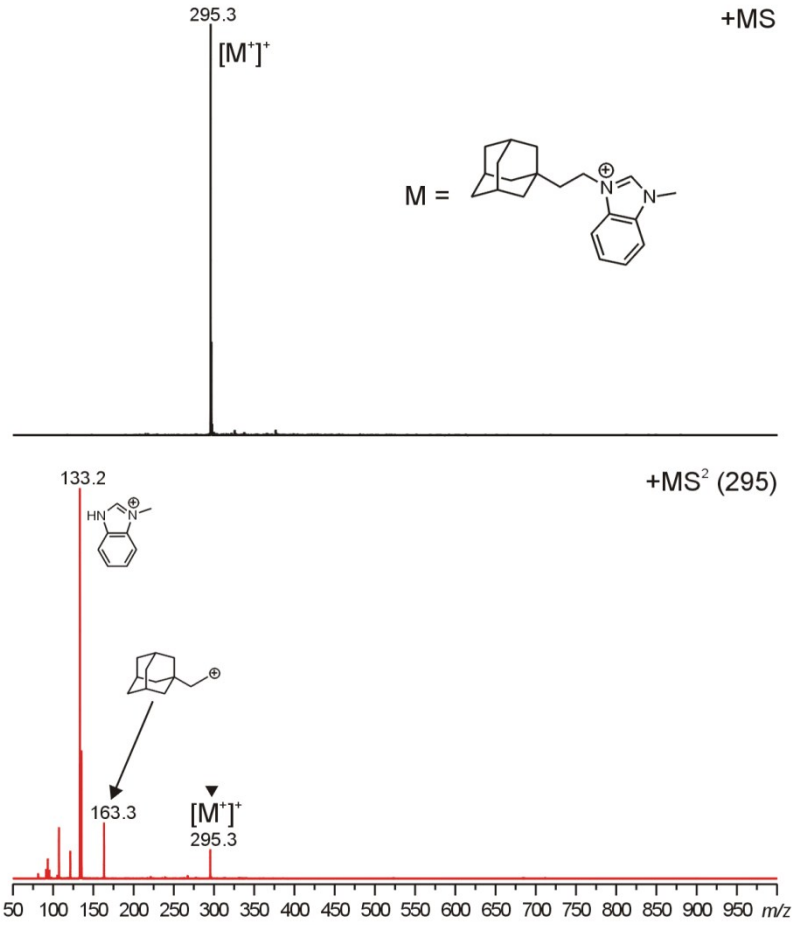

Figure S13: The positive-ion first-order ESI-MS (black) and tandem mass spectra MS^2 (red) of a MeOH:H_2O (1:1, v:v) solution of compound **10b**. The assignments for observed signals are shown in the brackets. The fragmented ion in tandem mass spectra is marked with a downward-facing triangle.

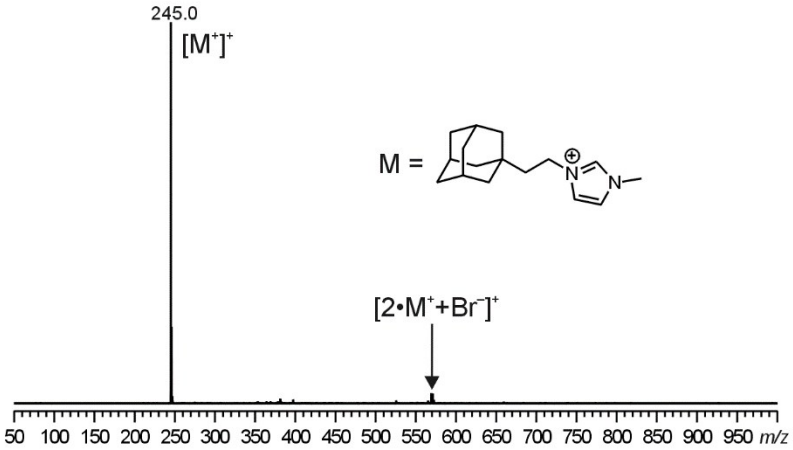

Figure S14: The positive-ion first-order ESI-MS a MeOH:H_2O (1:1, v:v) solution of compound **9b**. The assignments for observed signals are shown in the brackets.

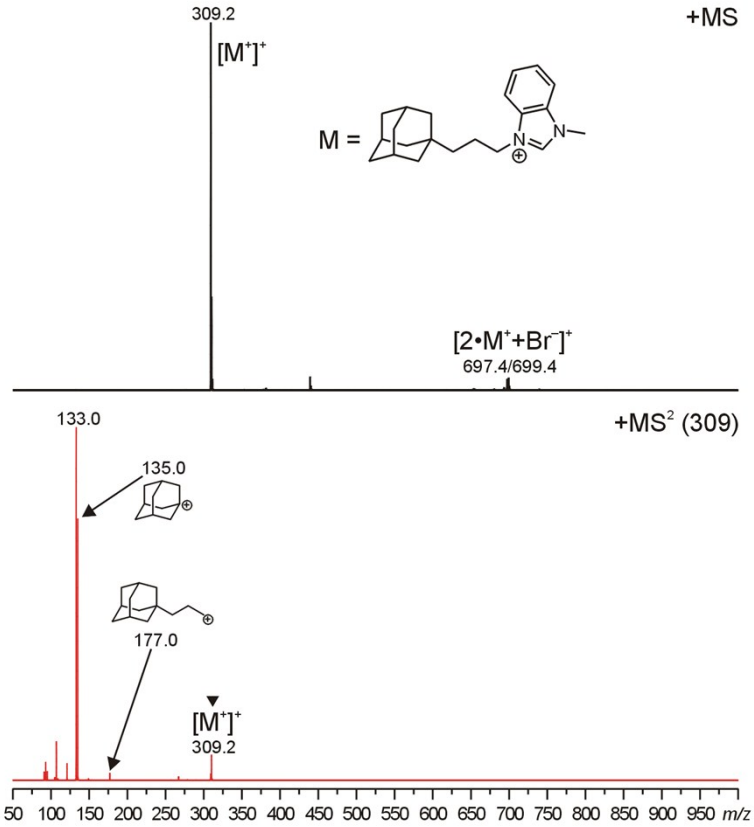

Figure S15: The positive-ion first-order ESI-MS (black) and tandem mass spectra MS^2 (red) of a MeOH:H_2O (1:1, v:v) solution of compound **10c**. The assignments for observed signals are shown in the brackets. The fragmented ion in tandem mass spectra is marked with a downward-facing triangle.

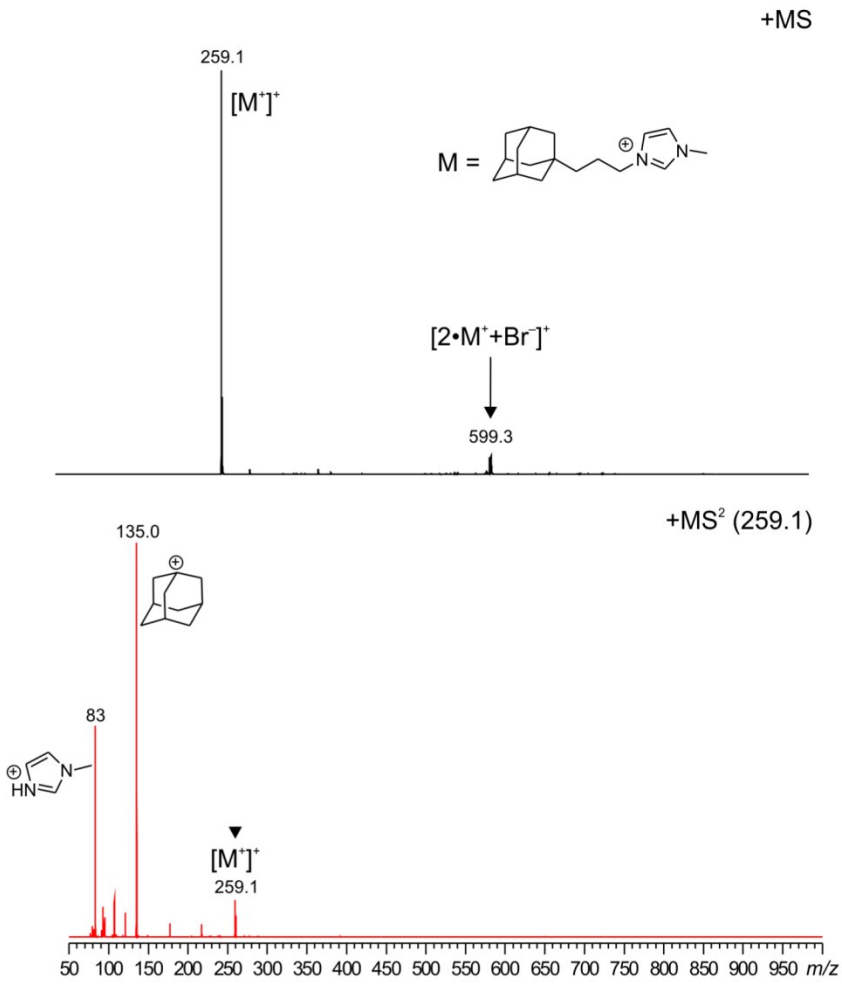

Figure S16: The positive-ion first-order ESI-MS (black) and tandem mass spectra MS^2 (red) of an MeOH:H_2O (1:1, v:v) solution of compound **9c**. The assignments for observed signals are shown in the brackets. The fragmented ion in tandem mass spectra is marked with a downward-facing triangle.

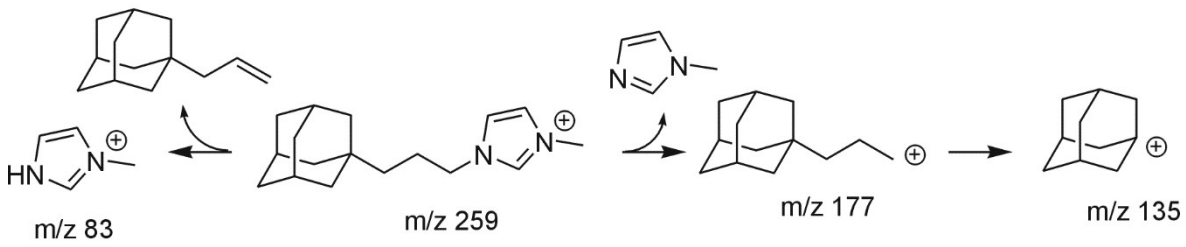

Scheme S1: Fragmentation pathways of the guest **9c**.

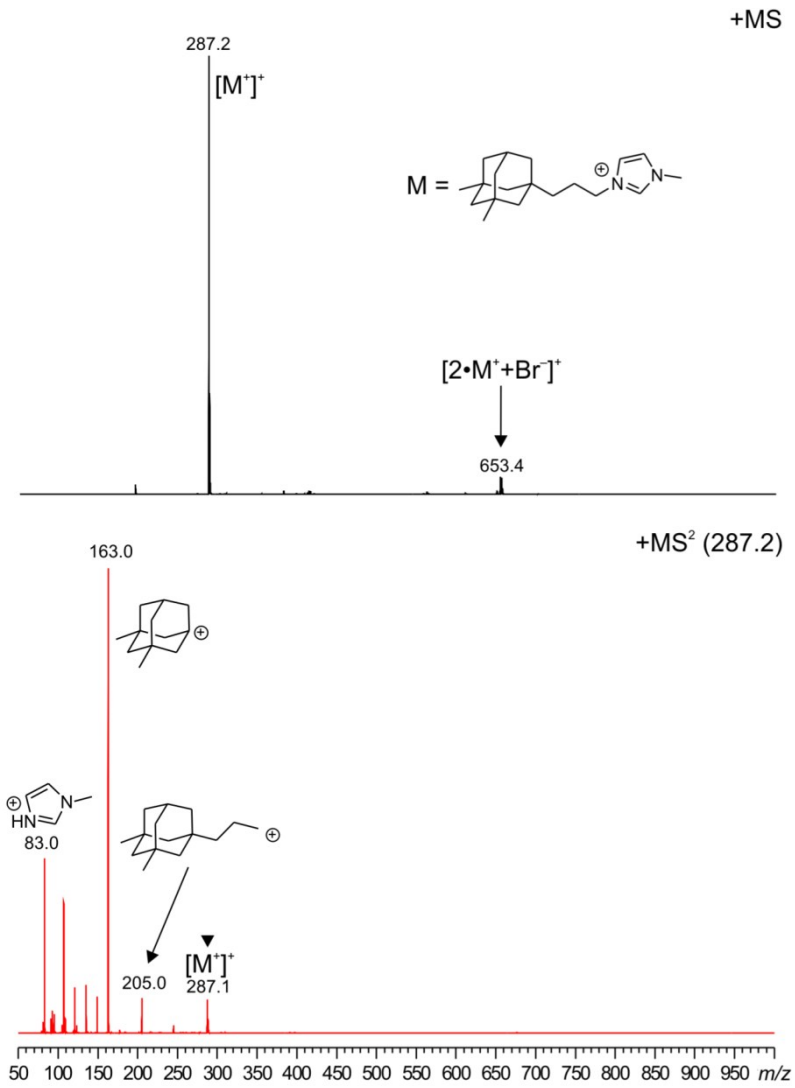

Figure S17: The positive-ion first-order ESI-MS (black) and tandem mass spectra MS^2 (red) of an MeOH:H_2O (1:1, v:v) solution of compound **9d**. The assignments for observed signals are shown in the brackets. The fragmented ion in tandem mass spectra is marked with a downward-facing triangle.

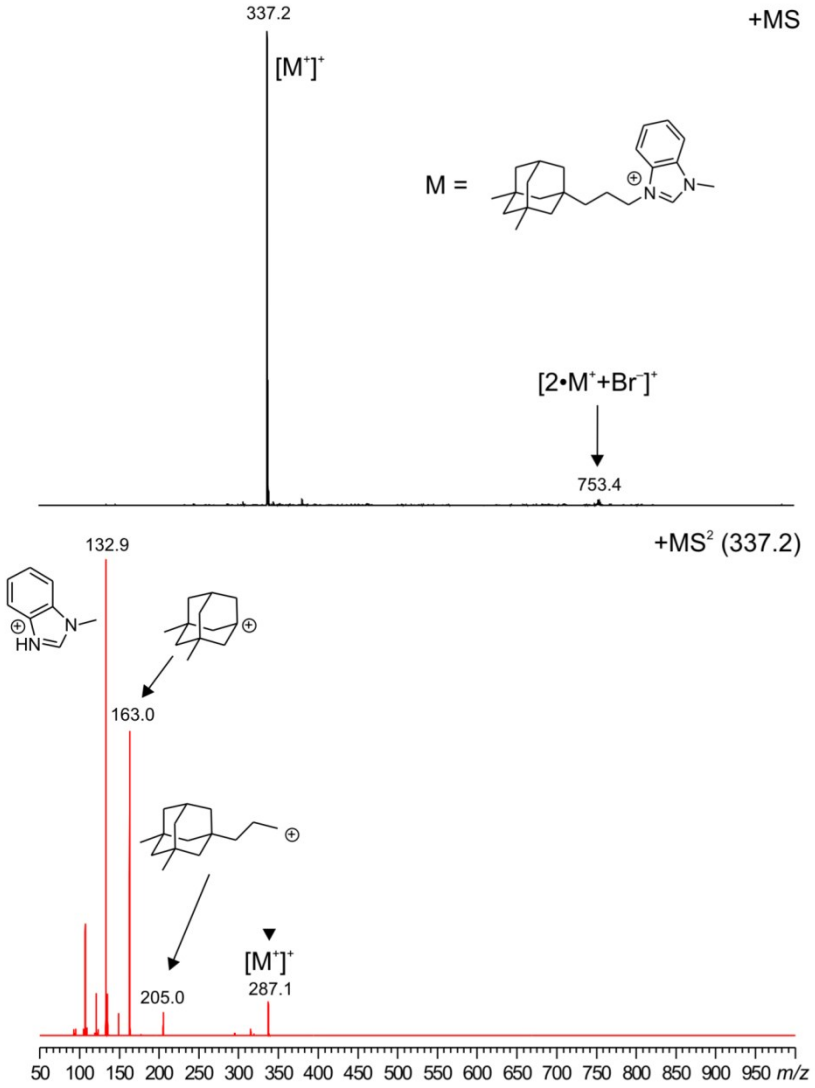

Figure S18: The positive-ion first-order ESI-MS (black) and tandem mass spectra MS^2 (red) of an MeOH:H_2O (1:1, v:v) solution of compound **10d**. The assignments for observed signals are shown in the brackets. The fragmented ion in tandem mass spectra is marked with a downward-facing triangle.

Stacking plots of NMR titrations

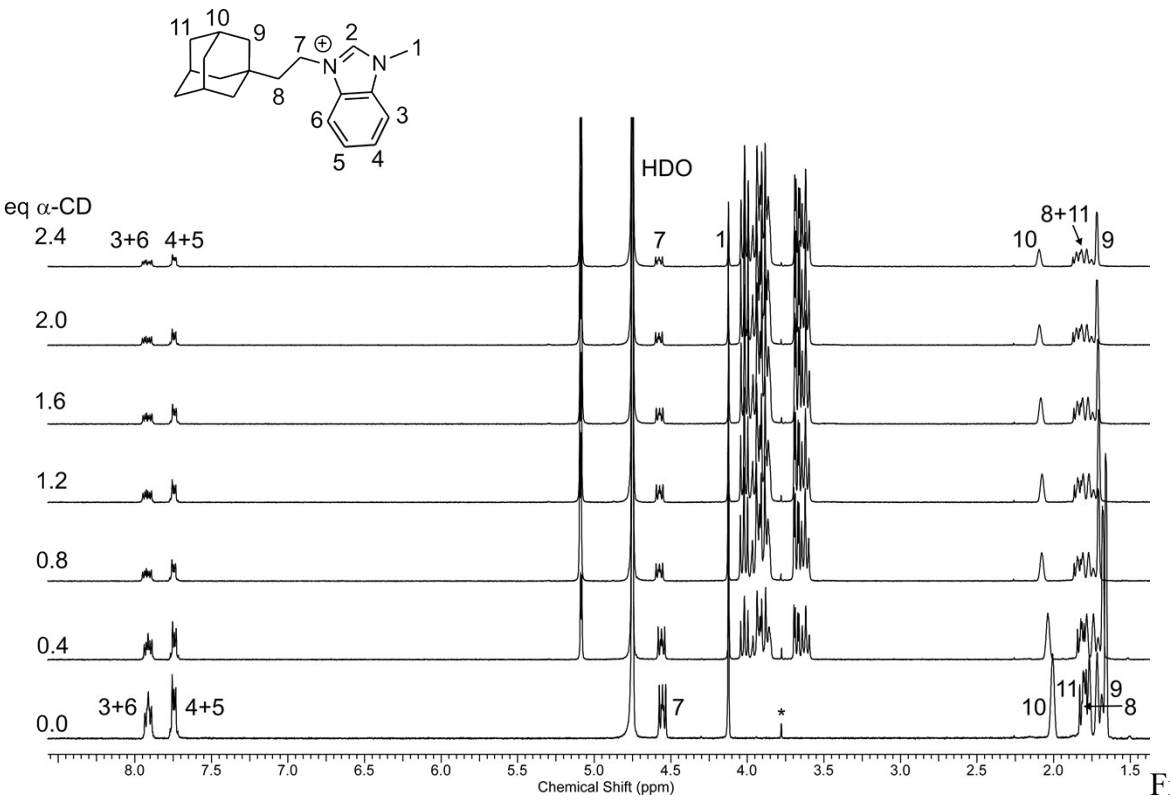

Figure S19: Stacking plot of ^{1}H NMR spectra (400 MHz) of mixtures of **10b** with α-CD in D_2O at 30 °C. Initial concentration of **10b** was 1.85 mM, concentration of α-CD stock solution was 4.41 mM. * residual MeI

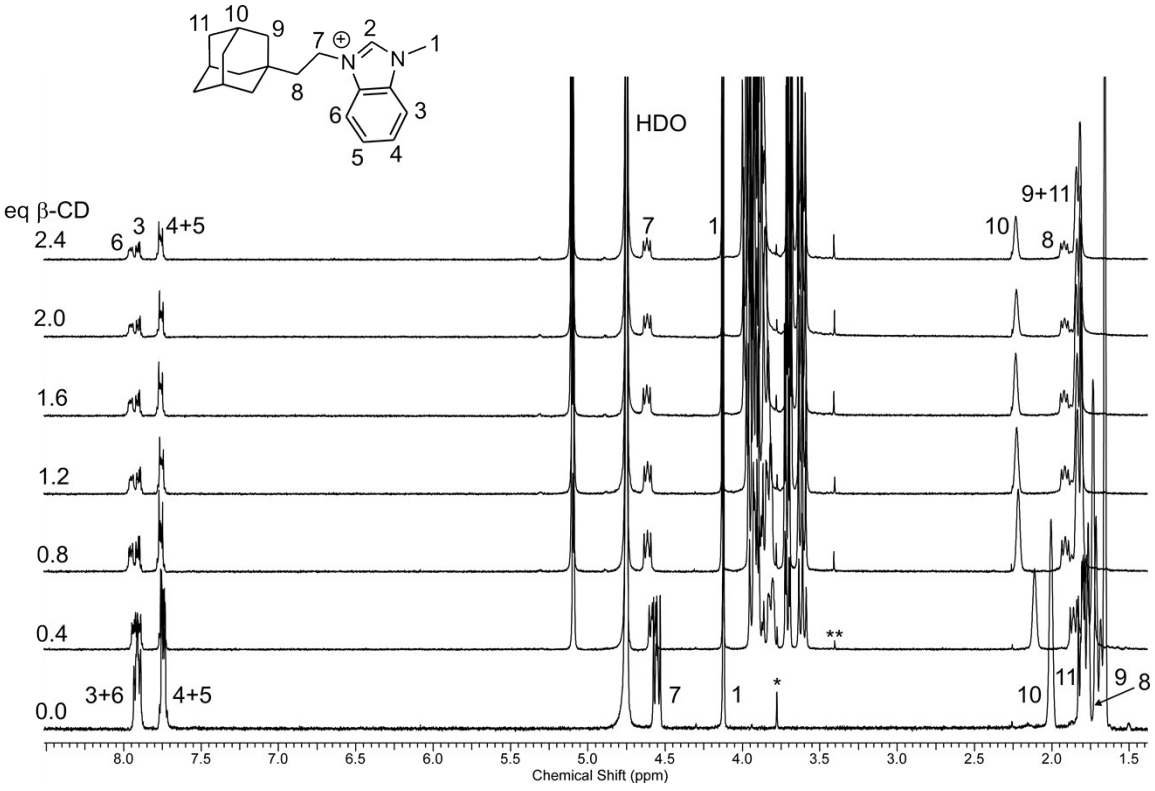

Figure S20: Stacking plot of ^{1}H NMR spectra (400 MHz) of mixtures of **10b** with β-CD in D_2O at 30 °C. Initial concentration of **10b** was 1.85 mM, concentration of β-CD stock solution was 4.40 mM. *residual MeI; **impurity from commercial β-CD

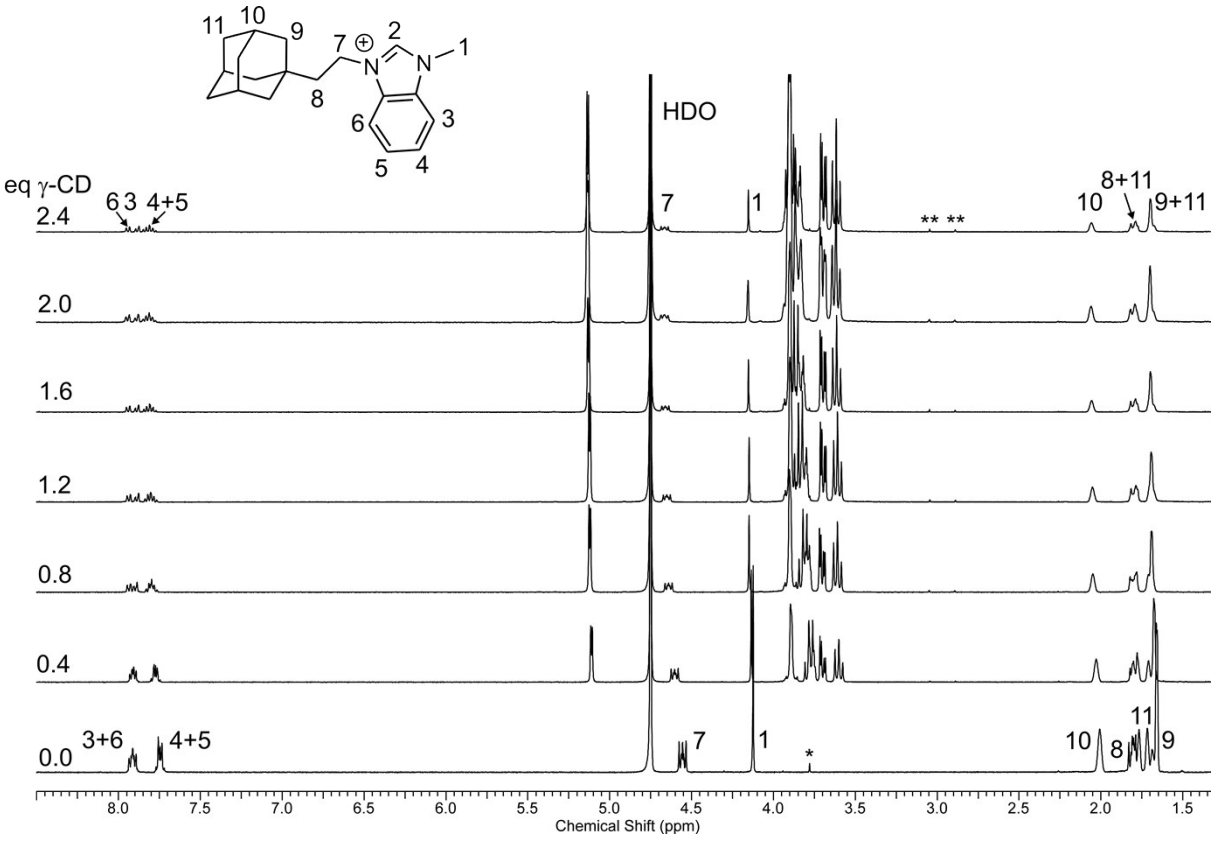

Figure S21: Stacking plot of ^{1}H NMR spectra (400 MHz) of mixtures of **10b** with γ-CD in D_2O at 30 °C. Initial concentration of **10b** was 1.85 mM, concentration of γ-CD stock solution was 4.47 mM. * residual MeI; **impurity from commercial γ-CD

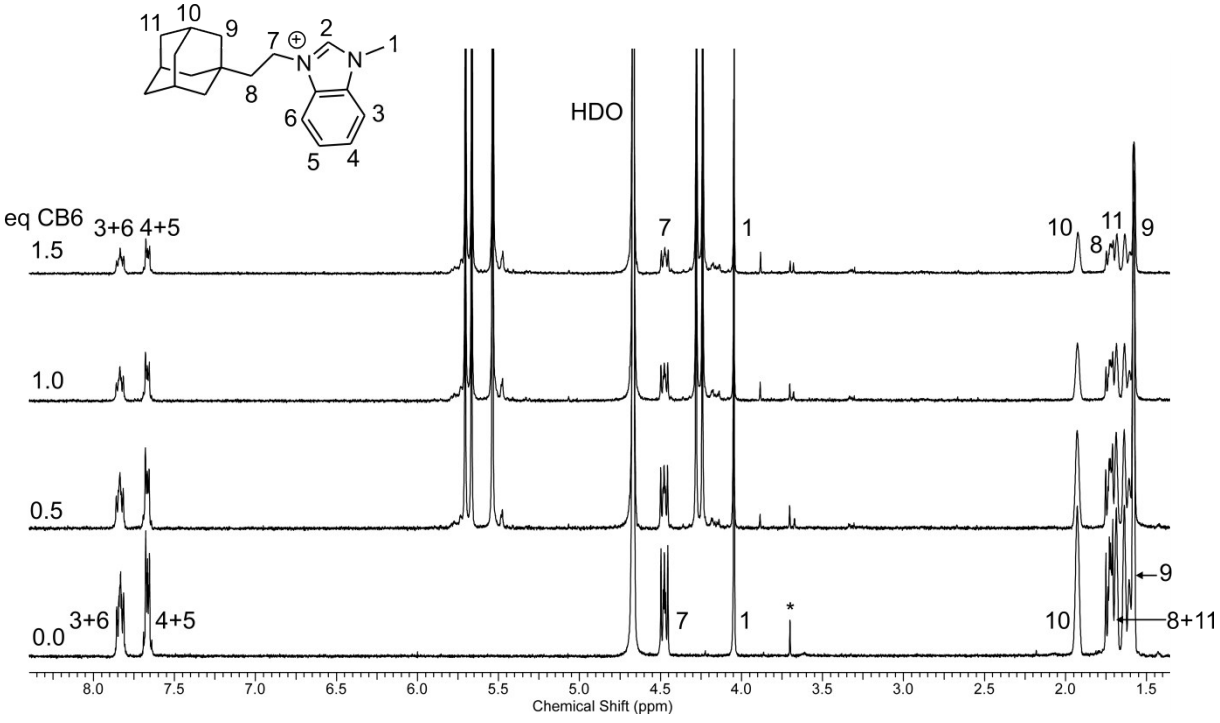

Figure S22: Stacking plot of ^{1}H NMR spectra (400 MHz) of mixtures of **10b** with CB6 in 50 mM NaCl in D_2O at 30 °C. Initial concentration of **10b** was 1.89 mM, concentration of CB6 stock solution was 2.19 mM. *residual MeI

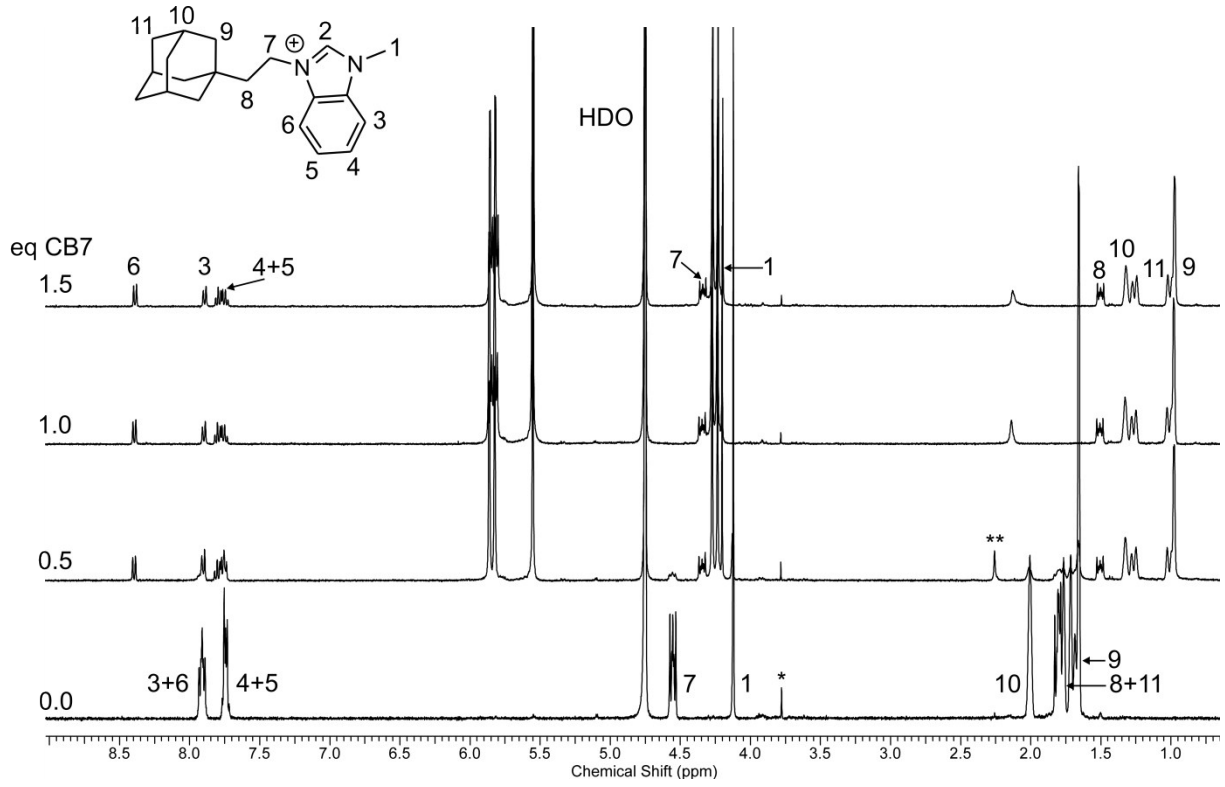

Figure S23: Stacking plot of ^{1}H NMR spectra (400 MHz) of mixtures of **10b** with CB7 in D_2O at 30 °C. Initial concentration of **10b** was 1.85 mM, concentration of CB7 stock solution was 2.24 mM. *residual MeI; **impurity from commercial CB7

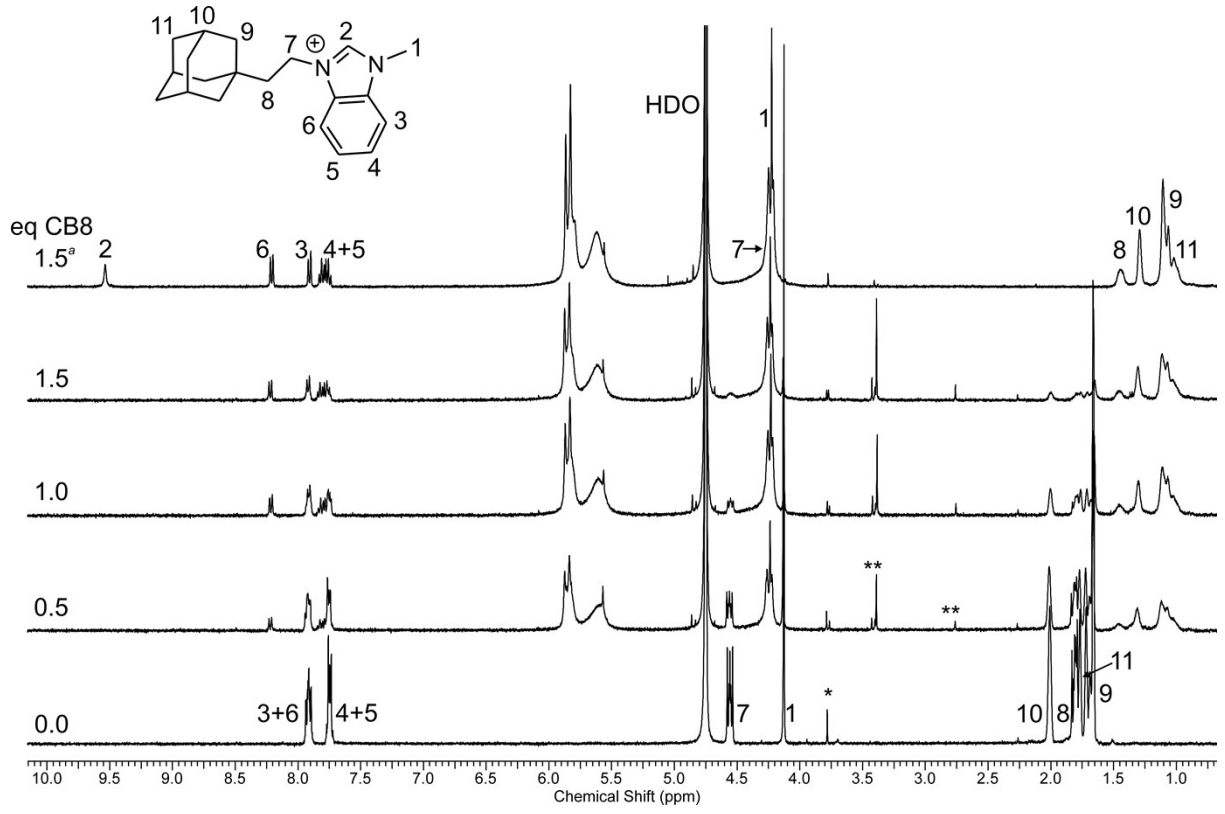

Figure S24: Stacking plot of ^{1}H NMR spectra (400 MHz) of mixtures of **10b** with CB8 in 50 mM NaCl in D_2O at 30 °C. Initial concentration of **10b** was 1.89 mM, concentration of the CB8 stock solution was 2.20 mM. *residual MeI; **impurities from commercial CB8

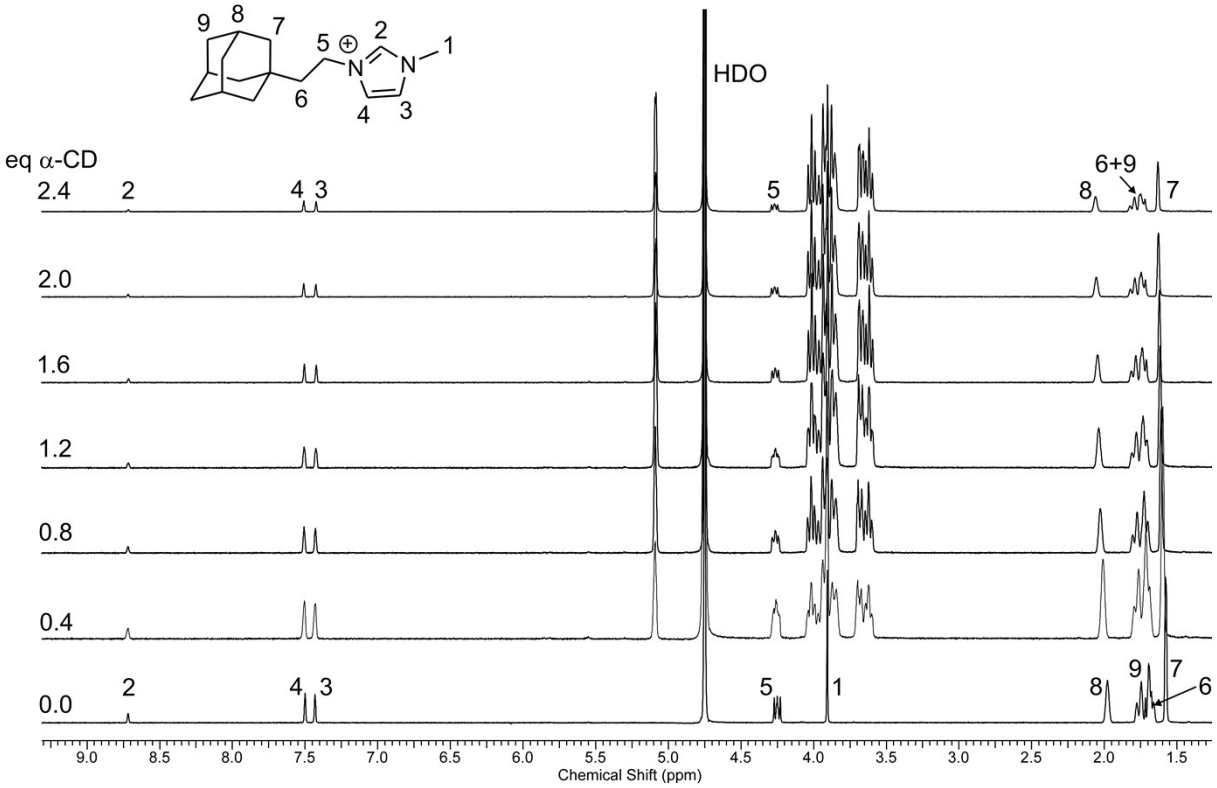

Figure S25: Stacking plot of ^{1}H NMR spectra (400 MHz) of mixtures of **9b** with α-CD in D_2O O at 30 °C. Initial concentration of **9b** was 1.89 mM, concentration of the α-CD stock solution was 4.45 mM.

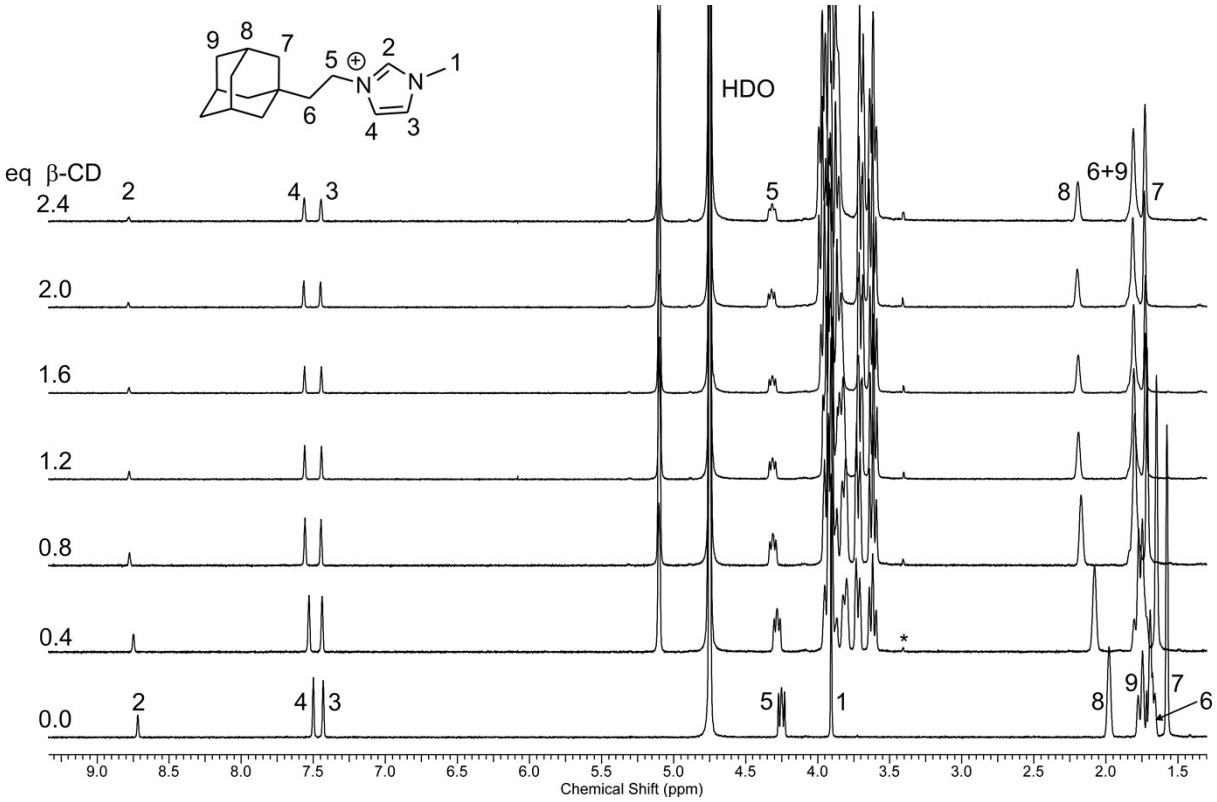

Figure S26: Stacking plot of ^{1}H NMR spectra (400 MHz) of mixtures of **9b** with β-CD in D_2O at 30 °C. Initial concentration of **9b** was 1.89 mM, concentration of the β-CD stock solution was 4.45 mM. *impurity from commercial β-CD

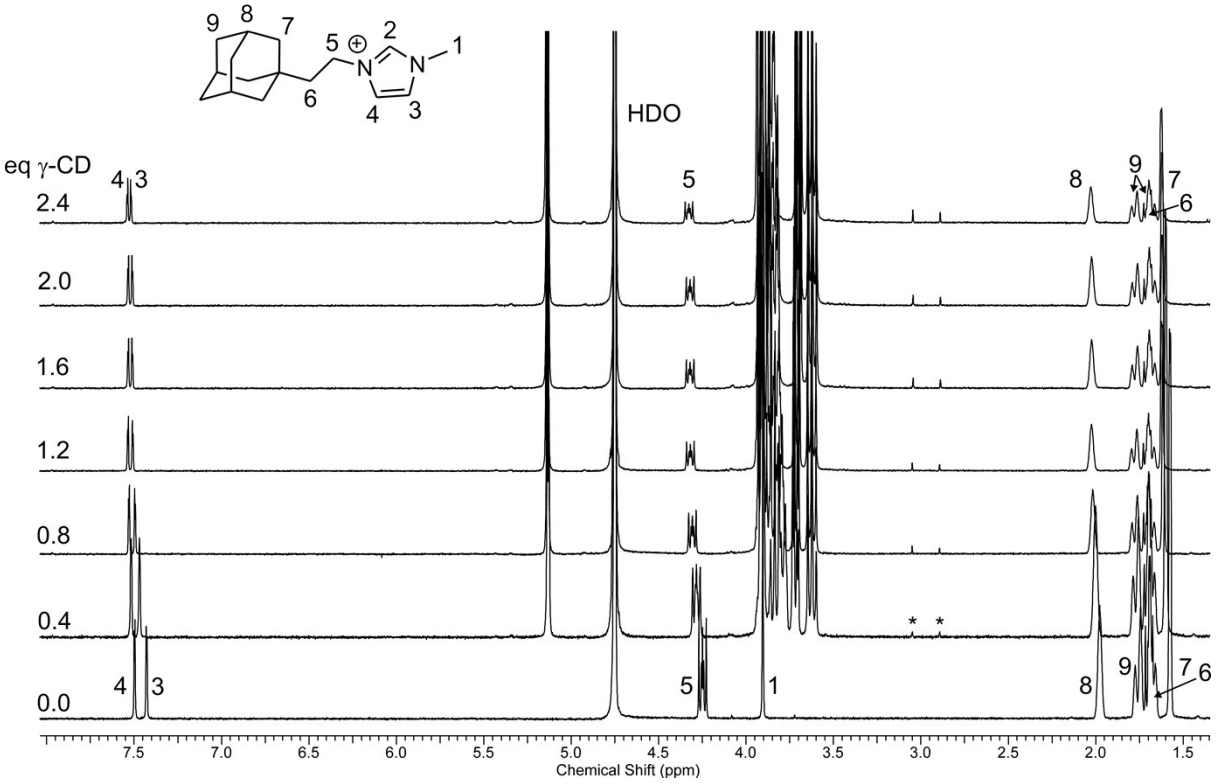

Figure S27: Stacking plot of ^{1}H NMR spectra (400 MHz) of mixtures of **9b** with γ-CD in D_2O at 30 °C. Initial concentration of **9b** was 1.89 mM, concentration of the γ-CD stock solution was 4.49 mM. *impurities from commercial γ-CD

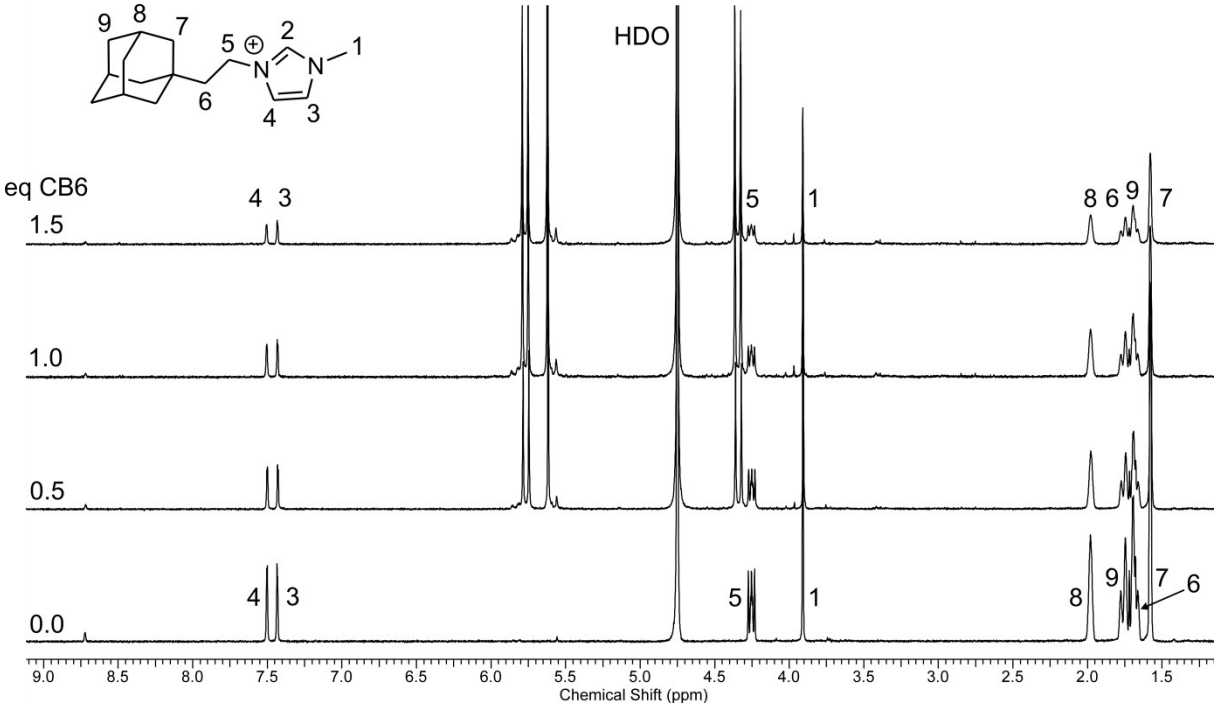

Figure S28: Stacking plot of ^{1}H NMR spectra (400 MHz) of mixtures of **9b** with CB6 in 50 mM NaCl in D_2O at 30 °C. Initial concentration of **9b** was 1.89 mM, concentration of the CB6 stock solution was 2.19 mM.

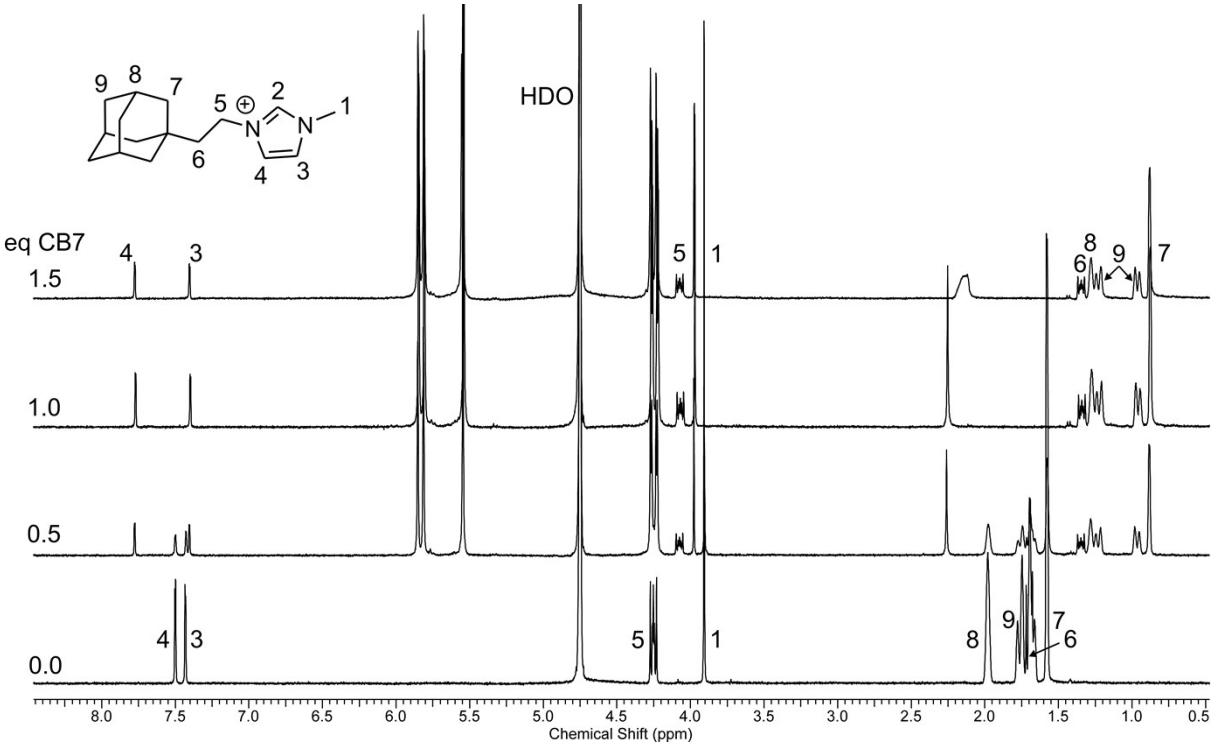

Figure S29: Stacking plot of ^{1}H NMR spectra (400 MHz) of mixtures of **9b** with CB7 in D_2O at 30 °C. Initial concentration of **9b** was 1.89 mM, concentration of the CB7 stock solution was 2.26 mM.

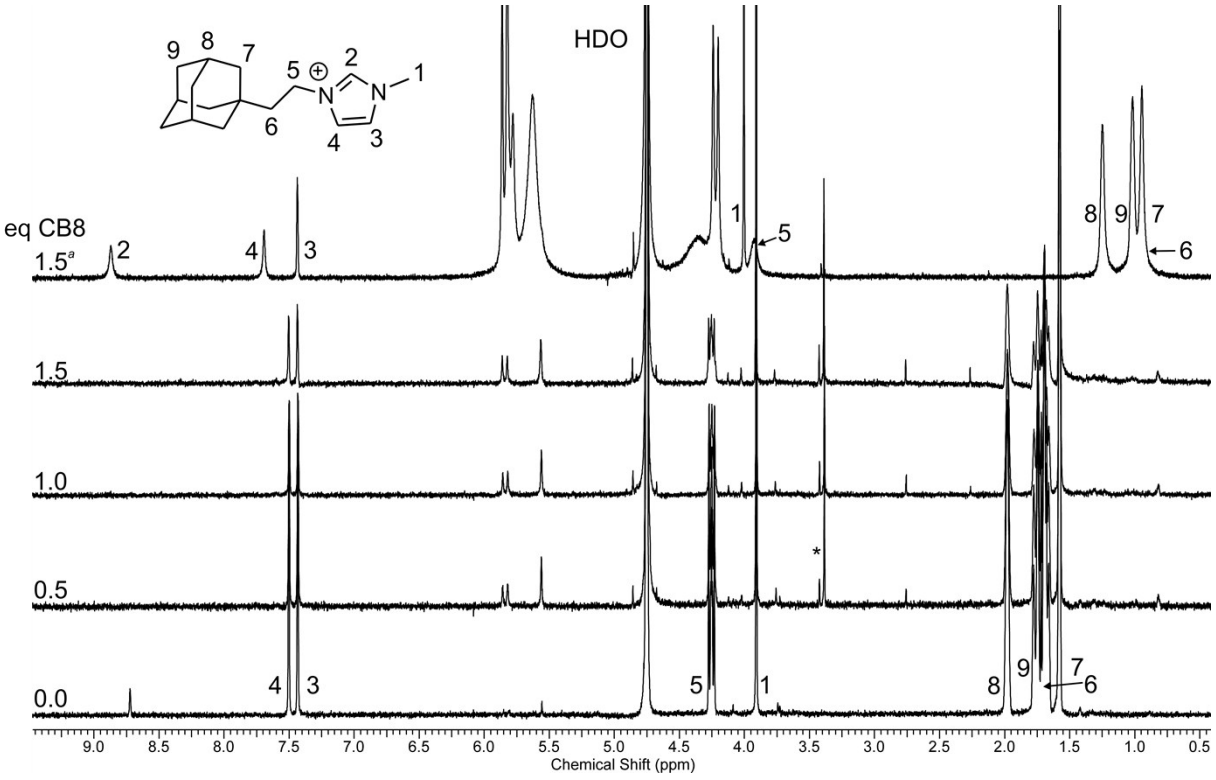

Figure S30: Stacking plot of ^{1}H NMR spectra (400 MHz) of mixtures of **9b** with CB8 in 50 mM NaCl in D_2O at 30 °C. Initial concentration of **9b** was 1.89 mM, concentration of the CB8 stock solution was 2.19 mM. *impurity from commercial CB8

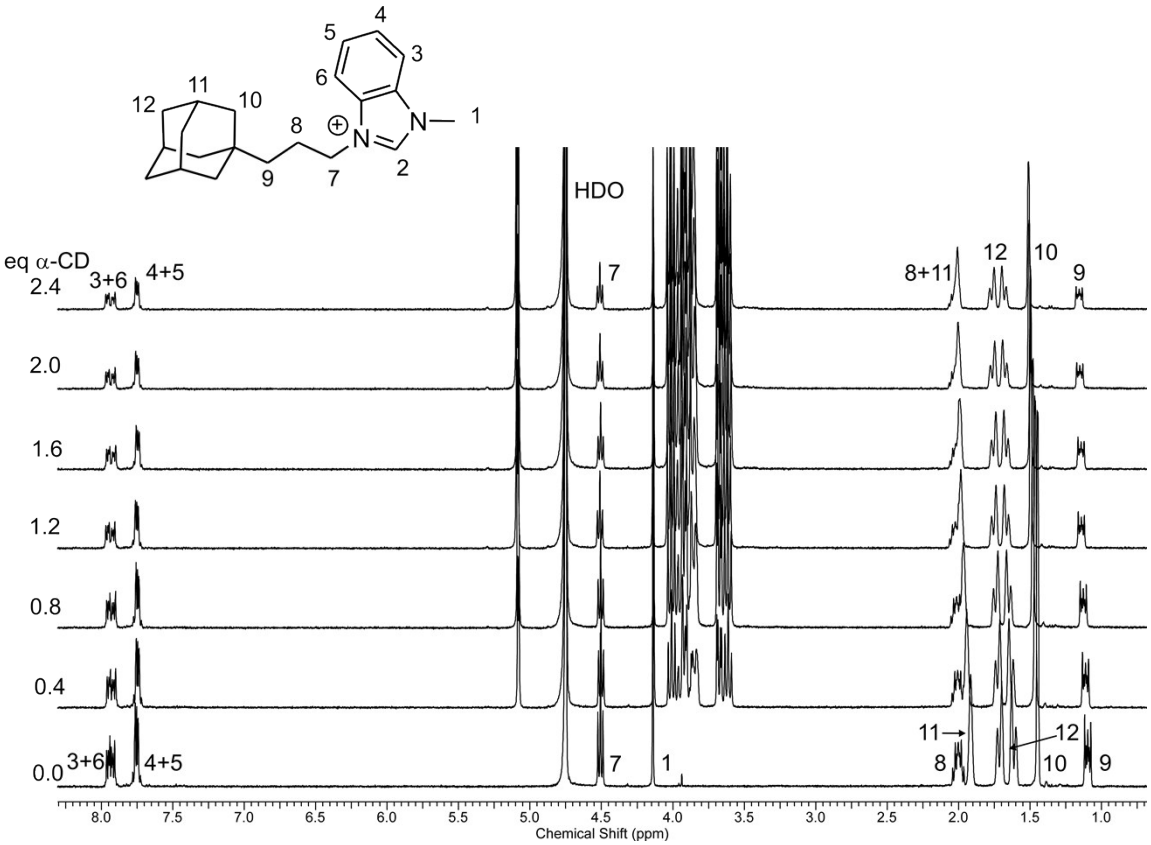

Figure S31: Stacking plot of ^{1}H NMR spectra (400 MHz) of mixtures of **10c** with α-CD in D_2O at 30 °C. Initial concentration of **10c** was 1.90 mM, concentration of the α-CD stock solution was 4.44 mM.

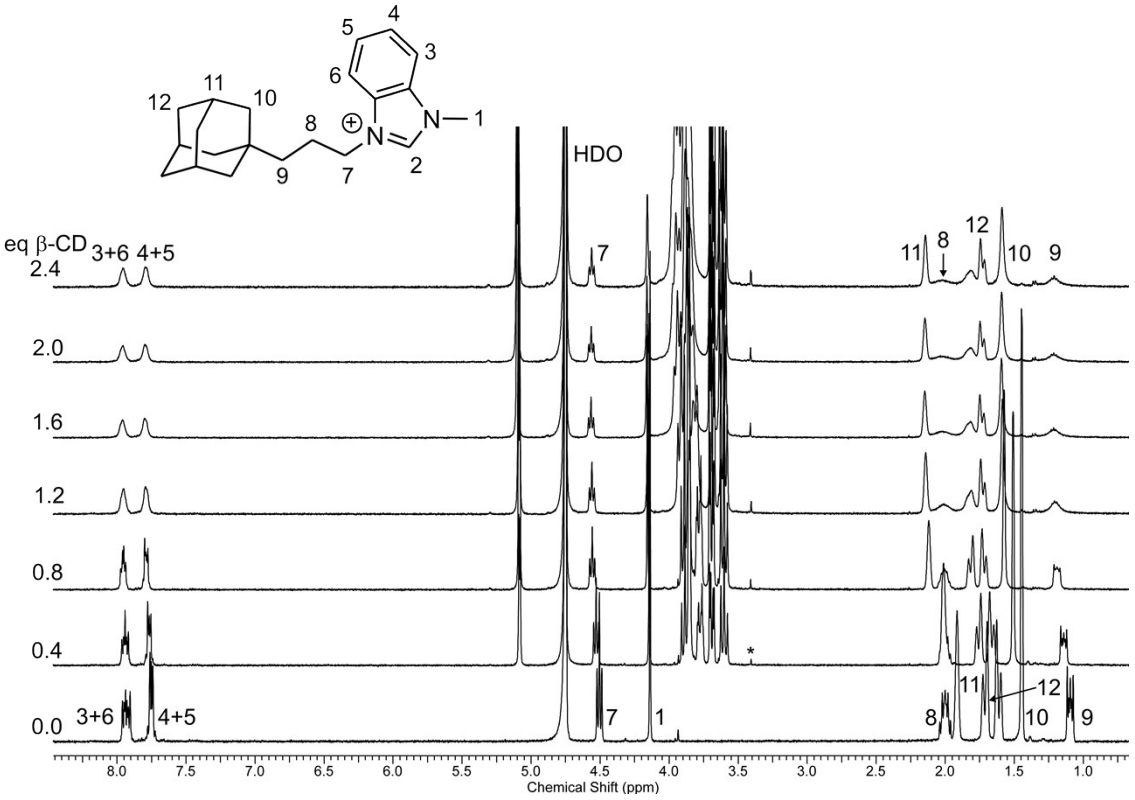

Figure S32: Stacking plot of ^{1}H NMR spectra (400 MHz) of mixtures of **10c** with β-CD in D_2O at 30 °C. Initial concentration of **10c** was 1.90 mM, concentration of the β-CD stock solution was 4.30 mM. *impurity from commercial β-CD

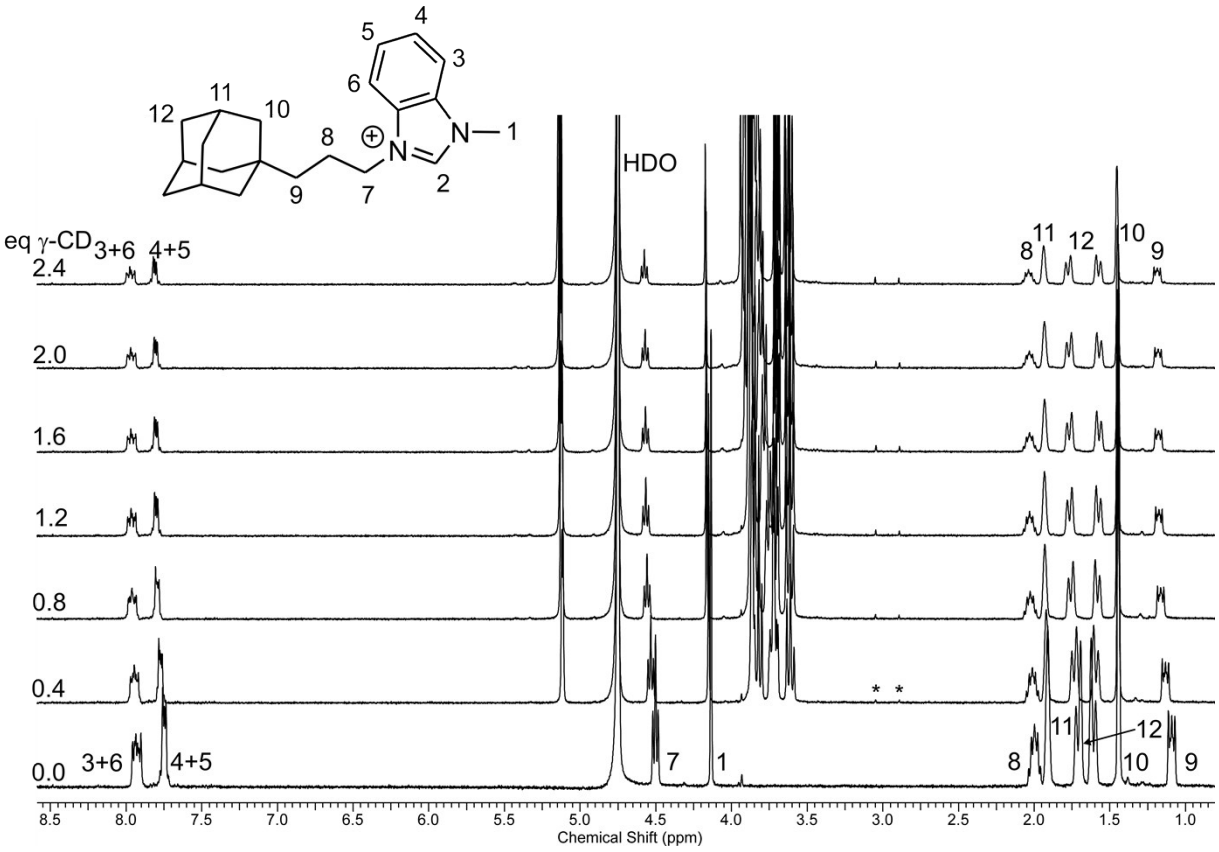

Figure S33: Stacking plot of ^{1}H NMR spectra (400 MHz) of mixtures of **10c** with γ-CD in D_2O at 30 °C. Initial concentration of **10c** was 1.90 mM, concentration of the γ-CD stock solution was 4.37 mM. *impurity from commercial γ-CD

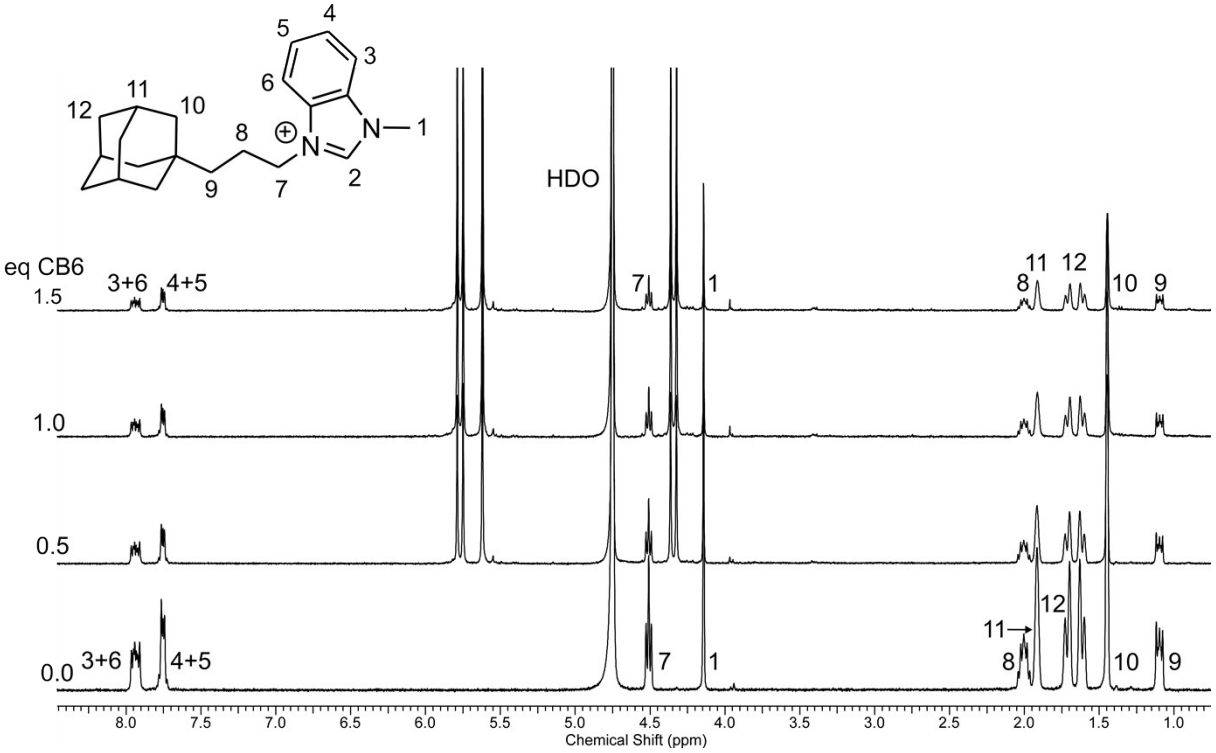

Figure S34: Stacking plot of ^{1}H NMR spectra (400 MHz) of mixtures of **10c** with CB6 in 50 mM NaCl in D_2O at 30 °C. Initial concentration of **10c** was 1.86 mM, concentration of the CB6 stock solution was 2.21 mM.

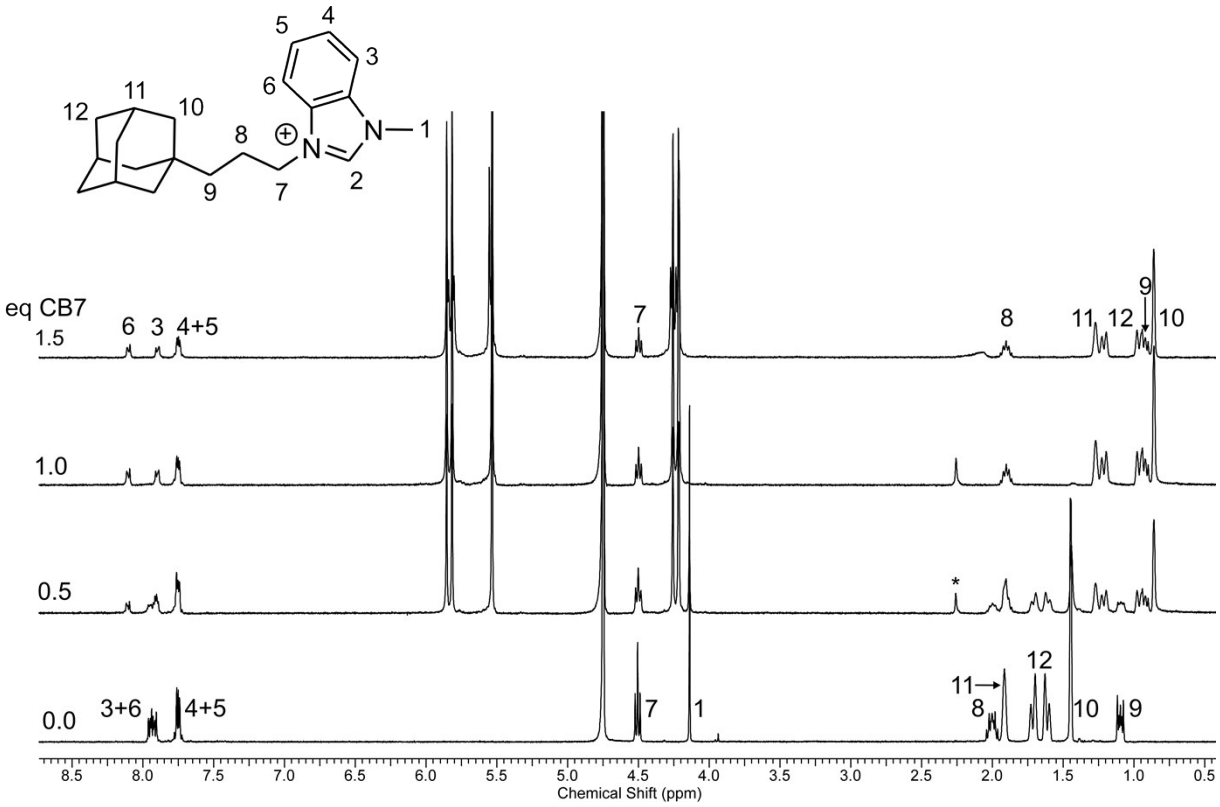

Figure S35: Stacking plot of ^{1}H NMR spectra (400 MHz) of mixtures of **10c** with CB7 in D_2O at 30 °C. Initial concentration of **10c** was 1.90 mM, concentration of the CB7 stock solution was 2.18 mM. *impurity from commercial CB7

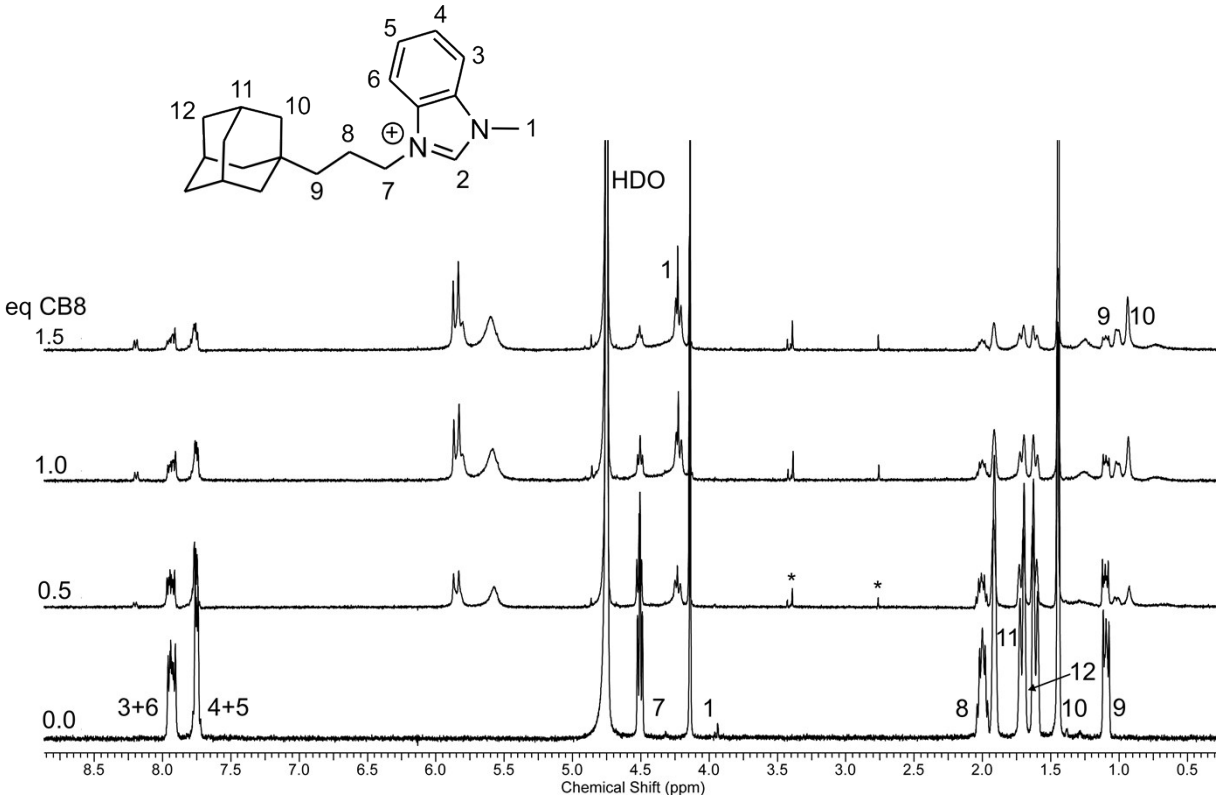

Figure S36: Stacking plot of ^{1}H NMR spectra (400 MHz) of mixtures of **10c** with CB8 in 50 mM NaCl in D_2O at 30 °C. Initial concentration of **10c** was 1.86 mM, concentration of the CB8 stock solution was 2.20 mM. *impurity from commercial CB8

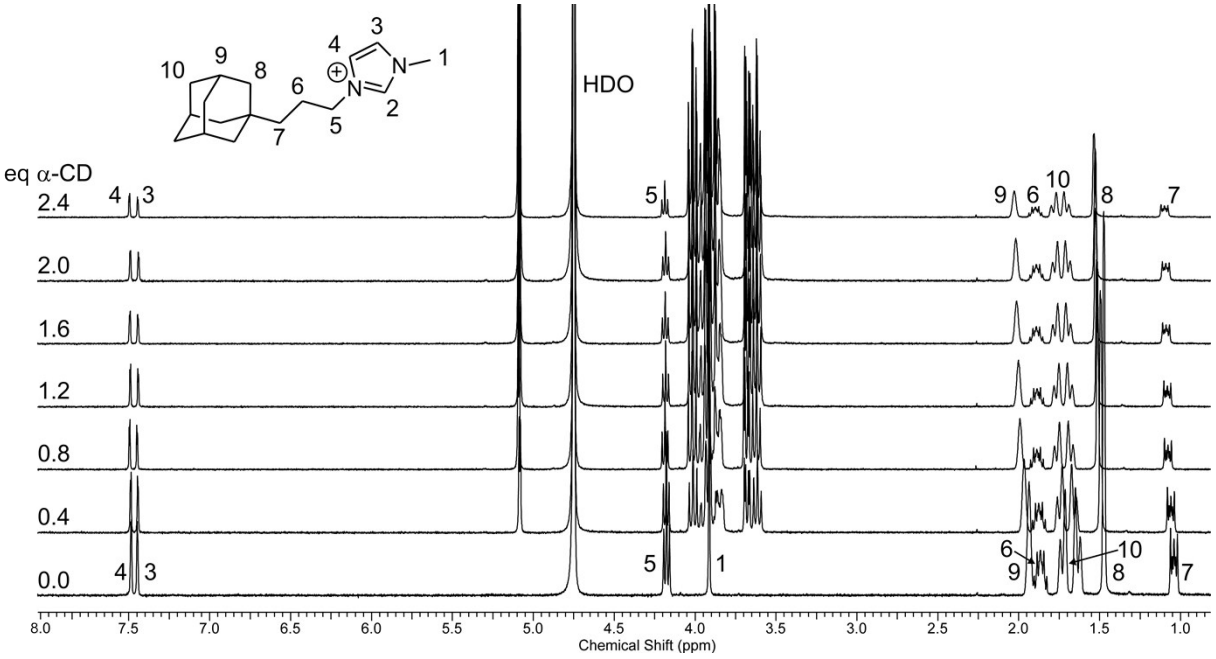

Figure S37: Stacking plot of ^{1}H NMR spectra (400 MHz) of mixtures of **9c** with α-CD in D_2O at 30 °C. Initial concentration of **9c** was 1.86 mM, concentration of the α-CD stock solution was 4.39 mM.

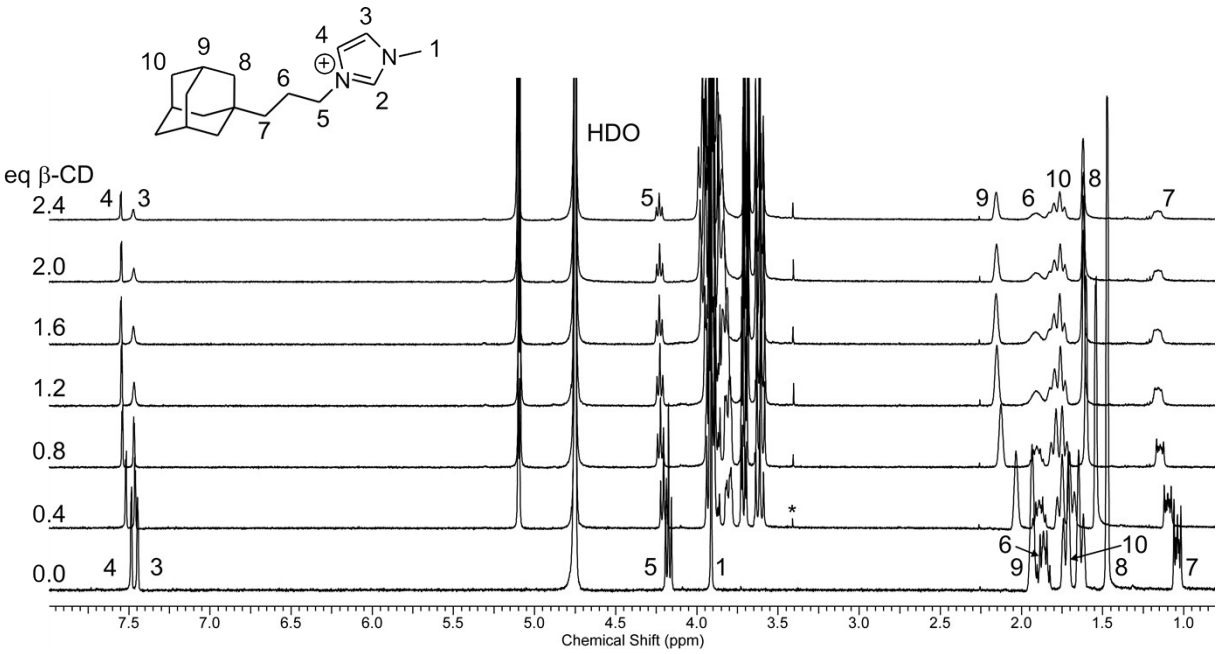

Figure S38: Stacking plot of ^{1}H NMR spectra (400 MHz) of mixtures of **9c** with β-CD in D_2O at 30 °C. Initial concentration of **9c** was 1.86 mM, concentration of the β-CD stock solution was 4.46 mM.

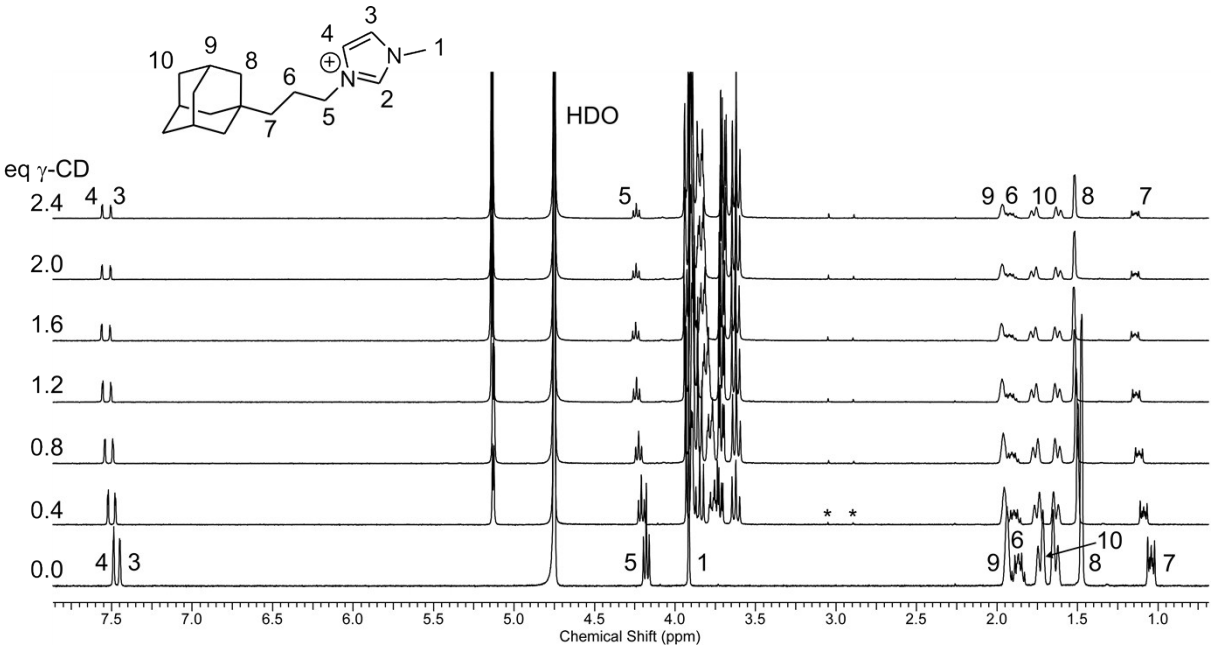

Figure S39: Stacking plot of ^{1}H NMR spectra (400 MHz) of mixtures of **9c** with γ-CD in D_2O at 30 °C. Initial concentration of **9c** was 1.86 mM, concentration of the γ-CD stock solution was 4.50 mM. *impurities from commercial γ-CD

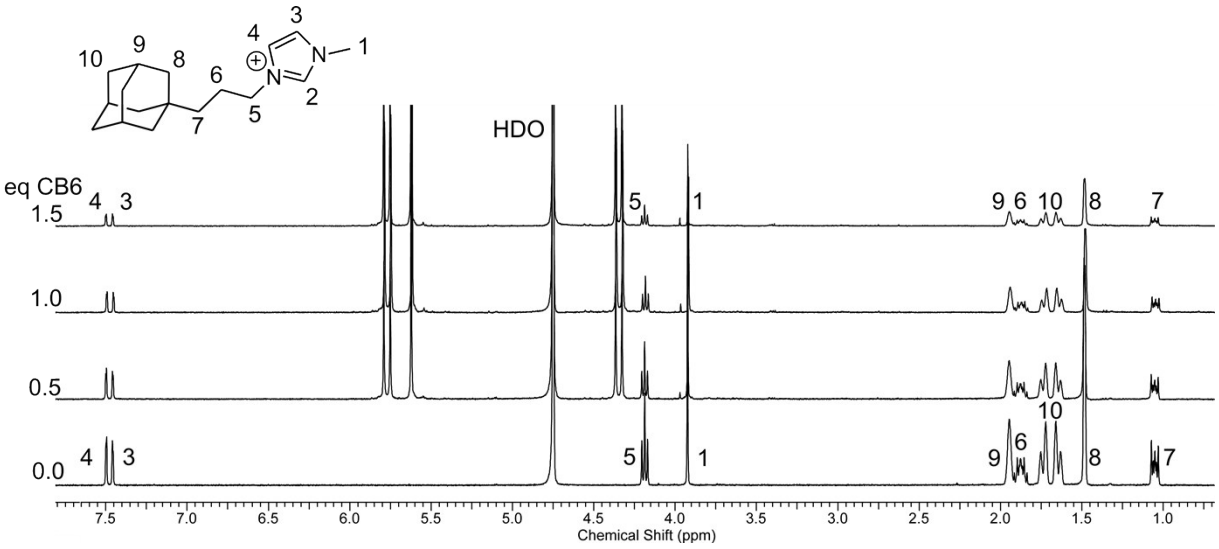

Figure S40: Stacking plot of ^{1}H NMR spectra (400 MHz) of mixtures of **9c** with CB6 in 50 mM NaCl in D_2O at 30 °C. Initial concentration of **9c** was 1.94 mM, concentration of the CB6 stock solution was 2.24 mM.

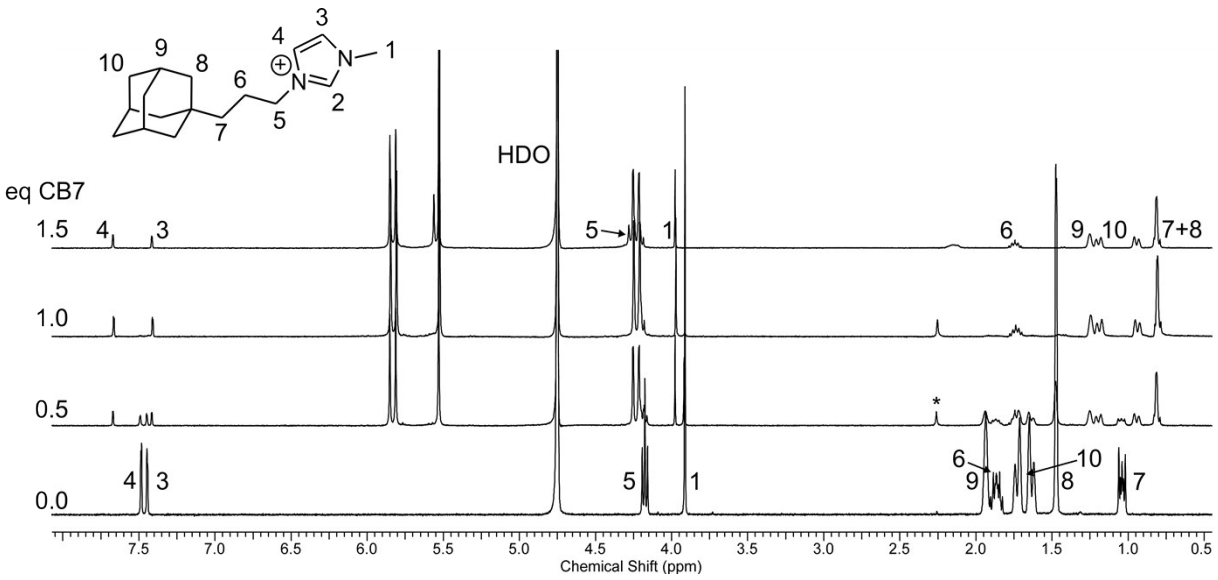

Figure S41: Stacking plot of ^{1}H NMR spectra (400 MHz) of mixtures of **9c** with CB7 in D_2O at 30 °C. Initial concentration of **9c** was 1.86 mM, concentration of the CB7 stock solution was 2.21 mM. *impurities from commercial CB7

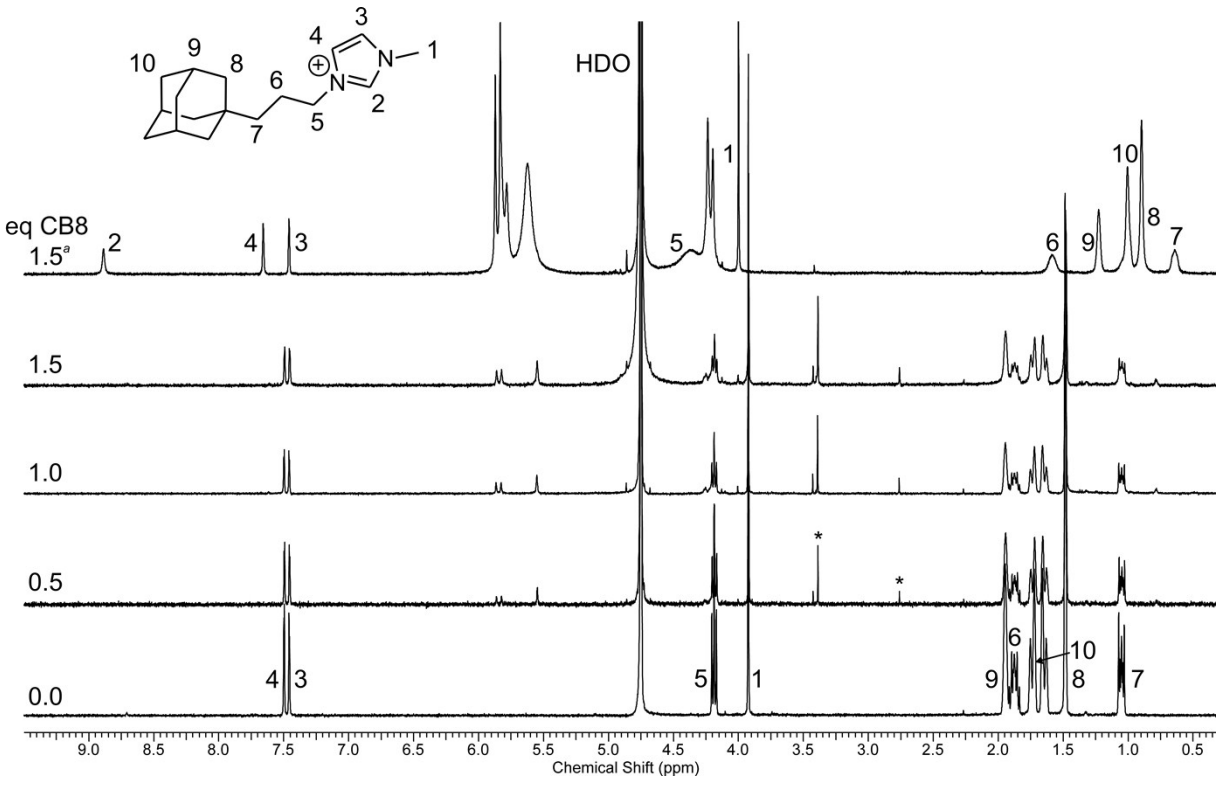

Figure S42: Stacking plot of ^{1}H NMR spectra (400 MHz) of mixtures of **9c** with CB8 in 50 mM NaCl in D_2O at 30 °C. Initial concentration of **9c** was 1.94 mM, concentration of the CB8 stock solution was 2.25 mM. *impurity from commercial CB8

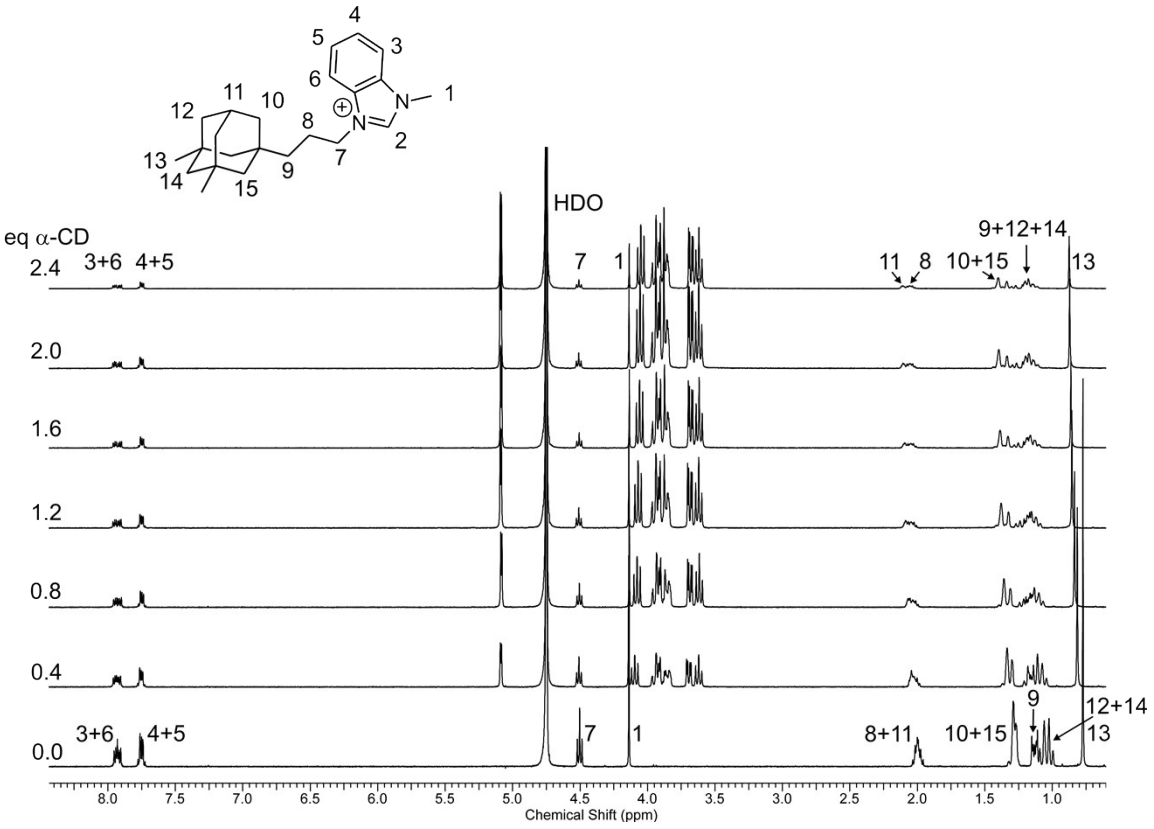

Figure S43: Stacking plot of ^{1}H NMR spectra (400 MHz) of mixtures of **10d** with α-CD in D_2O at 30 °C. Initial concentration of **10d** was 1.84 mM, concentration of the α-CD stock solution was 4.41 mM.

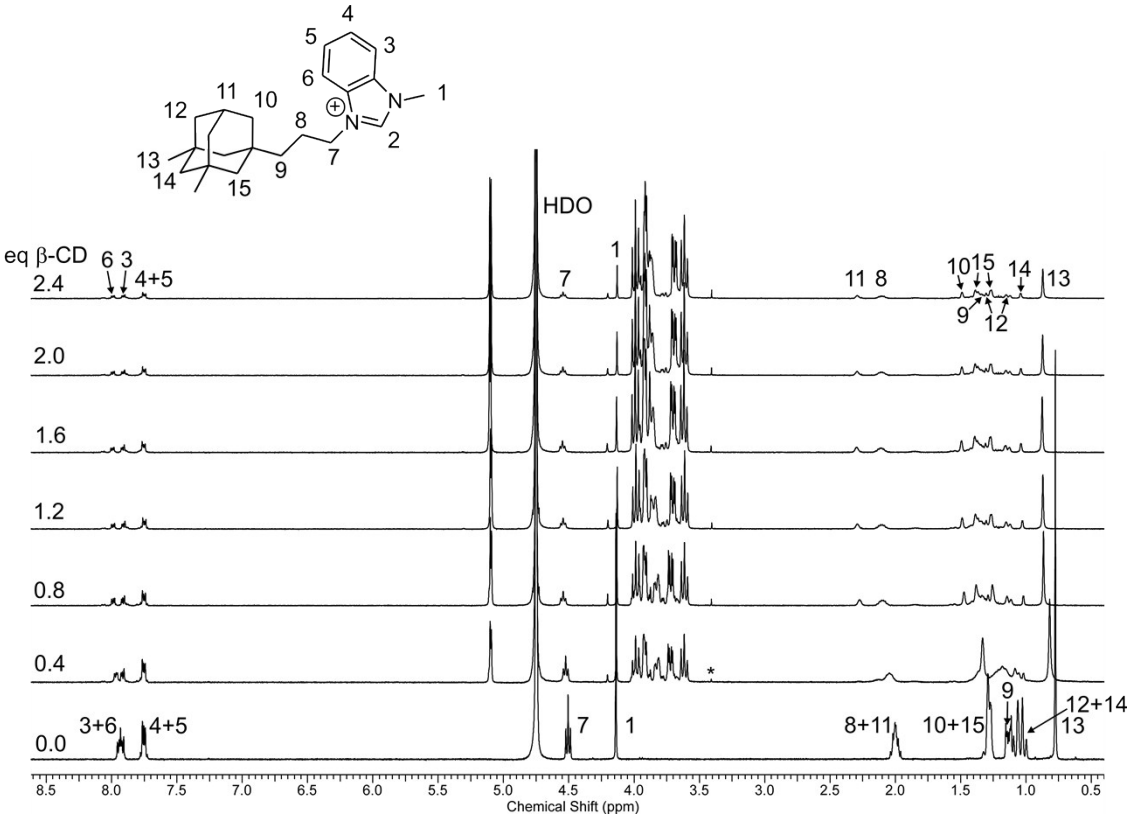

Figure S44: Stacking plot of ^{1}H NMR spectra (400 MHz) of mixtures of **10d** with β-CD in D_2O at 30 °C. Initial concentration of **10d** was 1.84 mM, concentration of the β-CD stock solution was 4.44 mM. *impurity from commercial β-CD

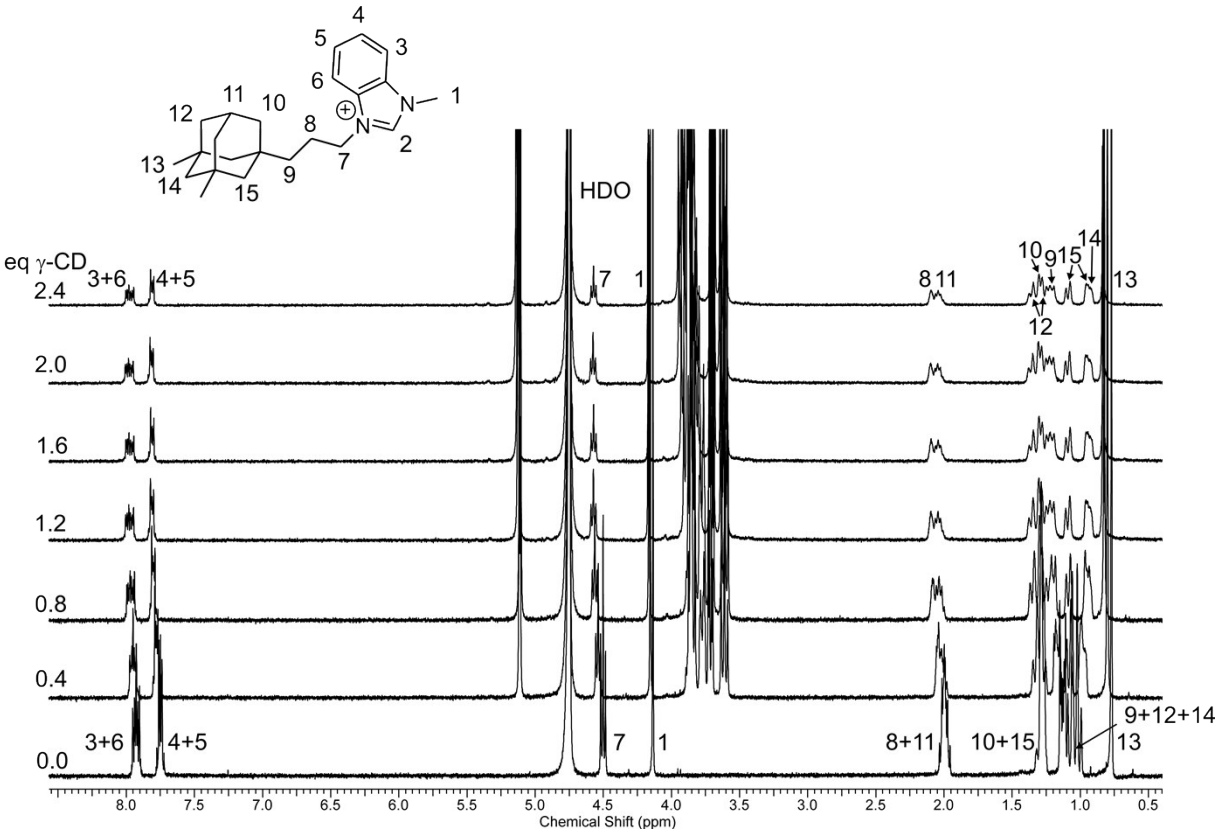

Figure S45: Stacking plot of ^{1}H NMR spectra (400 MHz) of mixtures of **10d** with γ-CD in D_2O at 30 °C. Initial concentration of **10d** was 1.84 mM, concentration of the γ-CD stock solution was 4.40 mM.

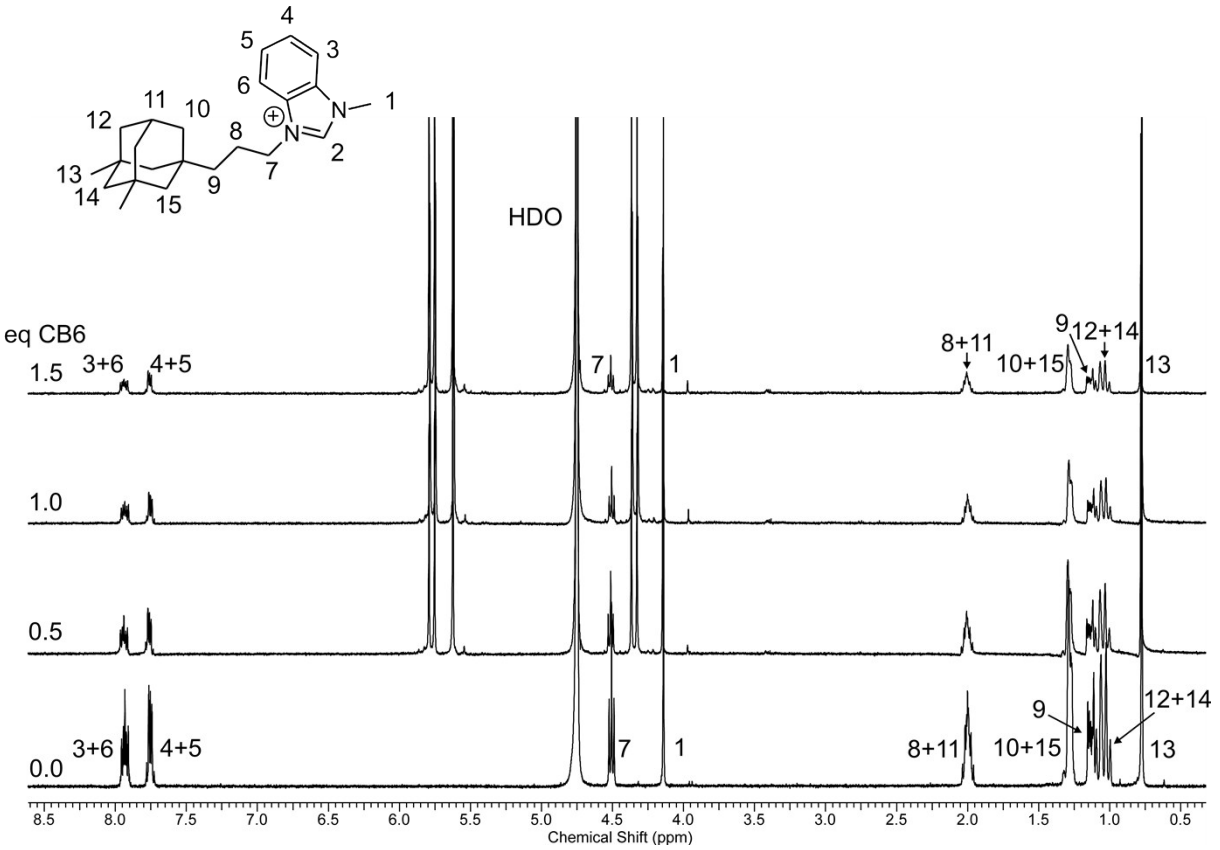

Figure S46: Stacking plot of ^{1}H NMR spectra (400 MHz) of mixtures of **10d** with CB6 in 50 mM NaCl in D_2O at 30 °C. Initial concentration of **10d** was 1.94 mM, concentration of the CB6 stock solution was 2.03 mM.

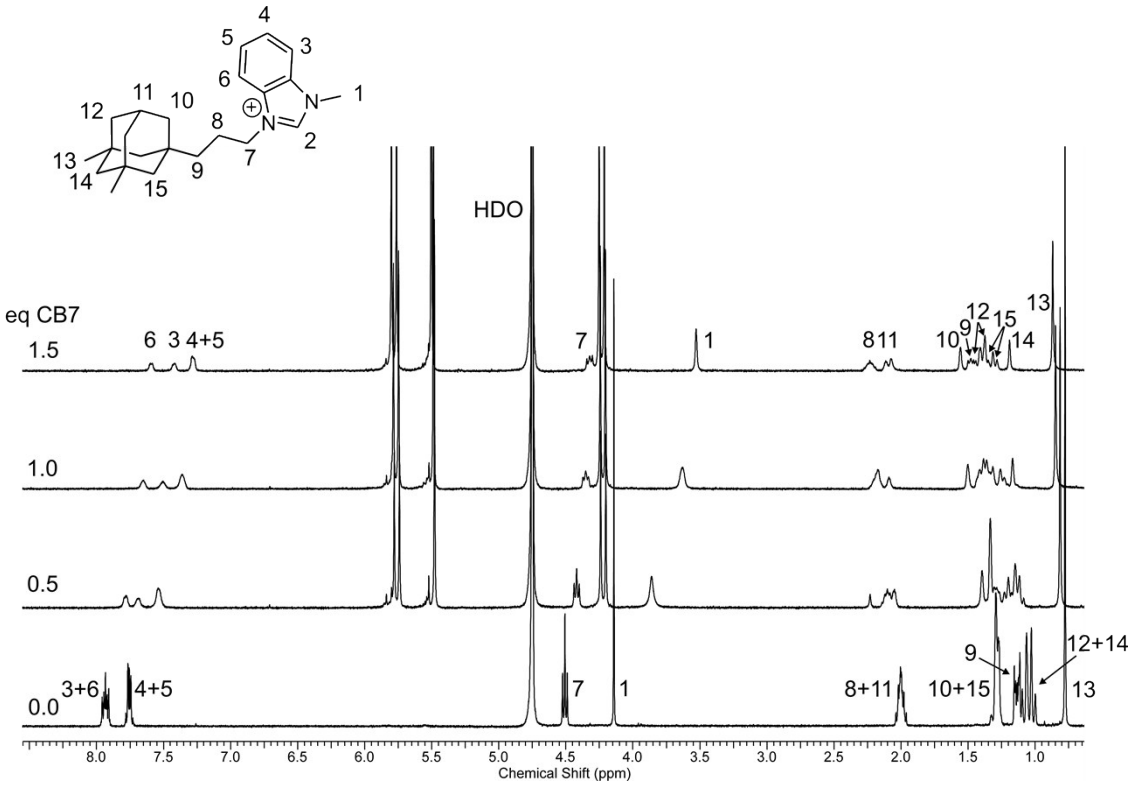

Figure S47: Stacking plot of ^{1}H NMR spectra (400 MHz) of mixtures of **10d** with CB7 in D_2O at 30 °C. Initial concentration of **10d** was 1.84 mM, concentration of the CB7 stock solution was 2.07 mM. *impurity from commercial CB7

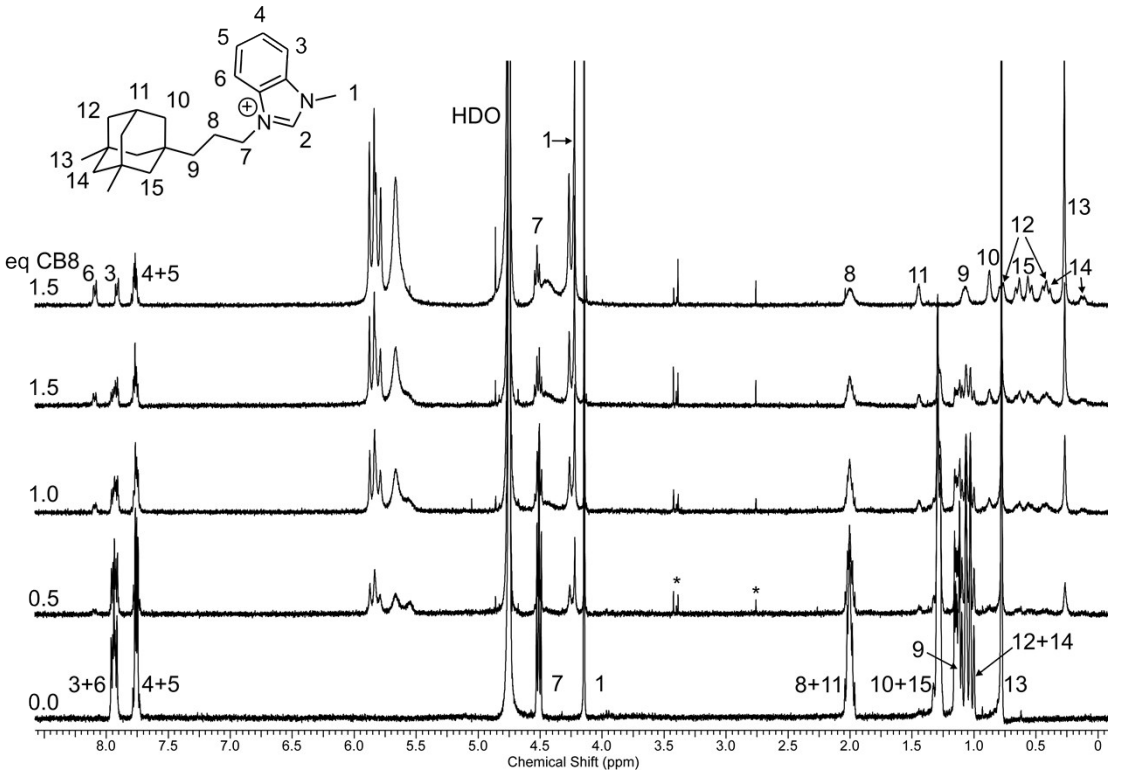

Figure S48: Stacking plot of ^{1}H NMR spectra (400 MHz) of mixtures of **10d** with CB8 in D_2O at 30 °C. Initial concentration of **10d** was 1.94 mM, concentration of the CB8 stock solution was 1.99 mM. *impurity from commercial CB8

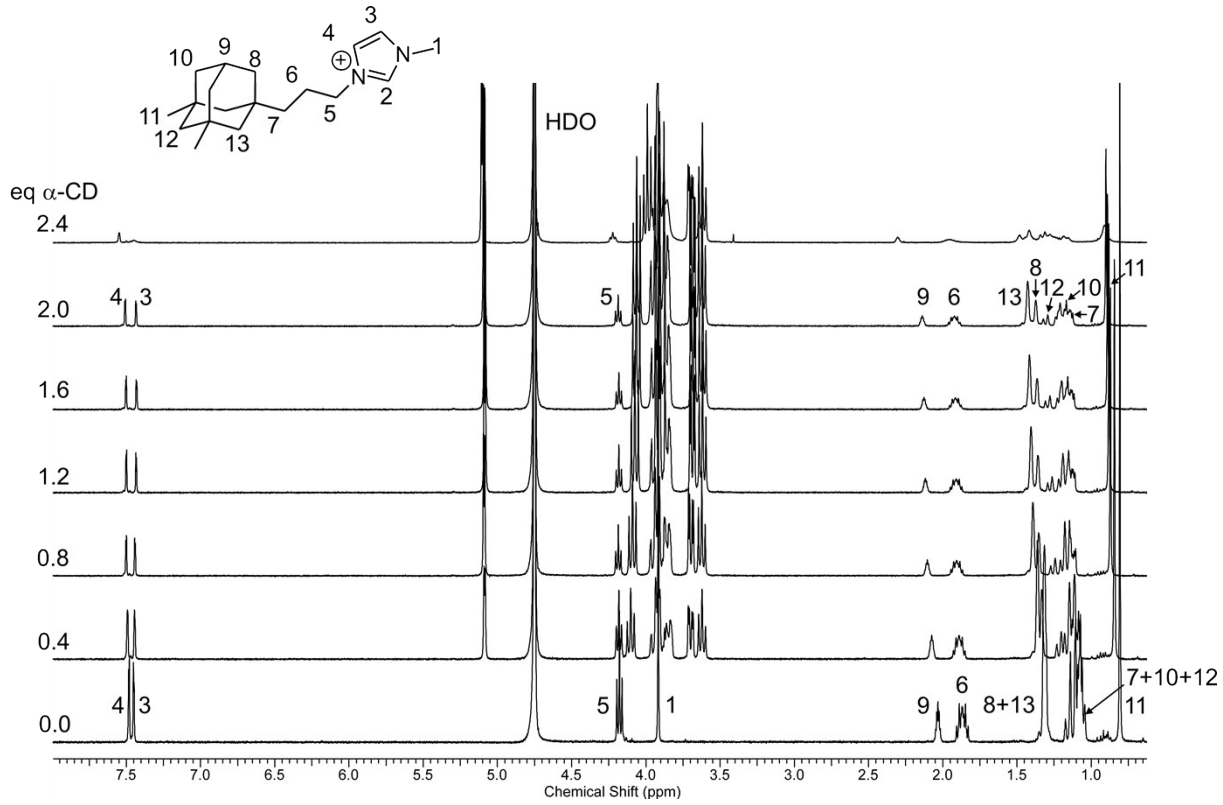

Figure S49: Stacking plot of ^{1}H NMR spectra (400 MHz) of mixtures of **9d** with α-CD in D_2O at 30 °C. Initial concentration of **9d** was 1.92 mM, concentration of the α-CD stock solution was 4.44 mM.

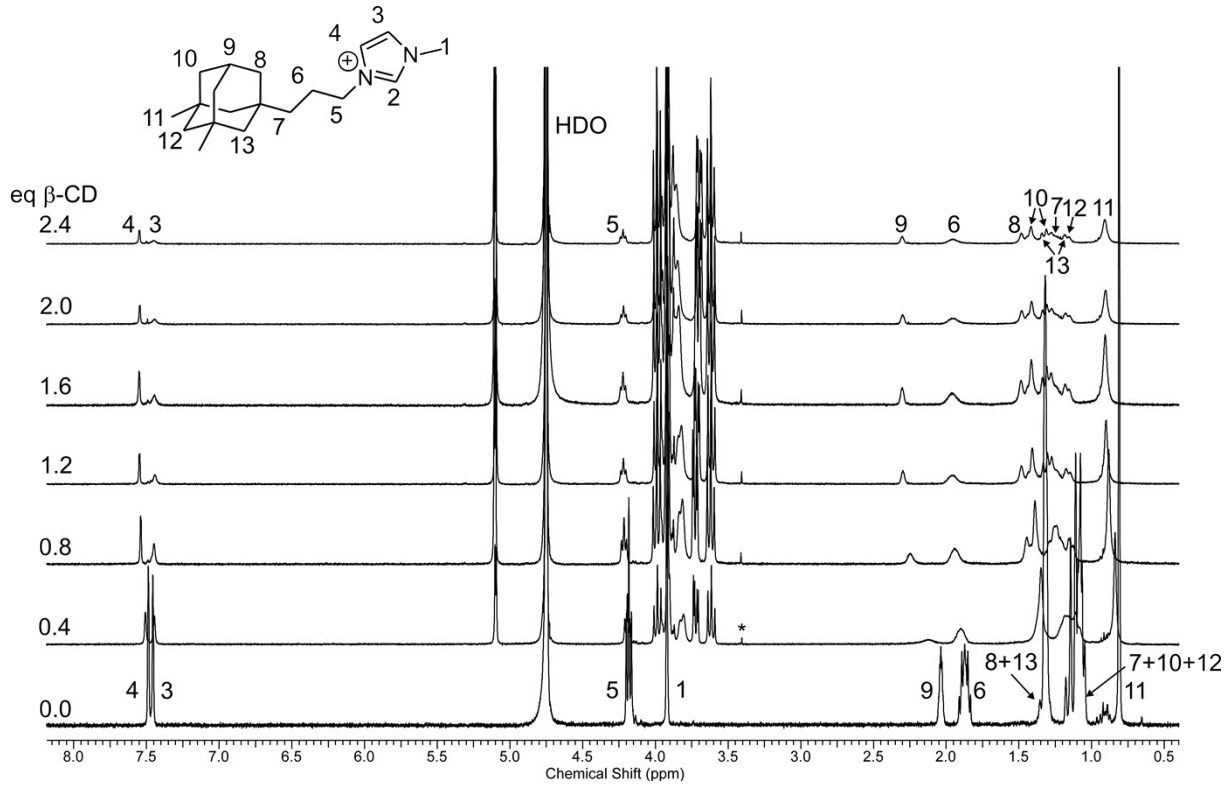

Figure S50: Stacking plot of ^{1}H NMR spectra (400 MHz) of mixtures of **9d** with β-CD in D_2O at 30 °C. Initial concentration of **9d** was 1.92 mM, concentration of the β-CD stock solution was 4.45 mM. * impurity from commercial β-CD

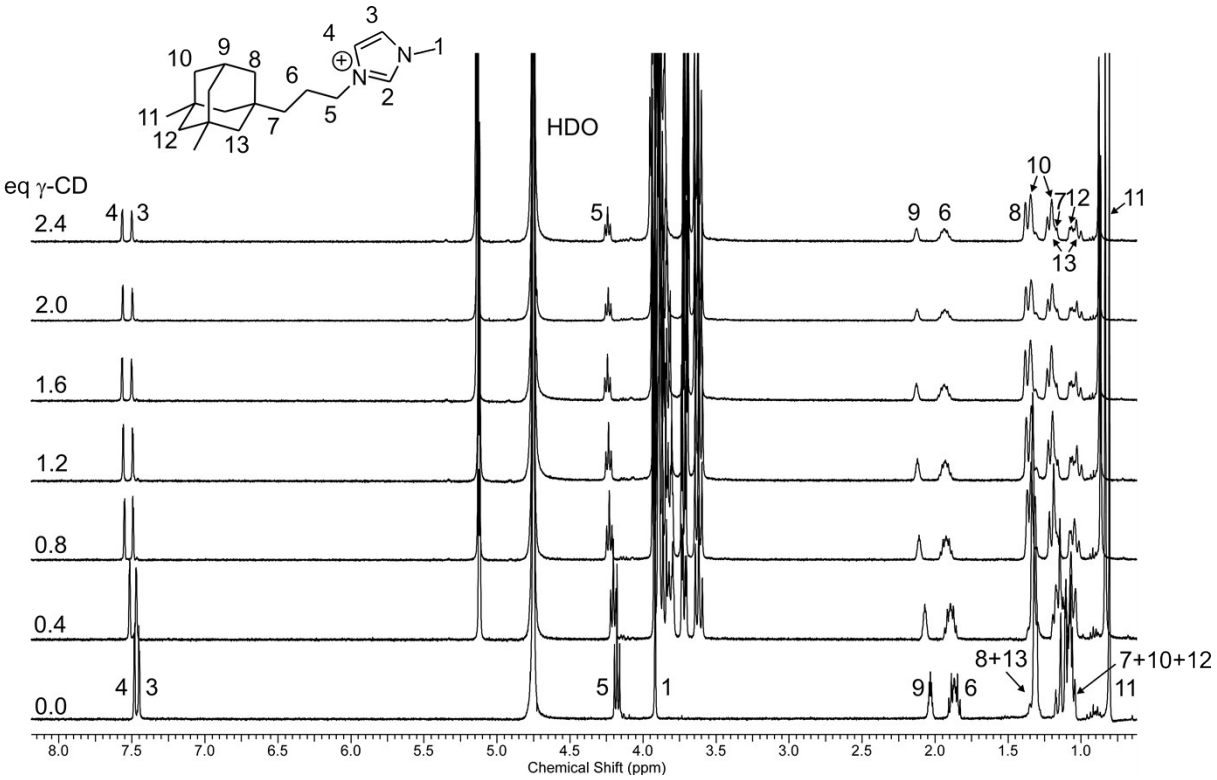

Figure S51: Stacking plot of ^{1}H NMR spectra (400 MHz) of mixtures of **9d** with γ-CD in D_2O at 30 °C. Initial concentration of **9d** was 1.92 mM, concentration of the γ-CD stock solution was 4.34 mM.

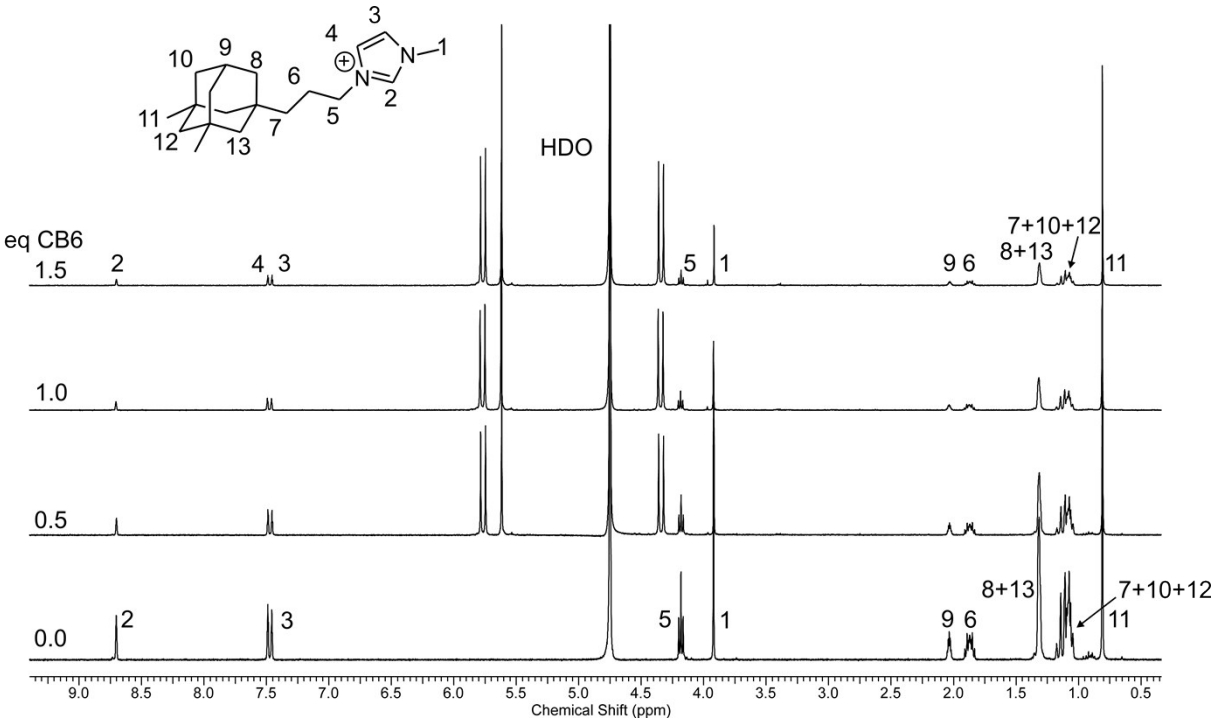

Figure S52: Stacking plot of ^{1}H NMR spectra (400 MHz) of mixtures of **9d** with CB6 in 50 mM NaCl in D_2O at 30 °C. Initial concentration of **9d** was 1.85 mM, concentration of the CB6 stock solution was 2.25 mM.

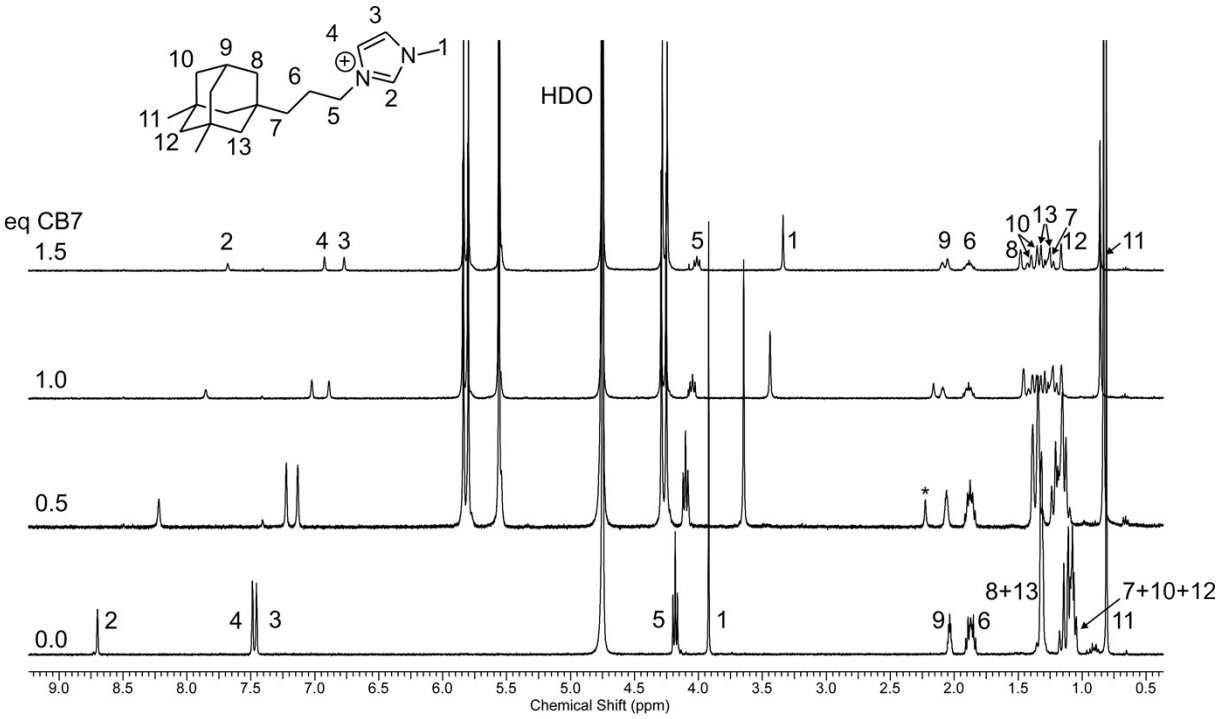

Figure S53: Stacking plot of ^{1}H NMR spectra (400 MHz) of mixtures of **9d** with CB7 in D_2O at 30 °C. Initial concentration of **9d** was 1.92 mM, concentration of the CB7 stock solution was 2.15 mM.

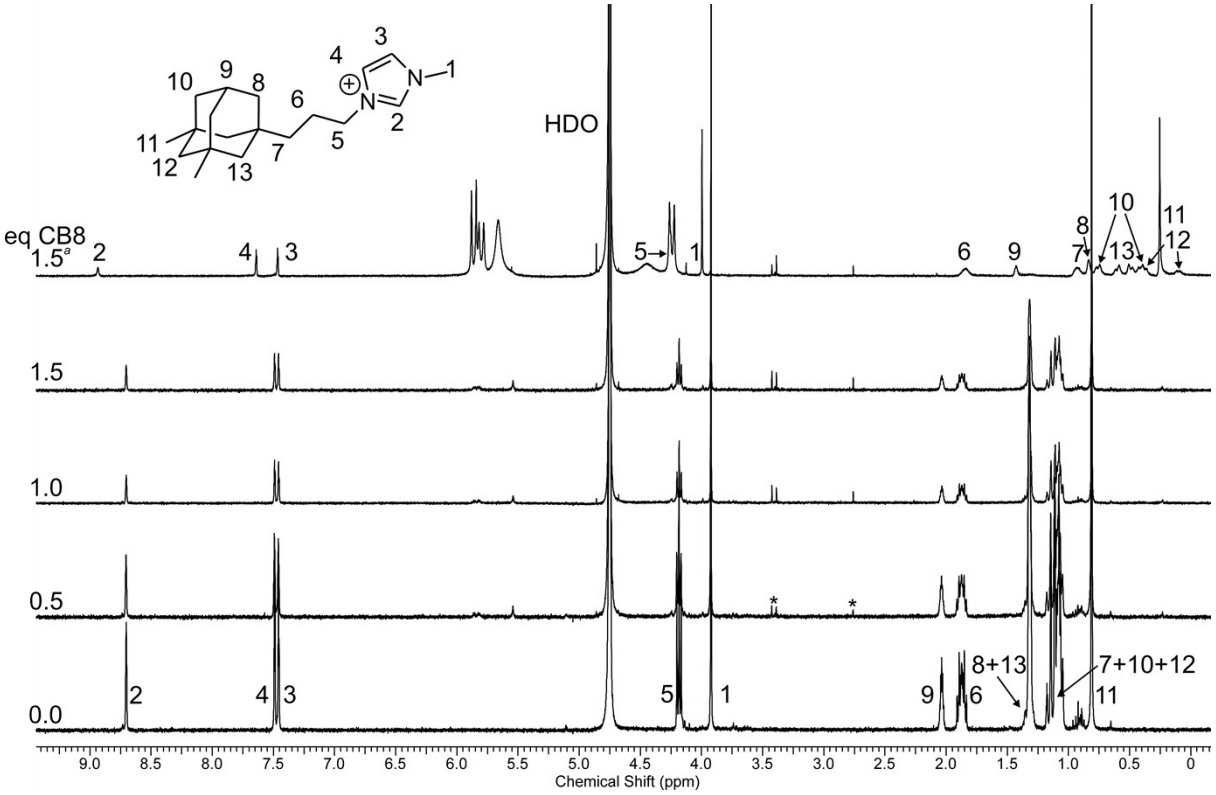

Figure S54: Stacking plot of ^{1}H NMR spectra (400 MHz) of mixtures of **9d** with CB8 in D_2O at 30 °C. Initial concentration of **9d** was 1.85 mM, concentration of the CB8 stock solution was 2.25 mM. *impurity from commercial CB8

ESI-MS of guests and host-guest complexes

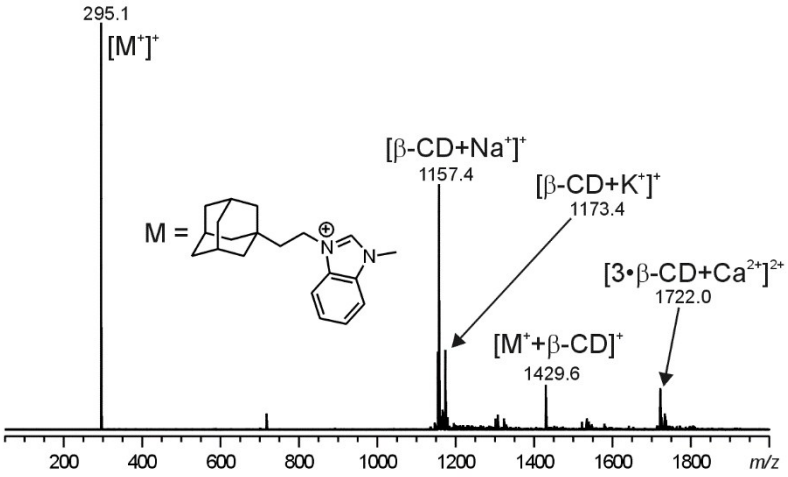

Figure S55: The positive-ion first-order ESI-MS of an aqueous solution of compound **10b**·β-CD. The assignments for observed signals are shown in the brackets.

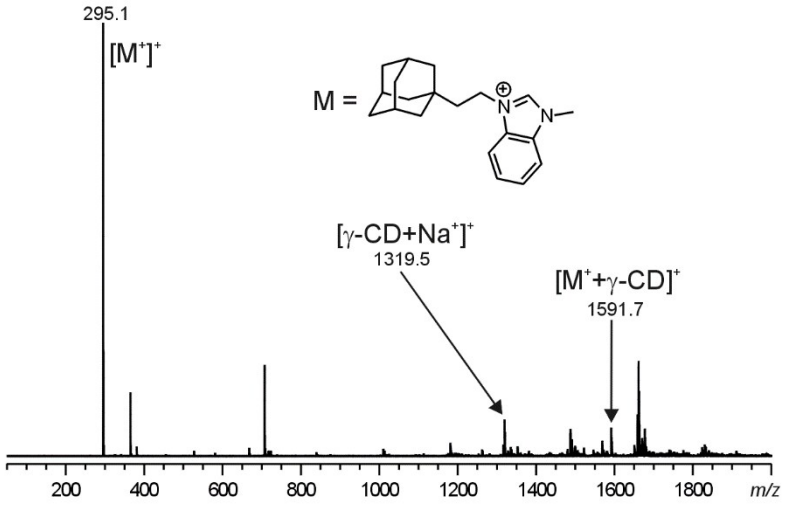

Figure S56: The positive-ion first-order ESI-MS of an aqueous solution of compound **10b**·γ-CD. The assignments for observed signals are shown in the brackets.

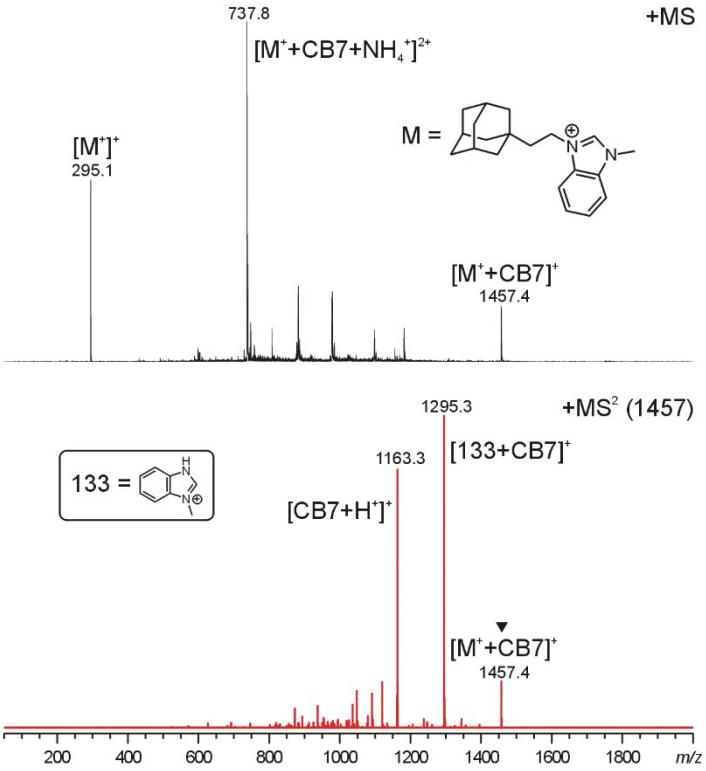

Figure S57: The positive-ion first-order ESI-MS (black) and tandem mass spectra MS^2 (red) of an aqueous solution of compound **10b**·CB7. The assignments for observed signals are shown in the brackets. The fragmented ions in tandem mass spectra are marked with downward-facing triangles.

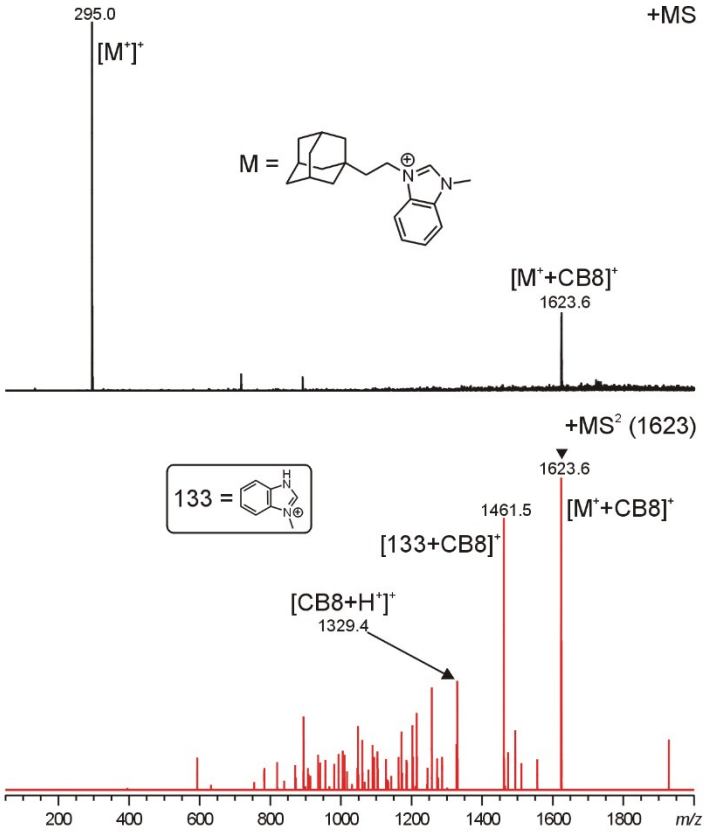

Figure S58: The positive-ion first-order ESI-MS (black) and tandem mass spectra MS^2 (red) of an aqueous solution of compound **10b**·CB8. The assignments for observed signals are shown in the brackets. The fragmented ions in tandem mass spectra are marked with downward-facing triangles.

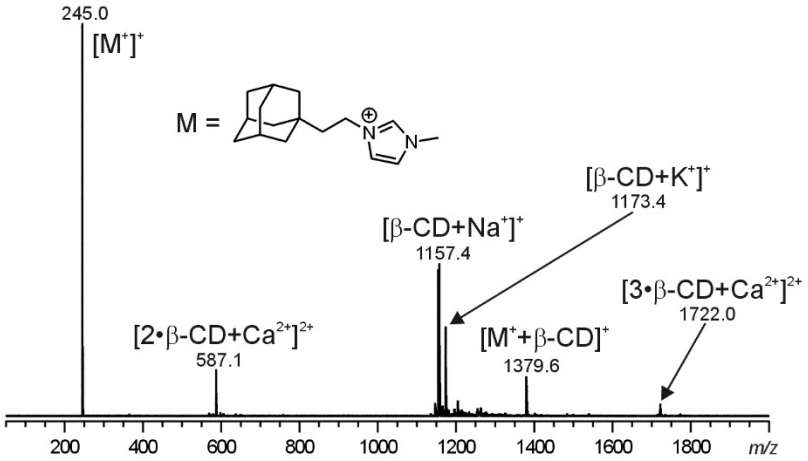

Figure S59: The positive-ion first-order ESI-MS of an aqueous solution of compound **9b**·β-CD. The assignments for observed signals are shown in the brackets.

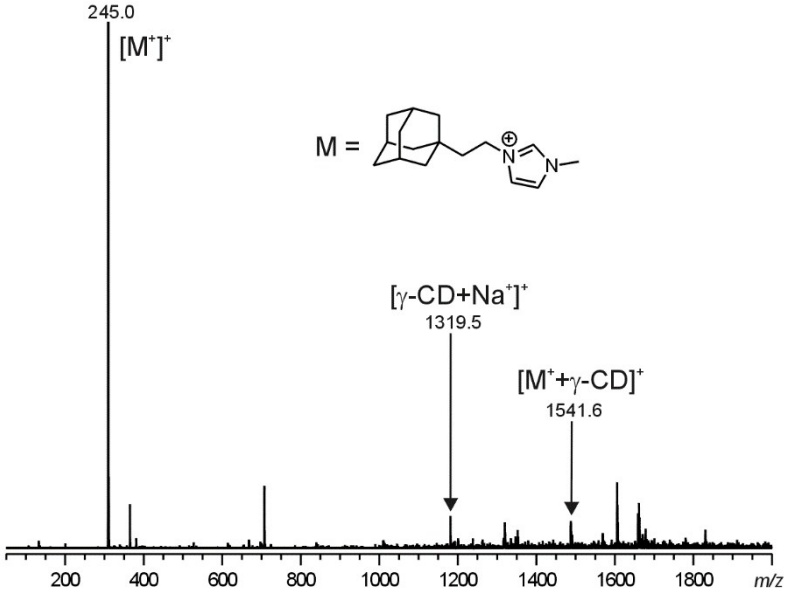

Figure S60: The positive-ion first-order ESI-MS of an aqueous solution of compound **9b**·γ-CD. The assignments for observed signals are shown in the brackets.

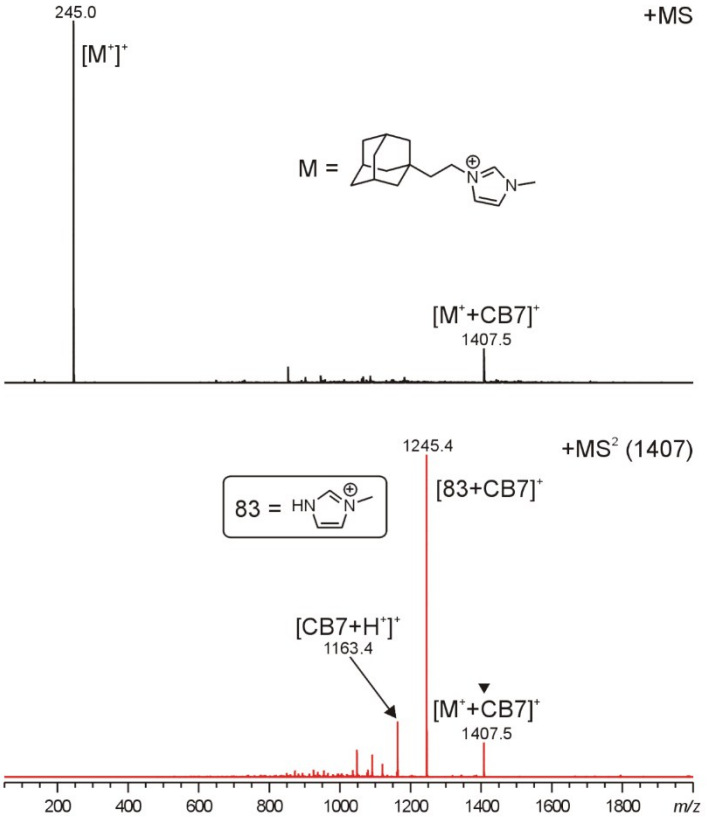

Figure S61: The positive-ion first-order ESI-MS (black) and tandem mass spectra MS^2 (red) of an aqueous solution of compound **9b**·CB7. The assignments for observed signals are shown in the brackets. The fragmented ions in tandem mass spectra are marked with downward-facing triangles.

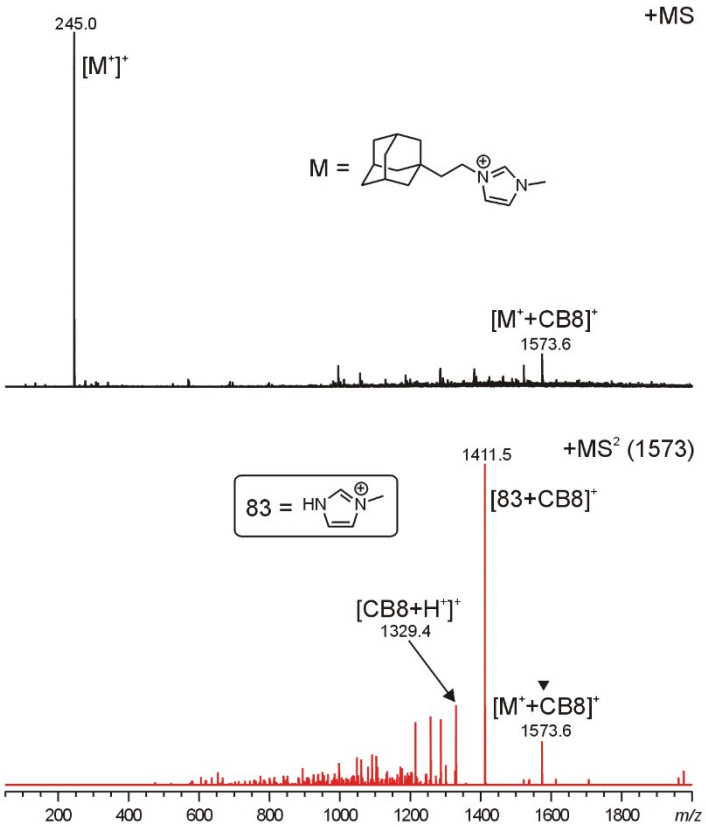

Figure S62: The positive-ion first-order ESI-MS (black) and tandem mass spectra MS^2 (red) of an aqueous solution of compound **9b**·CB8. The assignments for observed signals are shown in the brackets. The fragmented ions in tandem mass spectra are marked with downward-facing triangles.

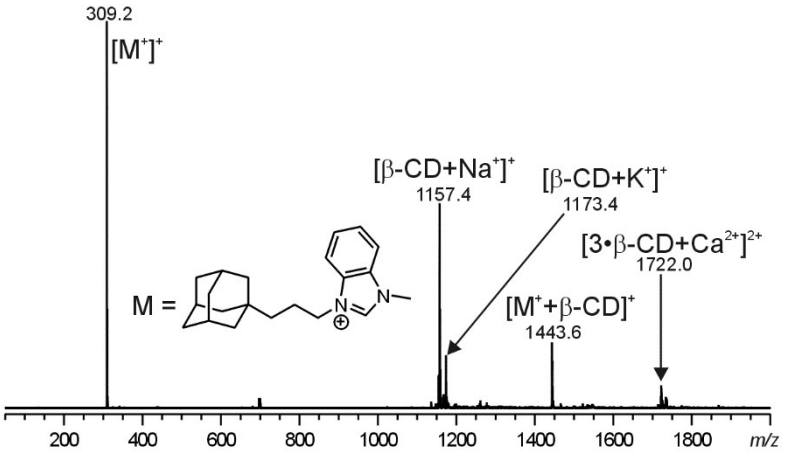

Figure S63: The positive-ion first-order ESI-MS of an aqueous solution of compound **10c**·β-CD. The assignments for observed signals are shown in the brackets.

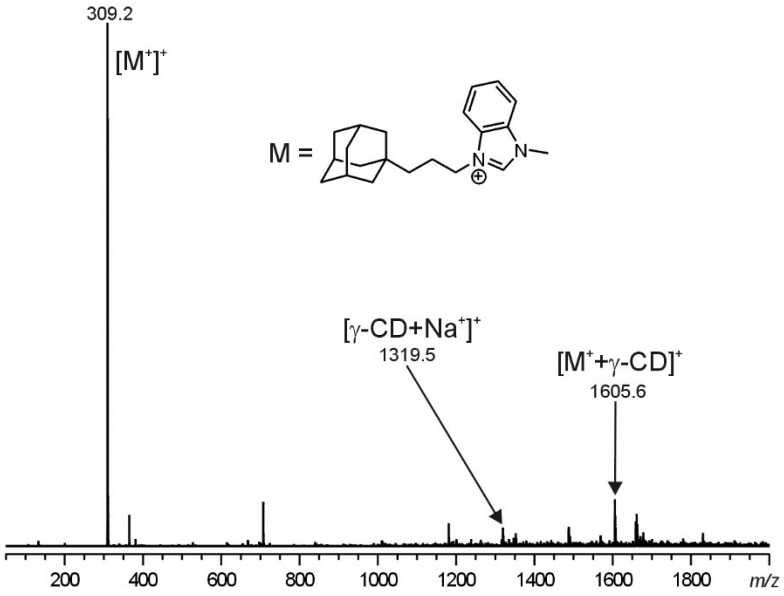

Figure S64: The positive-ion first-order ESI-MS of an aqueous solution of compound **10c**·γ-CD. The assignments for observed signals are shown in the brackets.

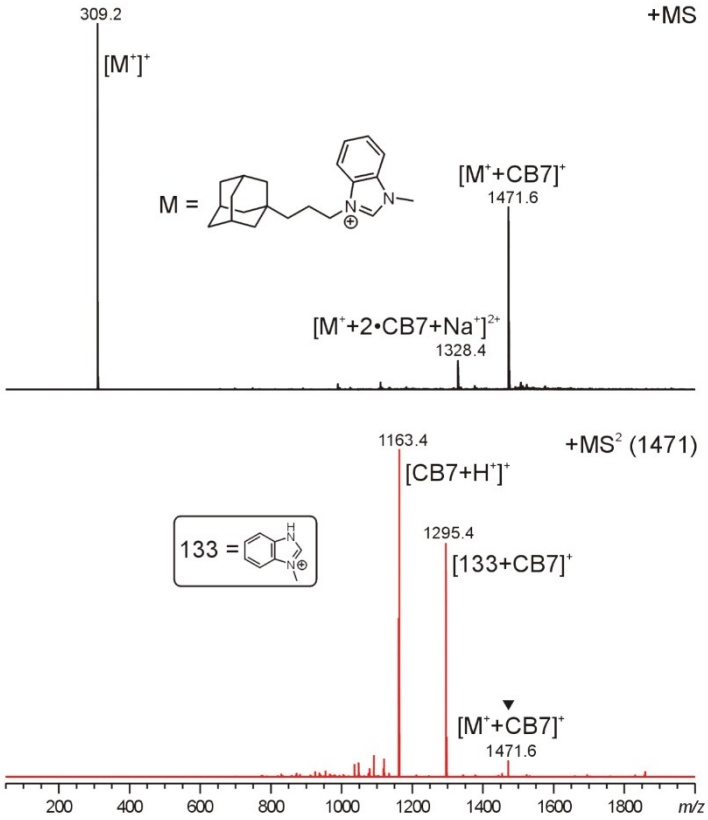

Figure S65: The positive-ion first-order ESI-MS (black) and tandem mass spectra MS^2 (red) of an aqueous solution of compound **10c**·CB7. The assignments for observed signals are shown in the brackets. The fragmented ions in tandem mass spectra are marked with downward-facing triangles.

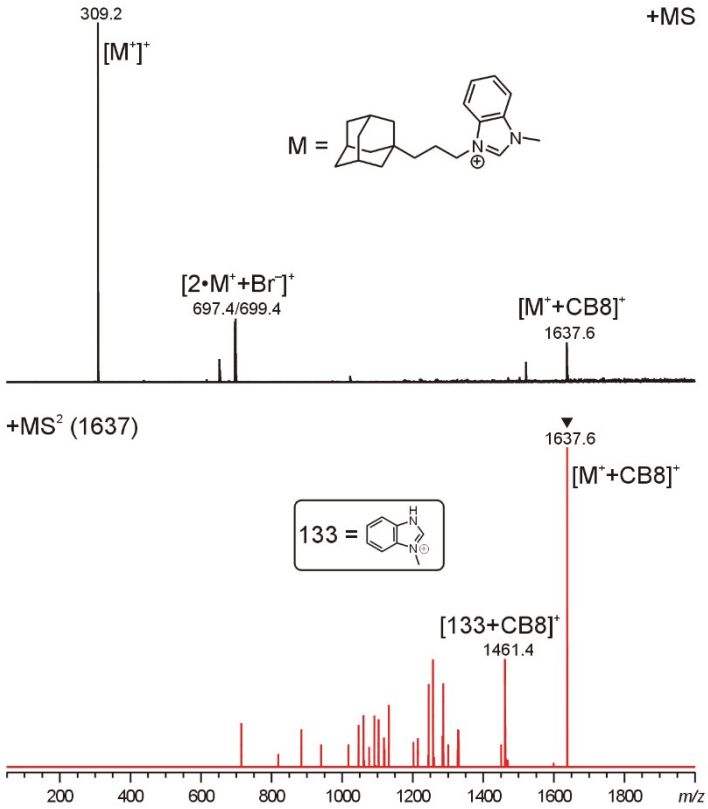

Figure S66: The positive-ion first-order ESI-MS (black) and tandem mass spectra MS^2 (red) of an aqueous solution of compound **10c**·CB8. The assignments for observed signals are shown in the brackets. The fragmented ions in tandem mass spectra are marked with downward-facing triangles.

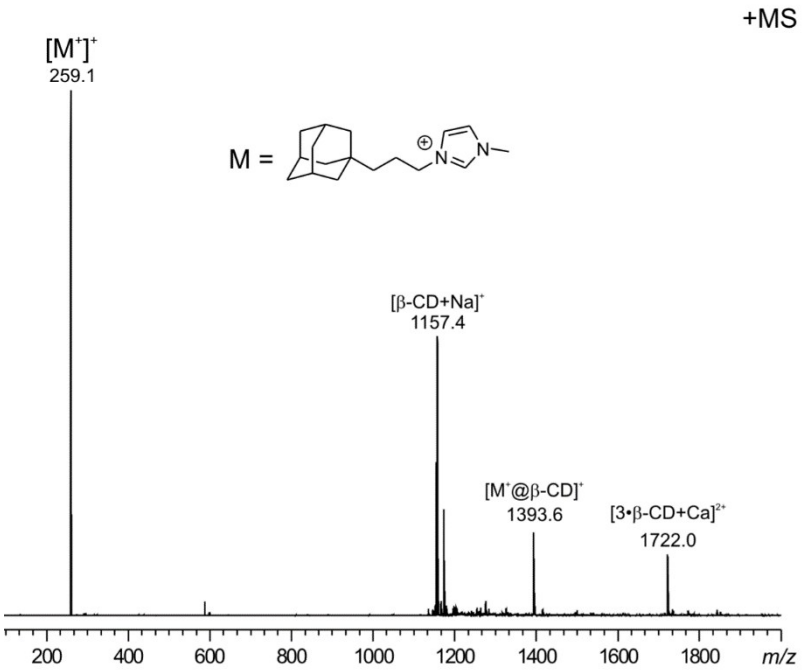

Figure S67: The positive-ion first-order ESI-MS of an aqueous solution of compound **9c**·β-CD. The assignments for observed signals are shown in the brackets.

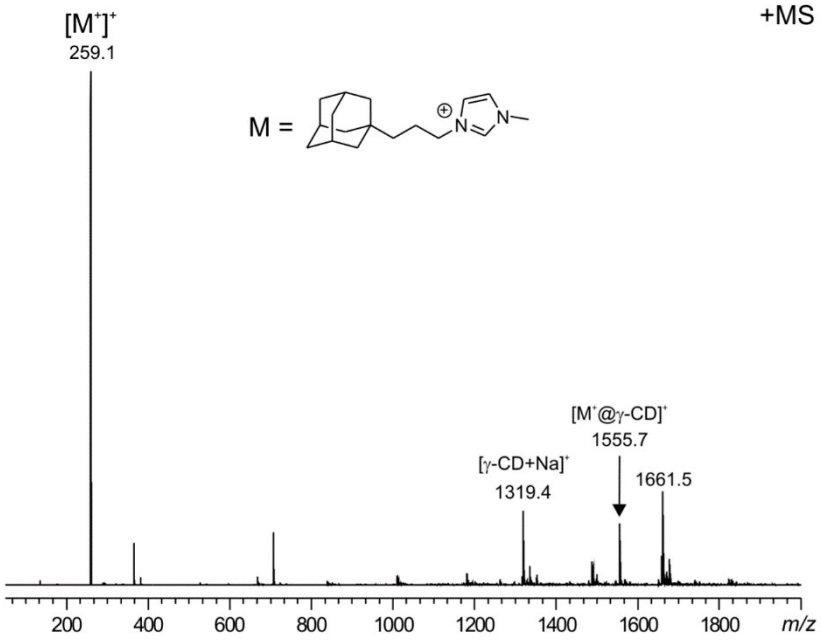

Figure S68: The positive-ion first-order ESI-MS of an aqueous solution of compound **9c**·γ-CD. The assignments for observed signals are shown in the brackets.

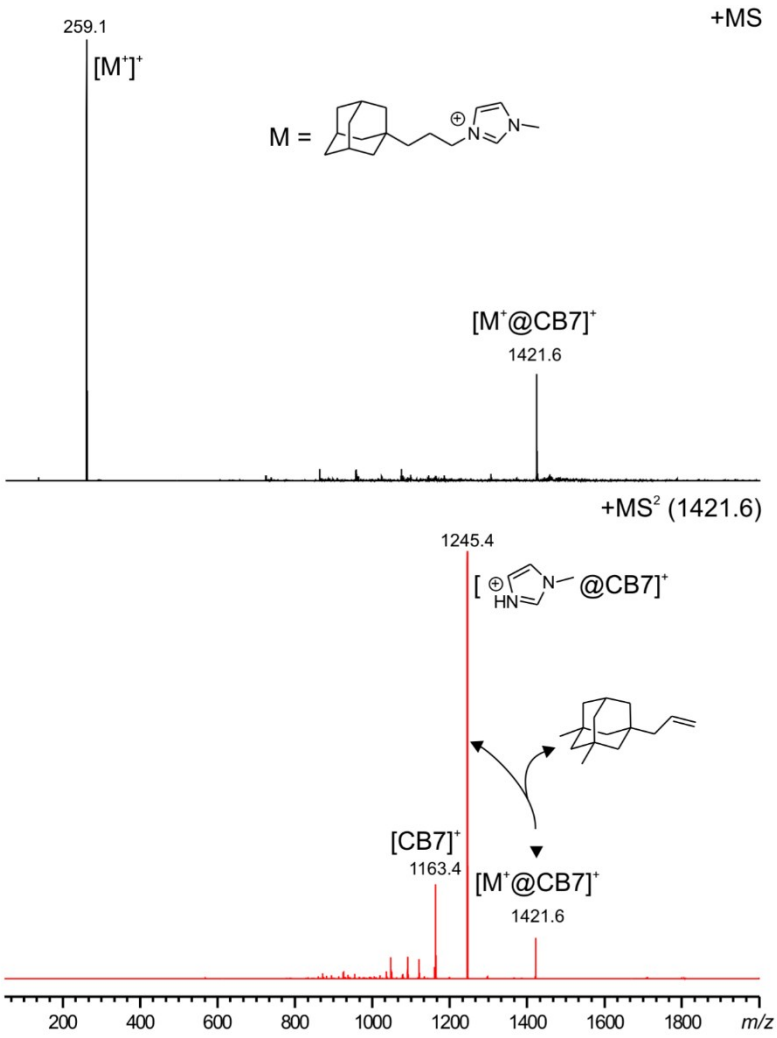

Figure S69: The positive-ion first-order ESI-MS (black) and tandem mass spectra MS^2 (red) of an aqueous solution of compound **9c**·CB7. The assignments for observed signals are shown in the brackets. The fragmented ions in tandem mass spectra are marked with downward-facing triangles.

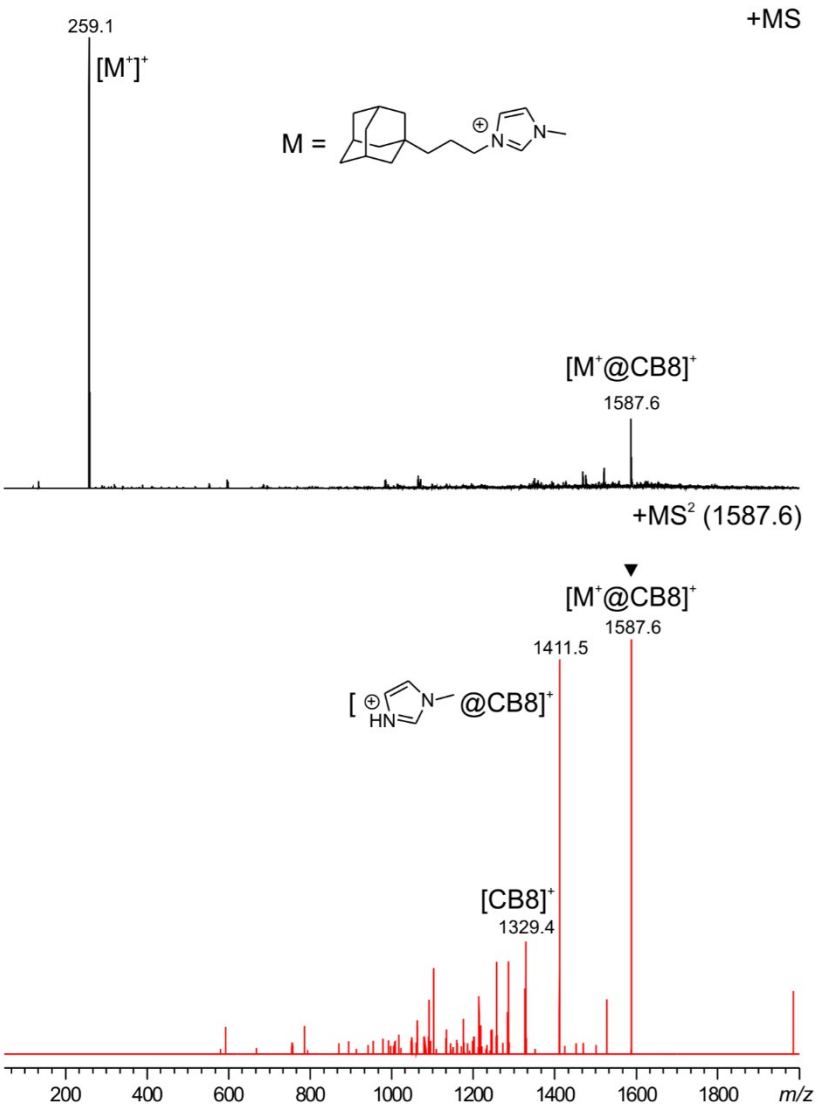

Figure S70: The positive-ion first-order ESI-MS (black) and tandem mass spectra MS^2 (red) of an aqueous solution of compound **9c**·CB8. The assignments for observed signals are shown in the brackets. The fragmented ions in tandem mass spectra are marked with downward-facing triangles.

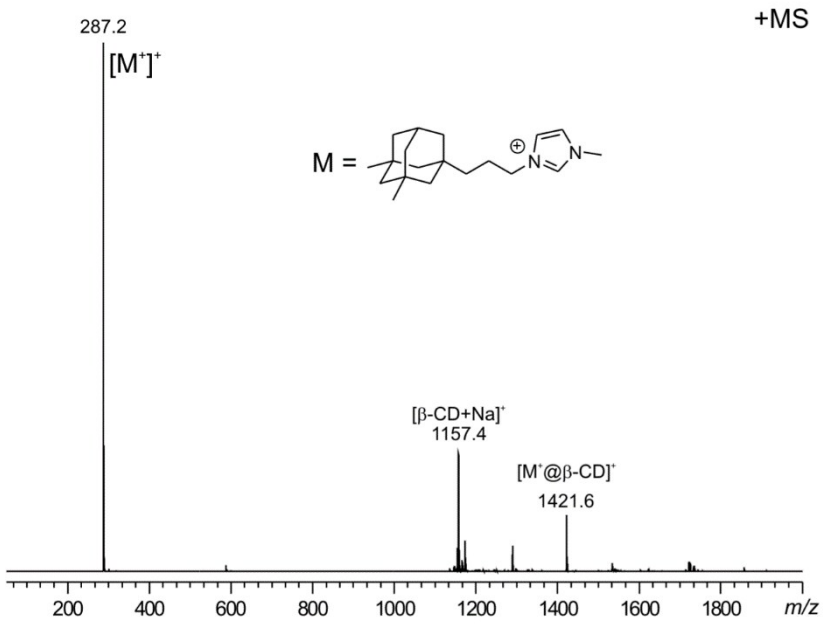

Figure S71: The positive-ion first-order ESI-MS of an aqueous solution of compound **9d**·β-CD. The assignments for observed signals are shown in the brackets.

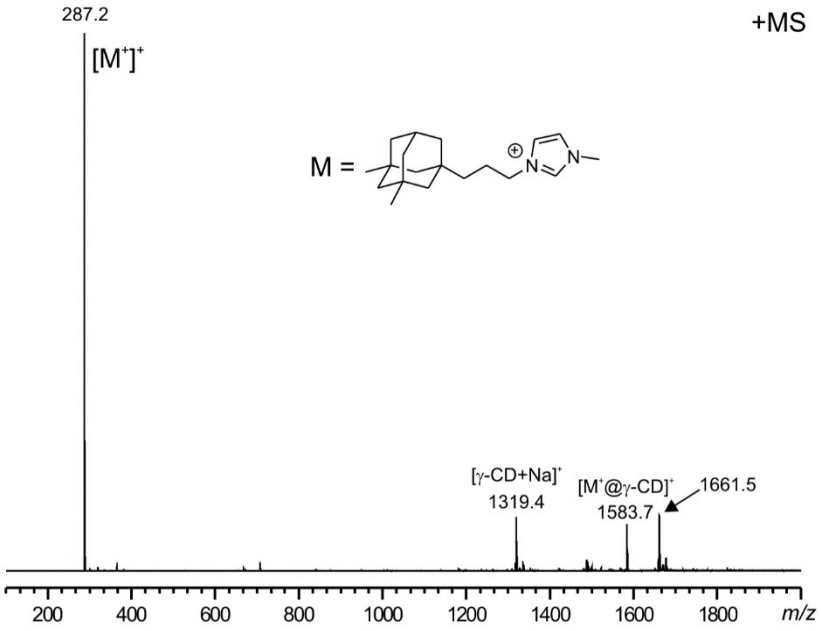

Figure S72: The positive-ion first-order ESI-MS of an aqueous solution of compound **9d**·γ-CD. The assignments for observed signals are shown in the brackets.

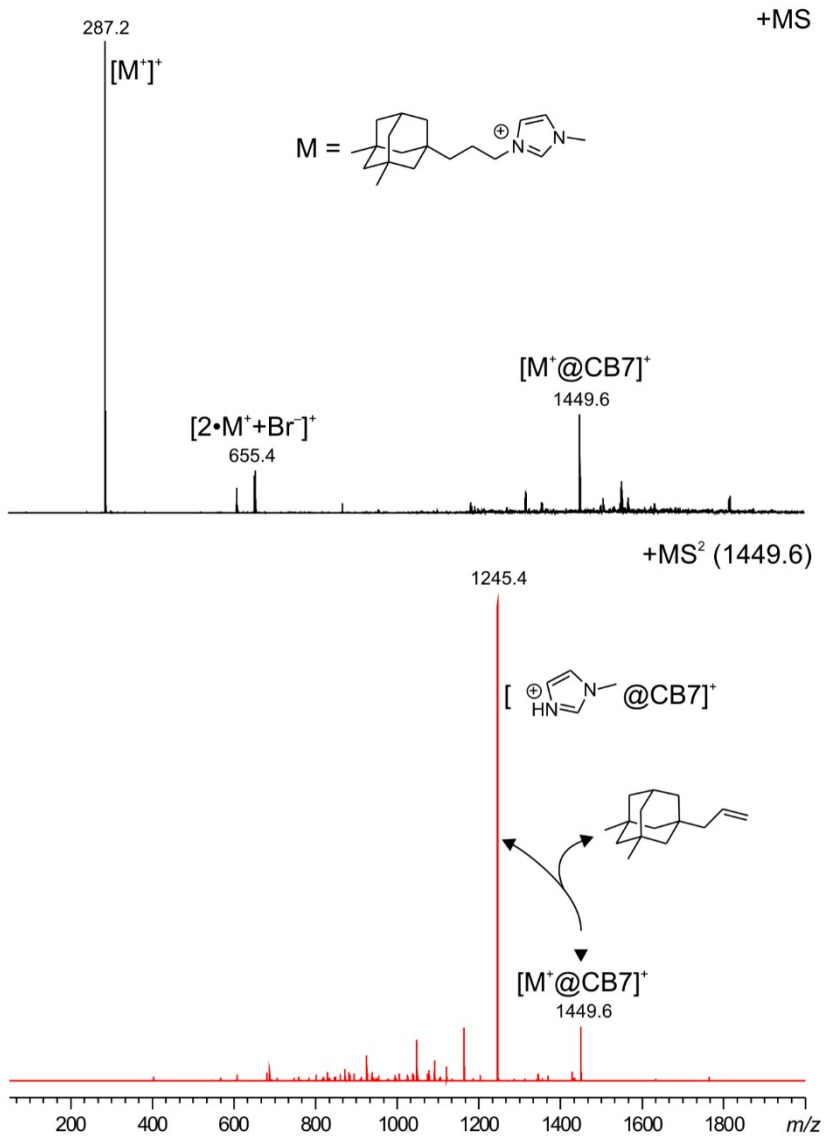

Figure S73: The positive-ion first-order ESI-MS (black) and tandem mass spectra MS^2 (red) of an aqueous solution of compound **9d**·CB7. The assignments for observed signals are shown in the brackets. The fragmented ions in tandem mass spectra are marked with downward-facing triangles.

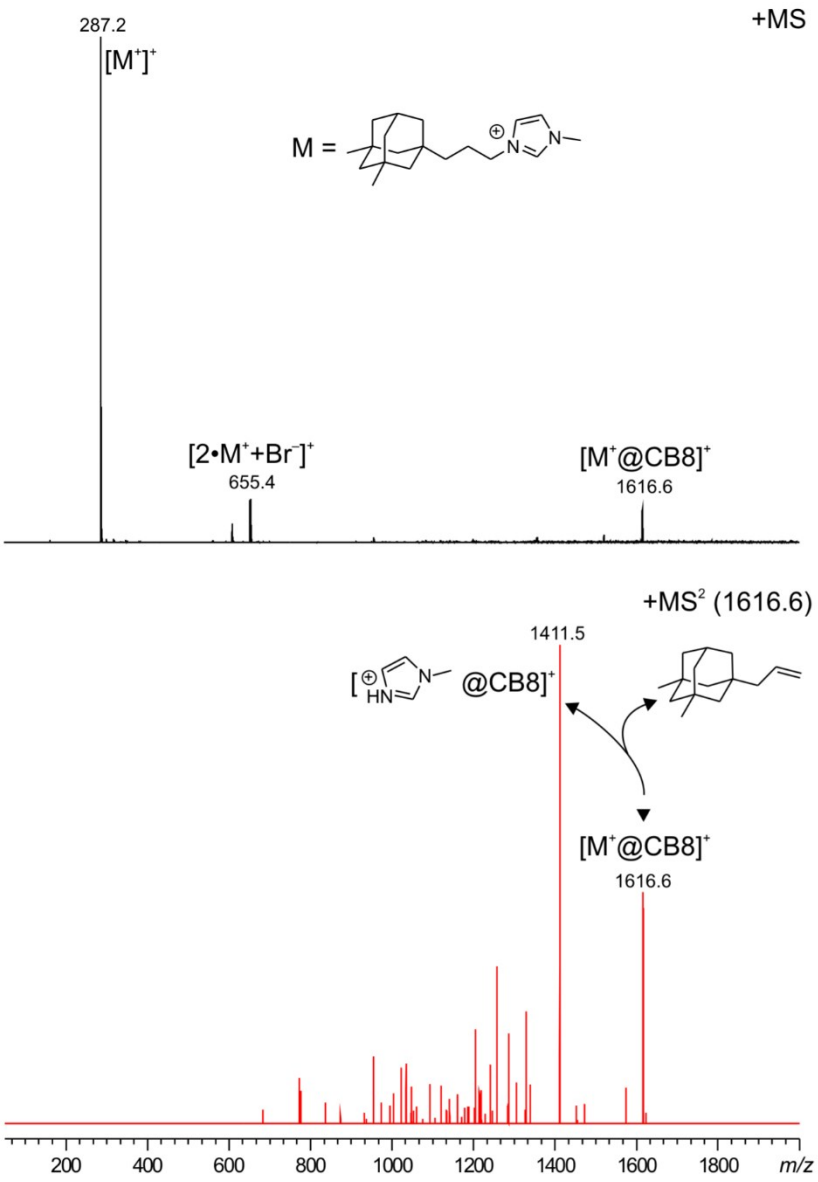

Figure S74: The positive-ion first-order ESI-MS (black) and tandem mass spectra MS^2 (red) of an aqueous solution of compound **9d**·CB8. The assignments for observed signals are shown in the brackets. The fragmented ions in tandem mass spectra are marked with downward-facing triangles.

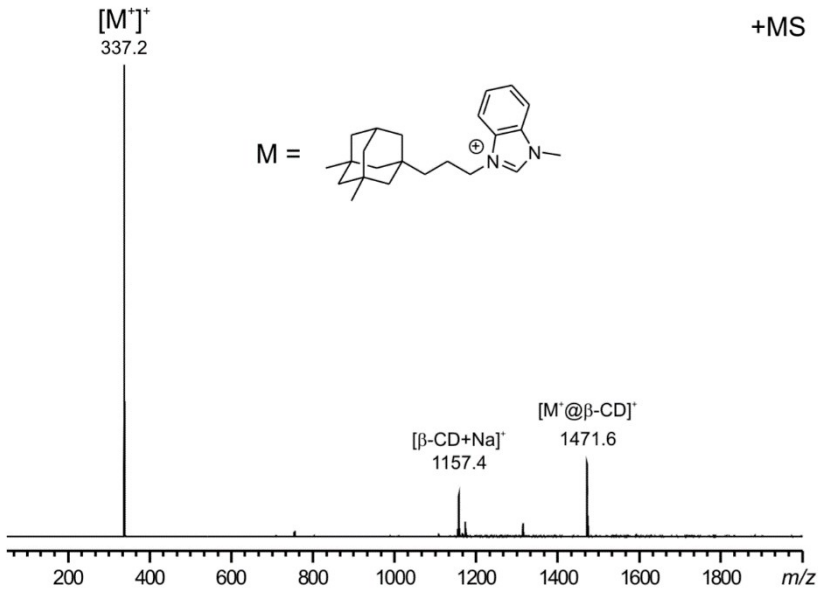

Figure S75: The positive-ion first-order ESI-MS of an aqueous solution of compound **10d**·β-CD. The assignments for observed signals are shown in the brackets.

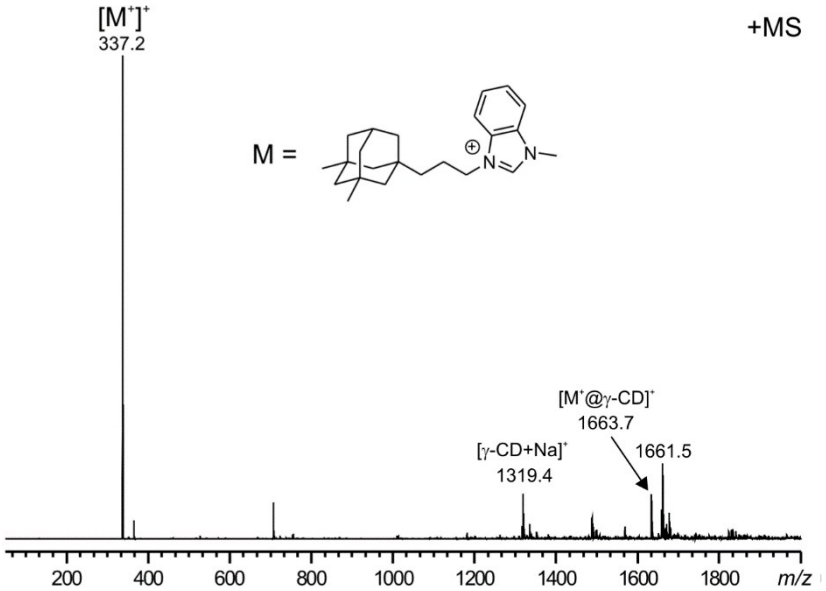

Figure S76: The positive-ion first-order ESI-MS of an aqueous solution of compound **10d**·γ-CD. The assignments for observed signals are shown in the brackets.

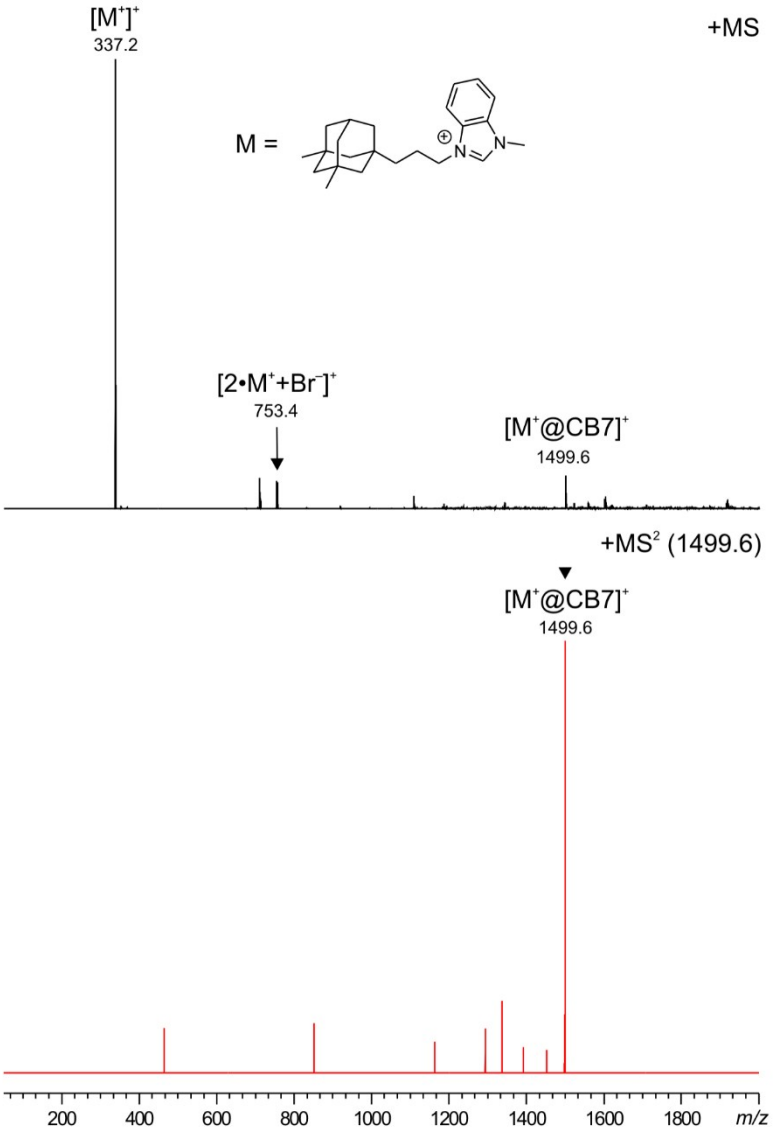

Figure S77: The positive-ion first-order ESI-MS (black) and tandem mass spectra MS^2 (red) of an aqueous solution of compound **10d**·CB7. The assignments for observed signals are shown in the brackets. The fragmented ions in tandem mass spectra are marked with downward-facing triangles.

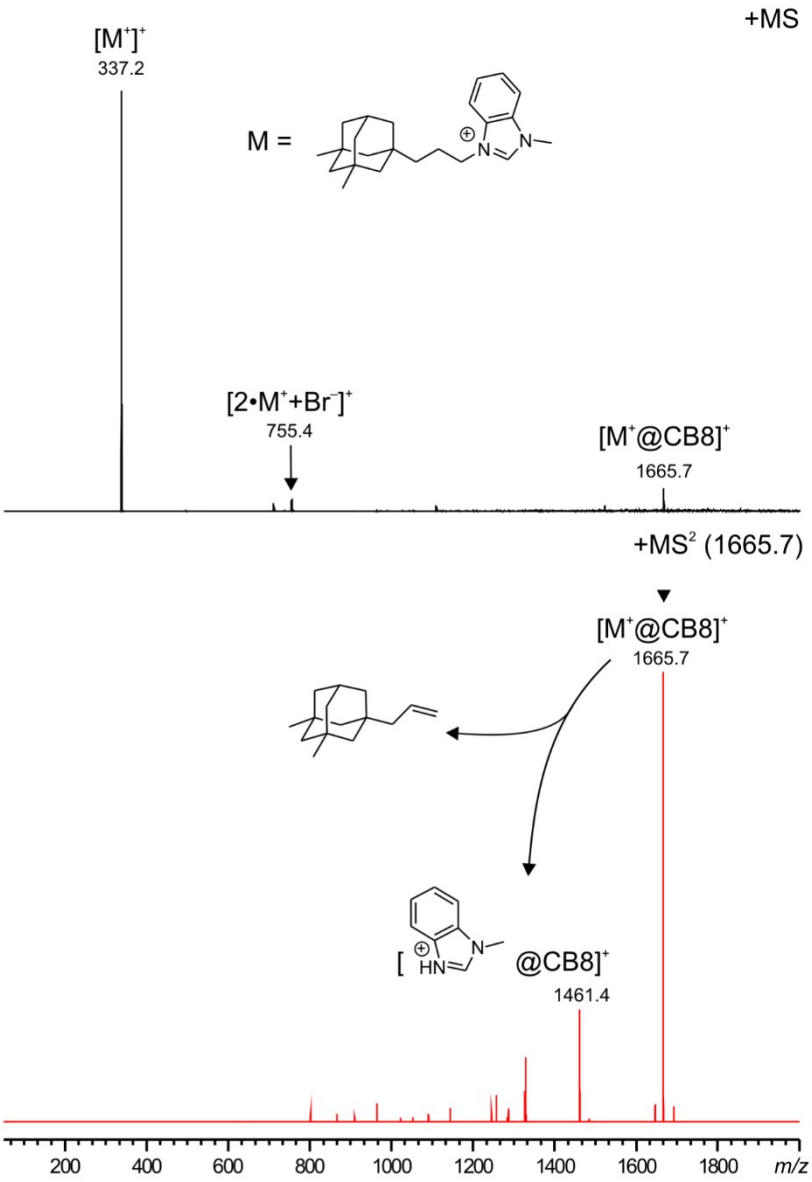

Figure S78: The positive-ion first-order ESI-MS (black) and tandem mass spectra MS^2 (red) of an aqueous solution of compound **10d**·CB8. The assignments for observed signals are shown in the brackets. The fragmented ions in tandem mass spectra are marked with downward-facing triangles.

Table S2: Calculated and experimental m/z values for examined complexes.

complex	m/z theor.	m/z exp.
9b@β-CD	1379.6	1379.6
9b@γ-CD	1541.6	1541.6
9b@CB7	1407.5	1407.5
9b@CB8	1573.6	1573.6
9c@β-CD	1393.6	1393.6
9c@γ-CD	1555.6	1555.7
9c@CB7	1421.6	1421.6
9c@CB8	1587.6	1587.6
9d@β-CD	1421.6	1421.6
9d@γ-CD	1583.7	1583.7
9d@CB7	1449.6	1449.6
9d@CB8	1615.6	1615.7
10b@β-CD	1429.6	1429.6
10b@γ-CD	1591.6	1591.7
10b@CB7	1457.6	1457.4
10b@CB8	1623.6	1623.6
10c@β-CD	1443.6	1443.6
10c@γ-CD	1605.6	1605.6
10c@CB7	1471.6	1471.6
10c@CB8	1637.6	1637.6
10d@β-CD	1471.6	1471.6
10d@γ-CD	1633.7	1633.7
10d@CB7	1499.6	1499.6
10d@CB8	1665.6	1665.7

Job's plots – Figures S79–S94

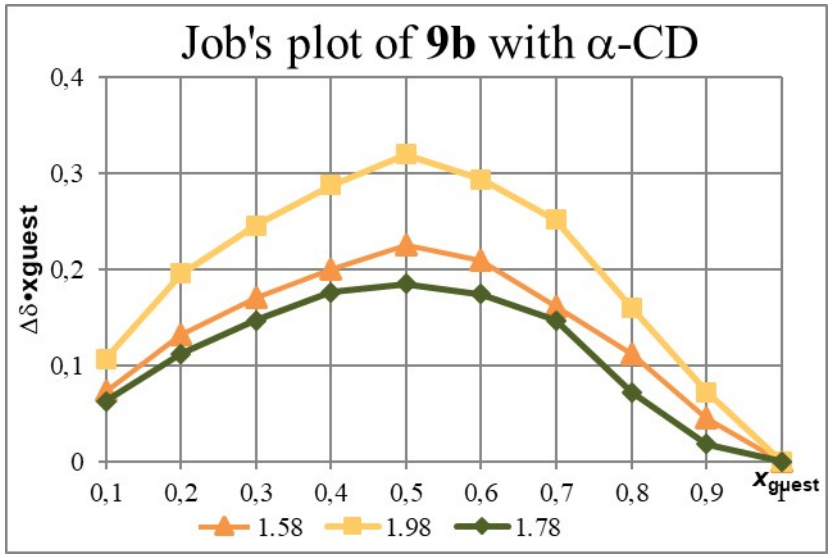

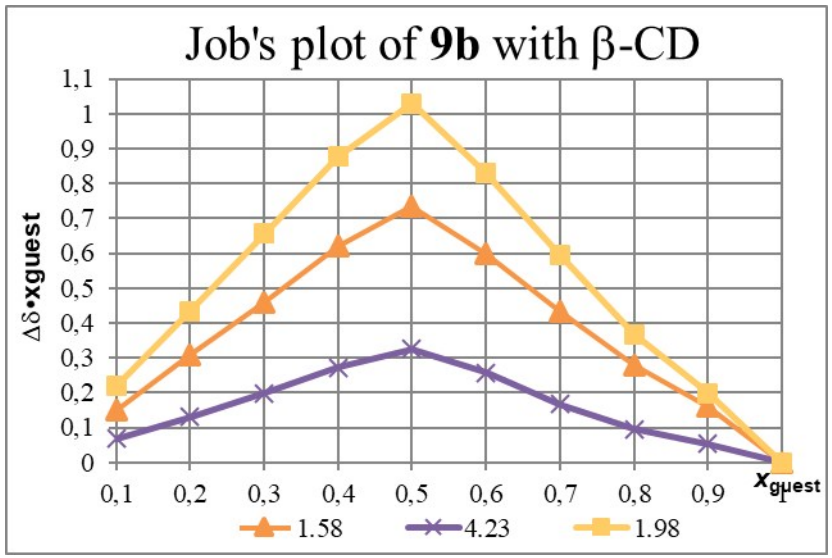

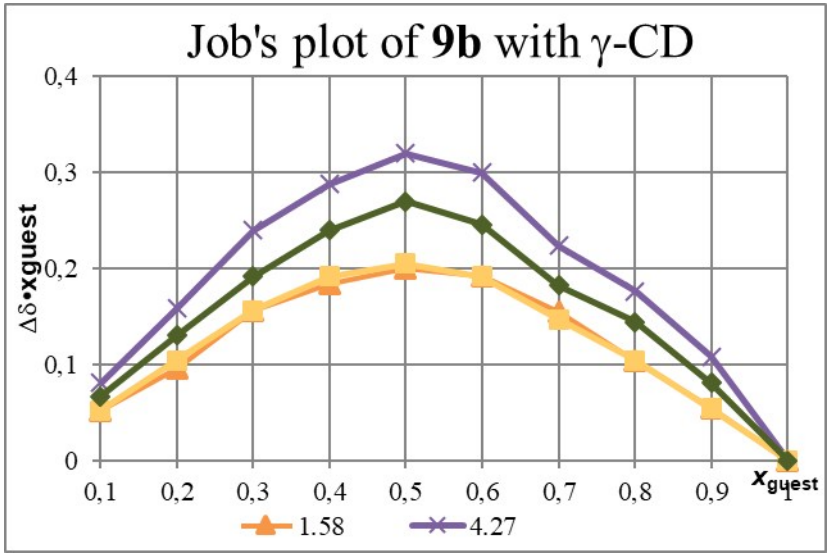

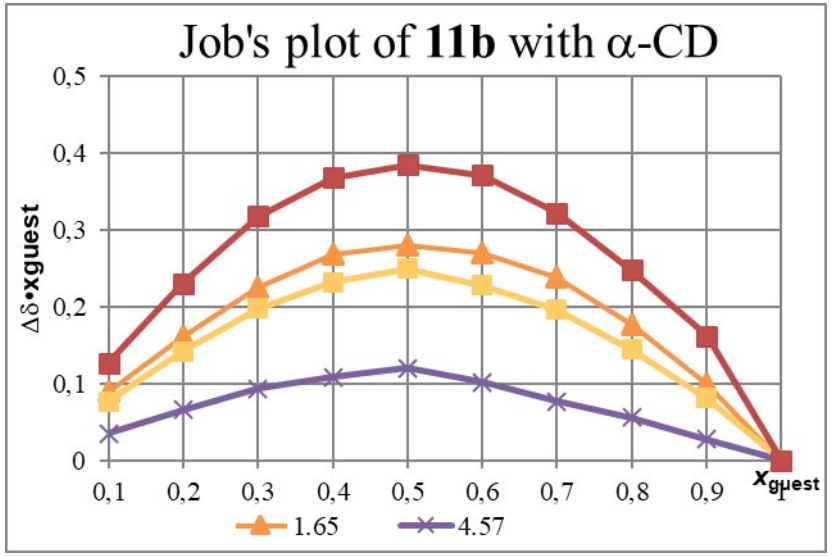

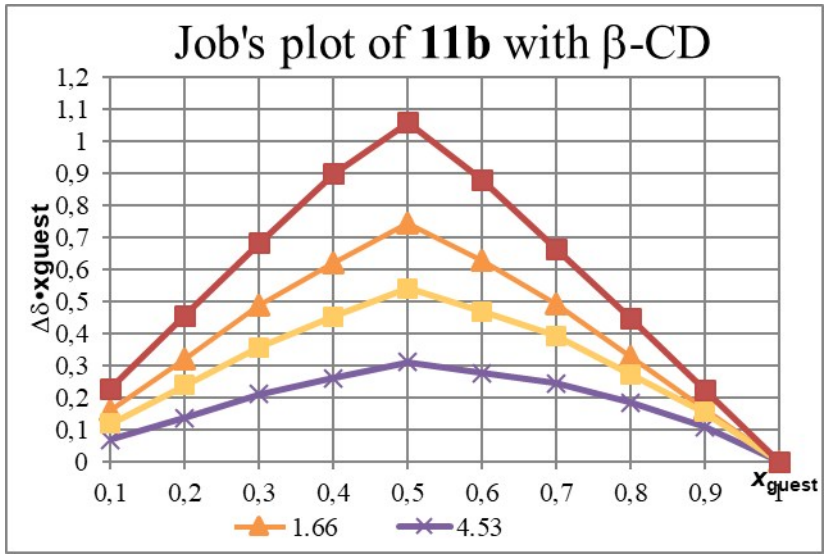
Job's plot of 11b with β-CD
Δδ•xguest
xguest
1.66
4.53

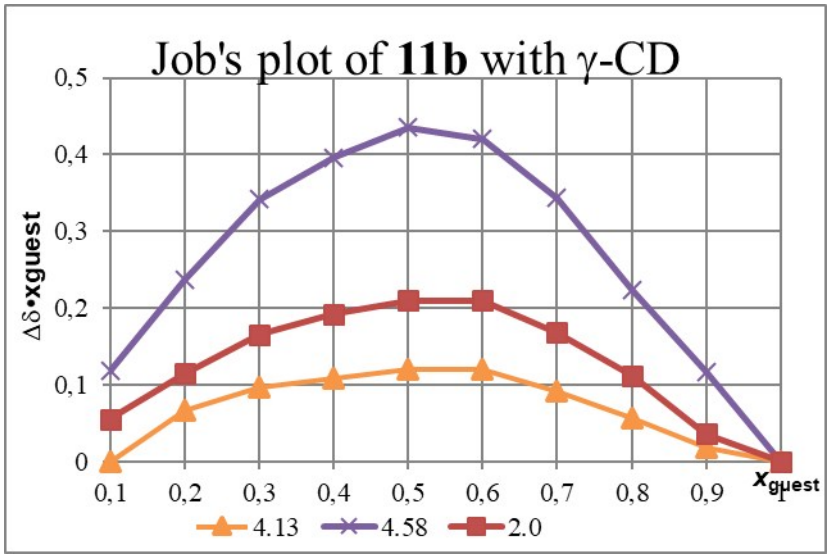
Job's plot of 11b with γ-CD
Δδ•xguest
xguest
4.13
4.58
2.0

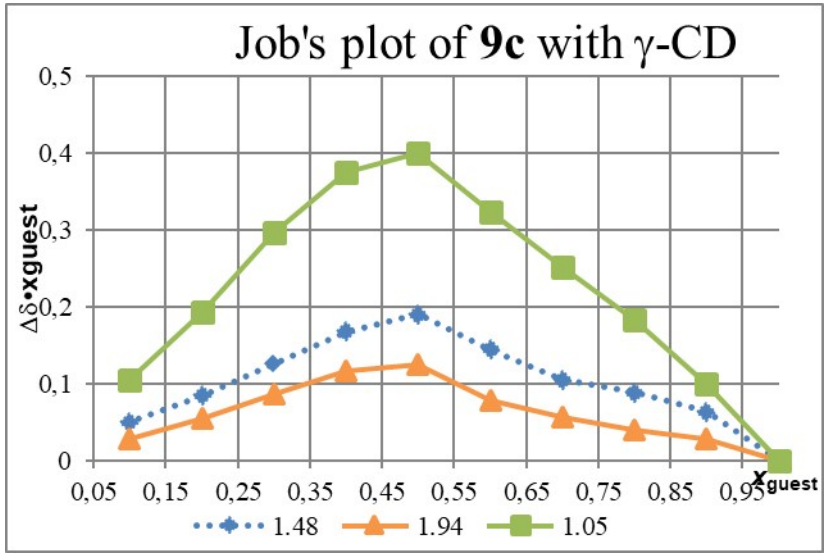
Job's plot of 9c with γ-CD
Δδ•xguest
xguest
1.48
1.94
1.05

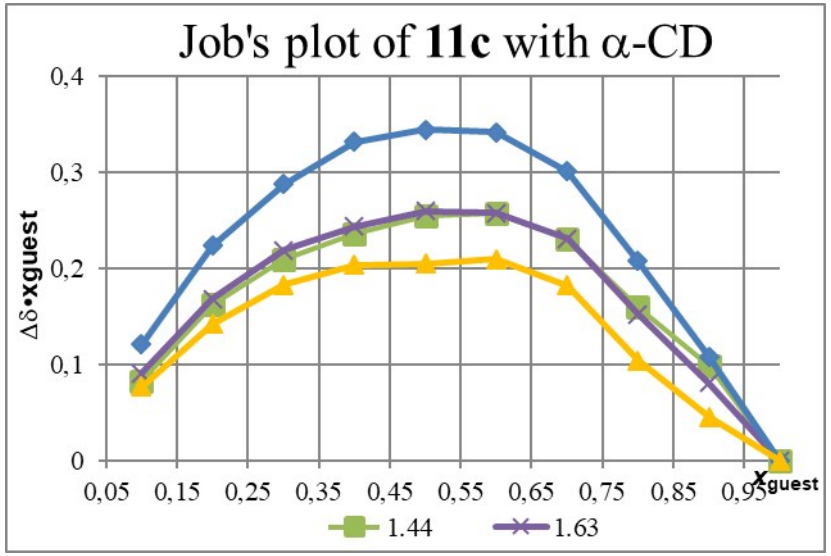
Job's plot of 11c with α-CD
Δδ•xguest
xguest
1.44
1.63

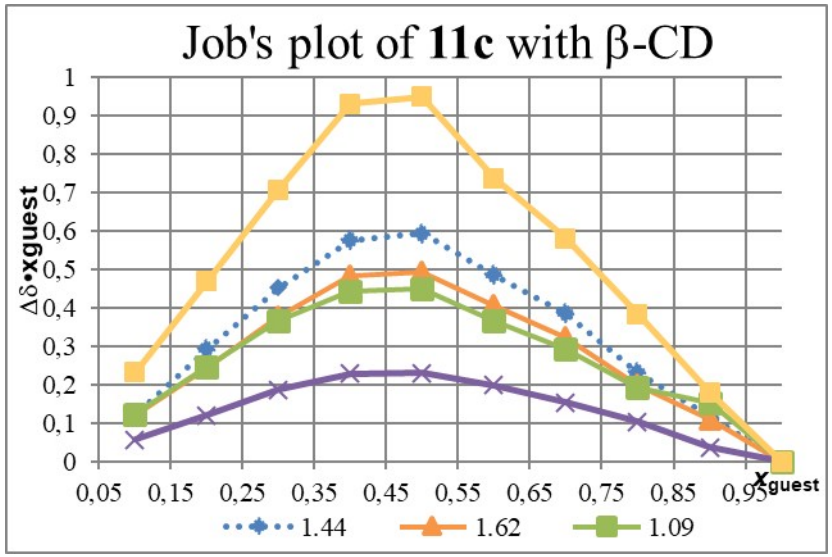
Job's plot of 11c with β-CD
Δδ•xguest
xguest
1.44
1.62
1.09

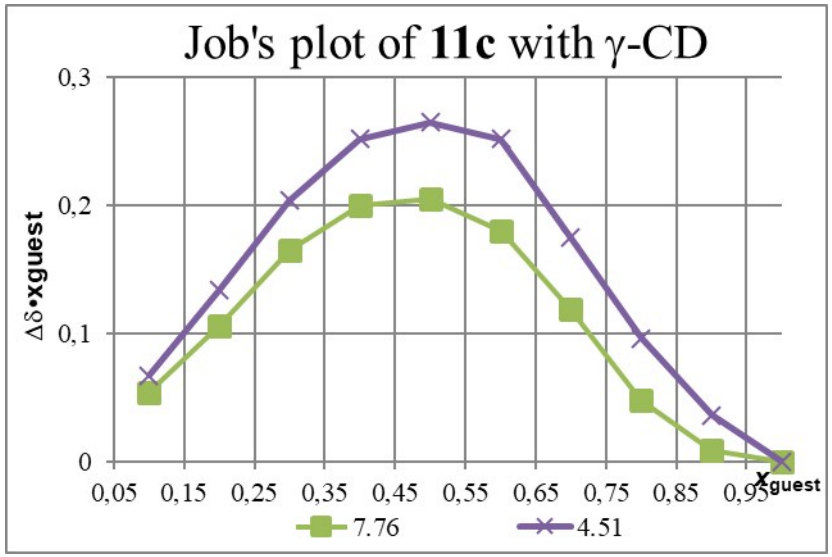
Job's plot of 11c with γ-CD
Δδ•xguest
xguest
7.76
4.51

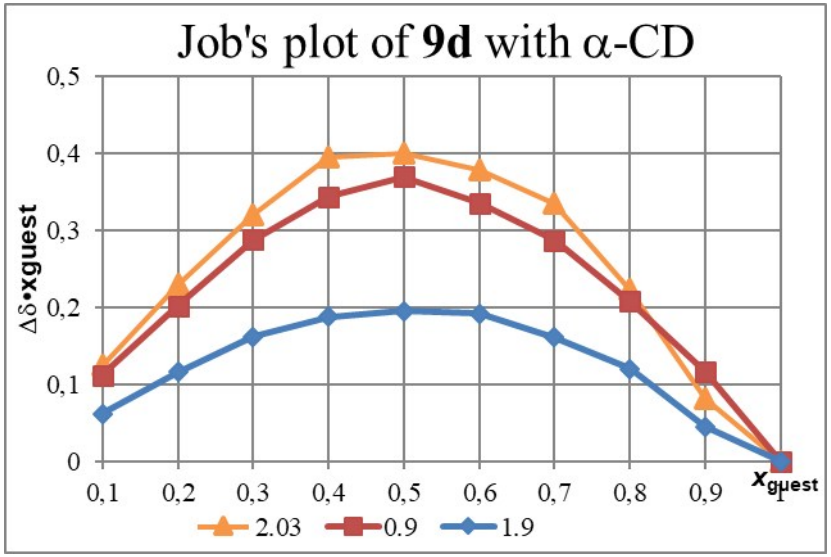
Job's plot of 9d with α-CD
Δδ•xguest
xguest
2.03
0.9
1.9

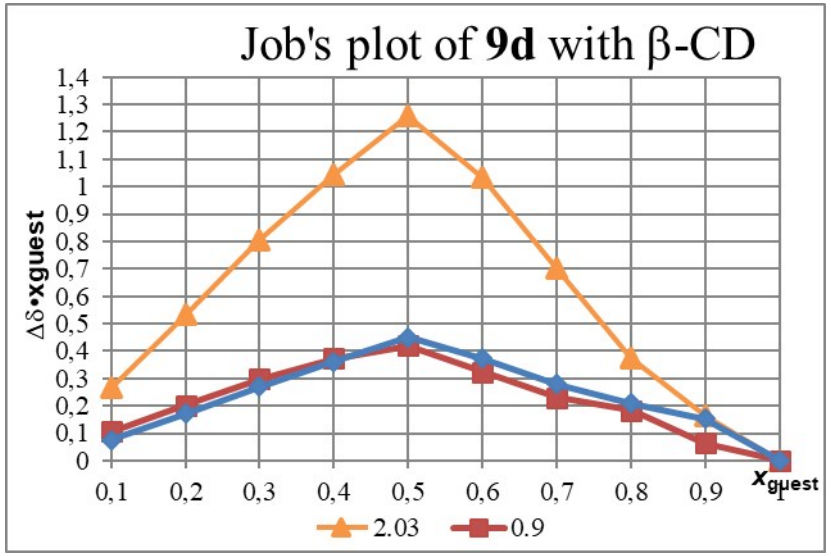
Job's plot of 9d with β-CD
Δδ•xguest
xguest
2.03
0.9

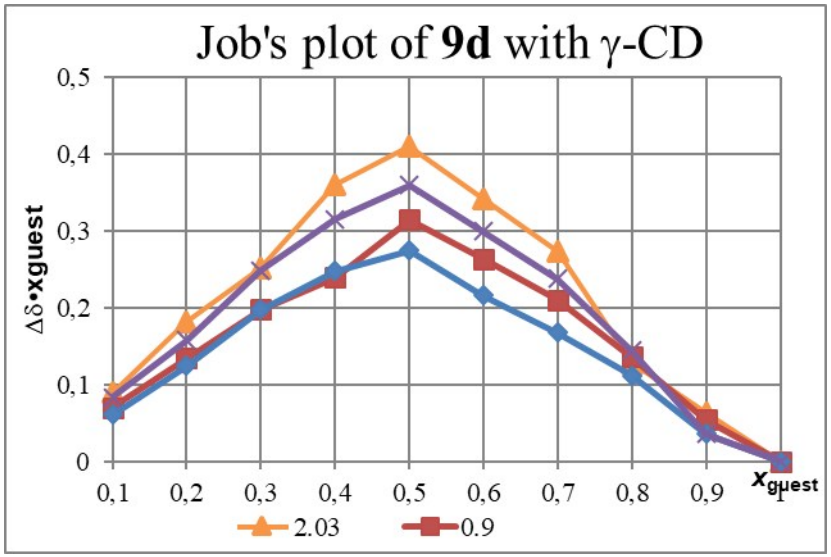
Job's plot of 9d with γ-CD
Δδ•xguest
xguest
2.03
0.9

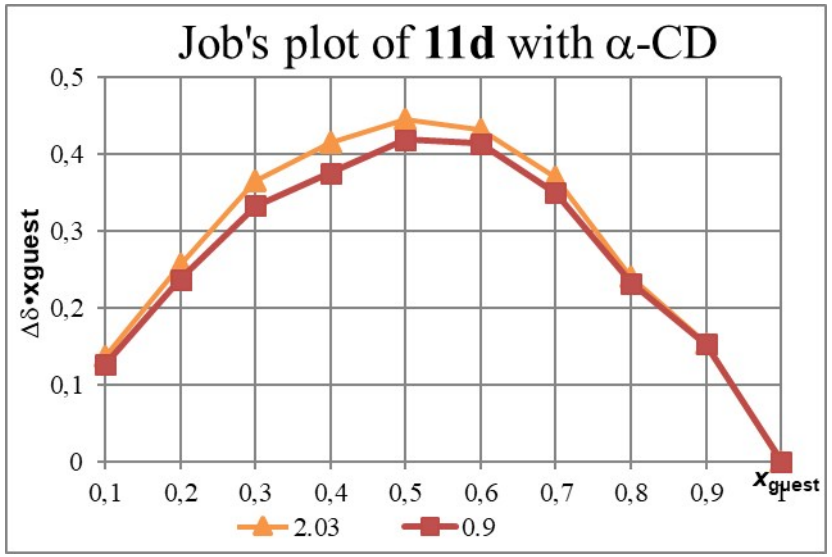
Job's plot of 11d with α-CD
Δδ•xguest
xguest
2.03
0.9

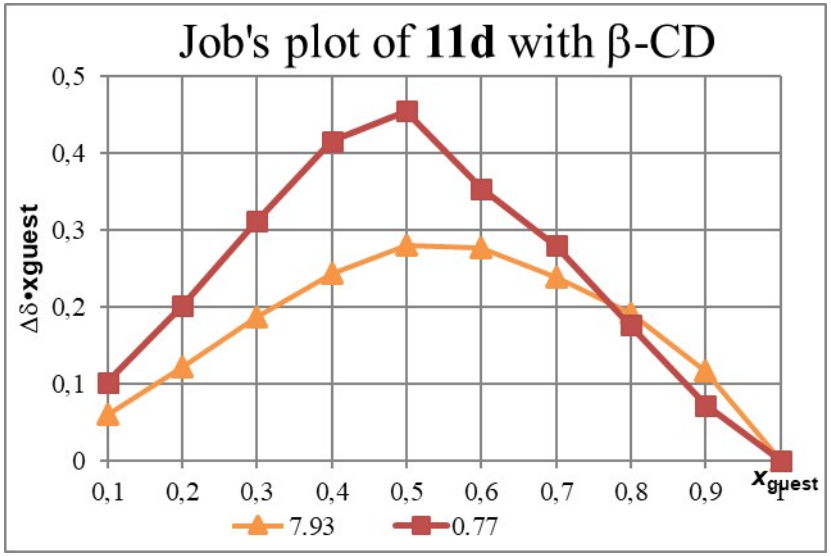
Job's plot of 11d with β-CD
Δδ•xguest
xguest
7.93
0.77

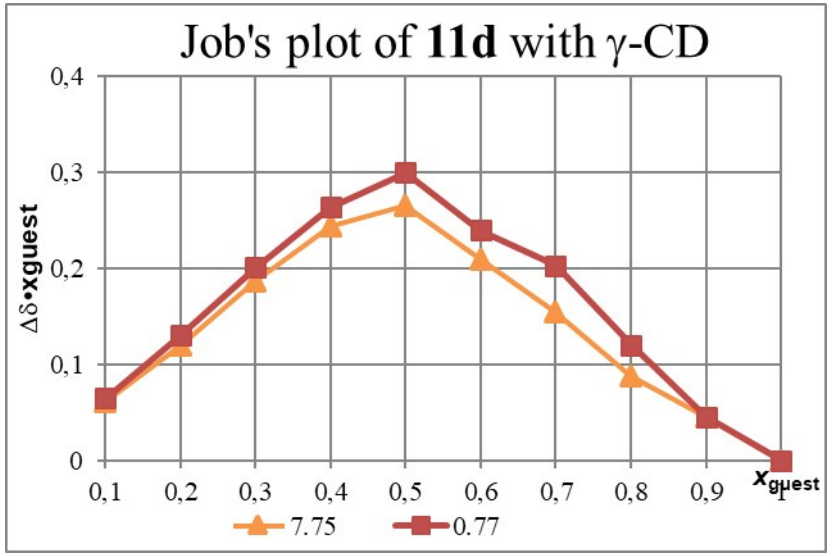
Job's plot of 11d with γ-CD
Δδ•xguest
xguest
7.75
0.77

Isothermal titration calorimetry results

The association constants and thermodynamic parameters for the complexation of guests **9a–9d** and **10a–10d** with CB7, CB8, α-CD, β-CD and γ-CD were determined by titration calorimetry using a MicroCal VP-ITC instrument. A solution of the host in water was placed in the sample cell, to which a solution of the guest was added in a series of 29 injections (10 μL). The heat evolved was recorded at 303 K. The net heat effect was obtained by subtracting the heat of guest dilution from the overall observed heat effect. Association constants exceeding 10^7 M^{-1} were determined by the multistep competition method as described by Rekharsky et al. A 1,6-hexamethylenediamine·2HCl (HMDCl), L-phenylalanine, methyl viologen dichloride (MV·2 HCl), and amantadine·HCl with respective association constants K_{CB7}=2.05×10^9 M^{-1}, K_{CB7}=5.16×10^5 M^{-1}, K_{CB8}=7.05×10^6 M^{-1}, K_{CB8}=2.89×10^9 M^{-1} were used as competitors. The data were analysed using the MicroCal Origin software. One Set of Sites model for data fitting were used. The complexation enthalpies for the multistep titration experiments were calculated as the sum of the enthalpies of each complexation step. The values of K obtained from the competitive titrations were verified using different concentrations of competitors. All titrations with CB7, CB8, and β-CD were performed in triplicate. Titrations with α-CD and γ-CD were performed only once.

Table S1 Isothermal titration calorimetry data

guest	host	K [dm^3·mol^{-1}]	n	$-\Delta H$ [kJ·mol^{-1}]	ΔS [J·mol^{-1}·K^{-1}]	$-\Delta G$ [kJ·mol^{-1}]	typical concentrations [mmol·dm^{-3}]		
							c (guest)	c (host)	c (comp)
9a	β-CD[a]	(6.8±0.3)×10^4	0.88±0.04	31.4±1.8	−11.1	28.1	1.3863	0.1556	na
	CB7[a]	(7.6±0.5)×10^{11}	0.97±0.01	91.3±1.2	−54.7	74.7	0.4950	0.0499	0.5455[b]
	CB8	(1.1±0.1)×10^{11}	0.89±0.04	53.08±1.1	36.4	64.1	0.5360	0.0480	6.1051[c]
9b	α-CD	2.9×10^2	1[d]	21	22	28	5.0273	0.4627	na
	β-CD	(1.9±0.5)×10^5	0.98±0.01	31.3±0.2	−2.4	30.6	1.6129	0.1641	na
	γ-CD	8.9×10^2	1.08	1.2	52.8	17.1	5.0337	0.4635	na
	CB7	(5.6±0.8)×10^{12}	1.01±0.03	89.4±1.3	−50.9	74	0.6271	0.0499	0.8540[b]
	CB8	(1.3±0.3)×10^{11}	1.00±0.03	52.3±0.9	40.2	64.4	0.6661	0.0527	3.0946[c]
9c	α-CD	3.0×10^2	1[d]	26	−39	14.4	5.1026	0.4985	na
	β-CD	(4.9±0.1)×10^5	0.96±0.02	33.21±0.15	−0.6	33.0	1.3616	0.1452	na
	γ-CD	1.2×10^4	0.95	−0.9	81.2	23.7	5.1015	0.5222	na
	CB7	(8.6±0.4)×10^{12}	0.97±0.05	85.7±1.4	−35.3	75.1	0.5364	0.0499	0.5319[b]
	CB8	(4.3±0.9)×10^{10}	1.01±0.03	49.5±1.2	40.2	61.7	0.5305	0.0480	4.6539[c]
9d	α-CD	7.7×10^2	1[d]	35	−59	16.7	4.9244	0.5076	na
	β-CD	(3.4±0.1)×10^5	0.95±0.01	39.6±0.9	−24.6	32.1	1.5389	0.1432	na
	γ-CD	8.4×10^4	0.93	12.6	52.8	28.6	4.9265	0.4996	na
	CB7	(8.3±1.5)×10^3	1.03±0.02	18.2±0.2	14.9	22.7	1.5425	0.1407	na
	CB8	(1.7±0.4)×10^{12}	1.04±0.01	67.3±1.2	12.0	70.9	0.5753	0.0502	1.3590[e]
10a	β-CD[a]	(5.0±0.4)×10^4	0.97±0.06	27.3±1.3	0.1	27.3	1.6001	0.1511	na
	CB7[a]	(1.0±0.6)×10^9	0.91±0.03	89±3	−120.7	52.0	0.5274	0.0499	0.2167[f]
	CB8	(3.0±0.4)×10^9	1.03±0.04	48.6±1.9	40.4	60.8	0.5780	0.0477	4.1647[c]
10b	α-CD	5.0×10^2	1[d]	14	5	15.7	4.6926	0.4750	na
	β-CD	(1.7±0.3)×10^5	1.02±0.01	30.2±0.2	0.5	30.3	1.8026	0.1953	na
	γ-CD	3.4×10^3	0.80	5.3	50.2	20.5	3.0780	0.2716	na
	CB7	(3.4±0.3)×10^{10}	0.97±0.03	89±3	−68.5	61.1	0.5241	0.0499	4.5753[f]
	CB8	(7.5±1.4)×10^{10}	1.08±0.03	50.9±1.1	41.1	63.3	0.5525	0.0480	5.4845[c]

Table S1 (continued) Isothermal titration calorimetry data

guest	host	K [dm^3·mol^{-1}]	n	$-\Delta H$ [kJ·mol^{-1}]	ΔS [J·mol^{-1}·K^{-1}]	$-\Delta G$ [kJ·mol^{-1}]	typical concentrations [mmol·dm^{-3}]		
							c (guest)	c (host)	c (comp)
10c	α-CD	2.7×10^2	1[d]	28	−46	14.1	5.0484	0.4701	na
	β-CD	$(5.0\pm0.1)\times10^5$	0.98±0.01	32.3±0.4	−33.1	33.1	1.5085	0.1684	na
	γ-CD	2.1×10^4	0.90	−1.19	86.7	25.1	5.0498	0.5034	na
	CB7	$(4.1\pm1.1)\times10^9$	0.99±0.01	84±4	−92.4	55.7	0.5719	0.0499	0.6199[f]
	CB8	$(5.9\pm0.8)\times10^{10}$	1.05±0.01	50.7±1.0	37.5	62.0	0.5753	0.0802	5.7210[e]
10d	α-CD	6.1×10^2	1[d]	36	−65	16.2	3.9005	0.3722	na
	β-CD	$(3.2\pm0.1)\times10^5$	0.96±0.03	39.8±1.5	−25.9	32	1.6482	0.1561	na
	γ-CD	8.0×10^4	1.02	12.2	53.6	28.5	3.9025	0.3972	na
	CB7	$(1.7\pm0.1)\times10^4$	1.04±0.02	26.9±0.6	−7.6	24.53	1.5108	0.1407	na
	CB8	$(2.0\pm0.3)\times10^{12}$	1.06±0.04	67.7±1.3	12.0	71.30	0.6005	0.0485	1.7634[e]

na = not applicable; [a] According to Branná *et al. J. Org. Chem.* **2016**, *81*, 9595–9604. Competitors were used as follows: [b] 1,6-hexamethylenediamine·2HCl, [c] methylviologen dichloride, [e] amantadine·HCl, [f] L-phenylalanine. [d] The n value was kept invariable during iteration process.

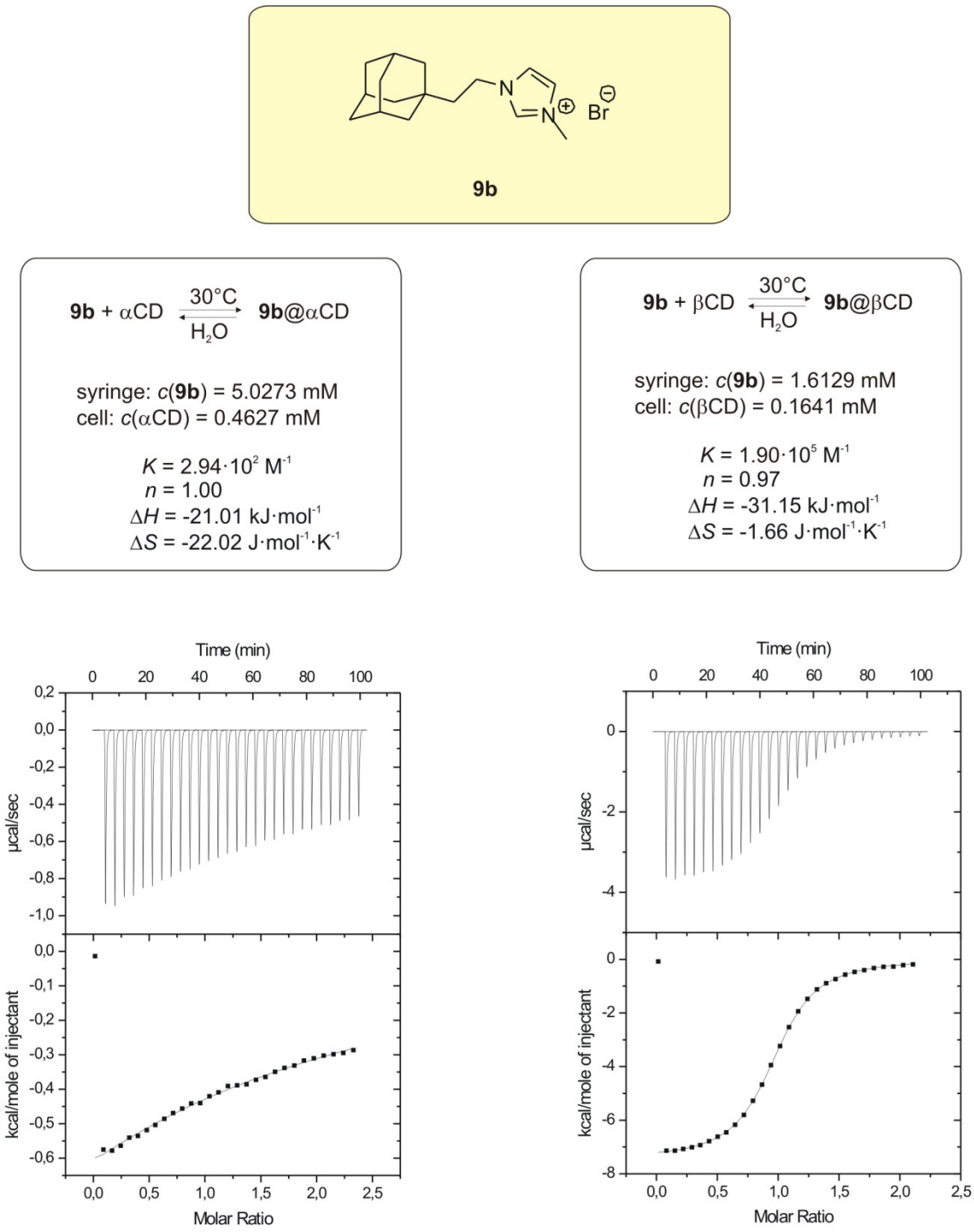

Figure S95: ITC experiments on complexation of **9b** with α-CD (left) and β-CD (right) in water at 30°C.

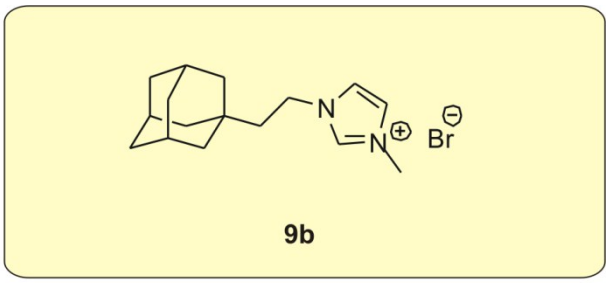

9b

9b + γCD $\underset{H_2O}{\overset{30°C}{\rightleftharpoons}}$ **9b**@γCD

syringe: c(**9b**) = 5.0337 mM
cell: c(γCD) = 0.4635 mM

$K = 8.86 \cdot 10^2\ M^{-1}$
$n = 1.08$
$\Delta H = -1.15\ kJ \cdot mol^{-1}$
$\Delta S = 52.76\ J \cdot mol^{-1} \cdot K^{-1}$

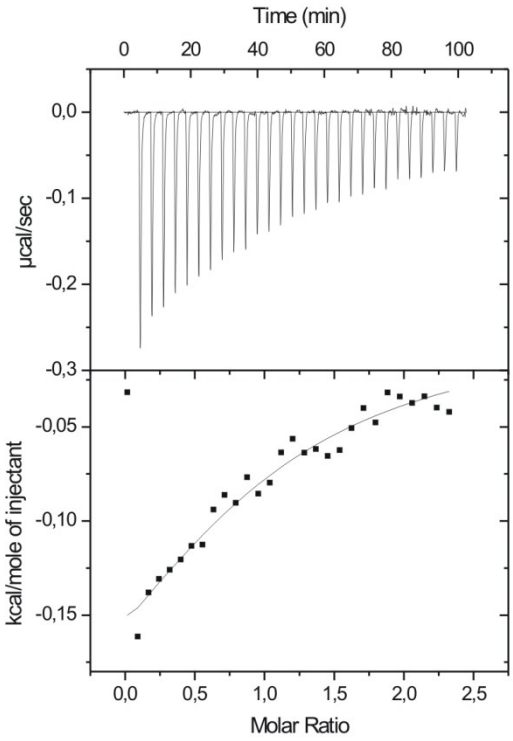

Figure S96: ITC experiment on complexation of **9b** with γ-CD in water at 30°C.

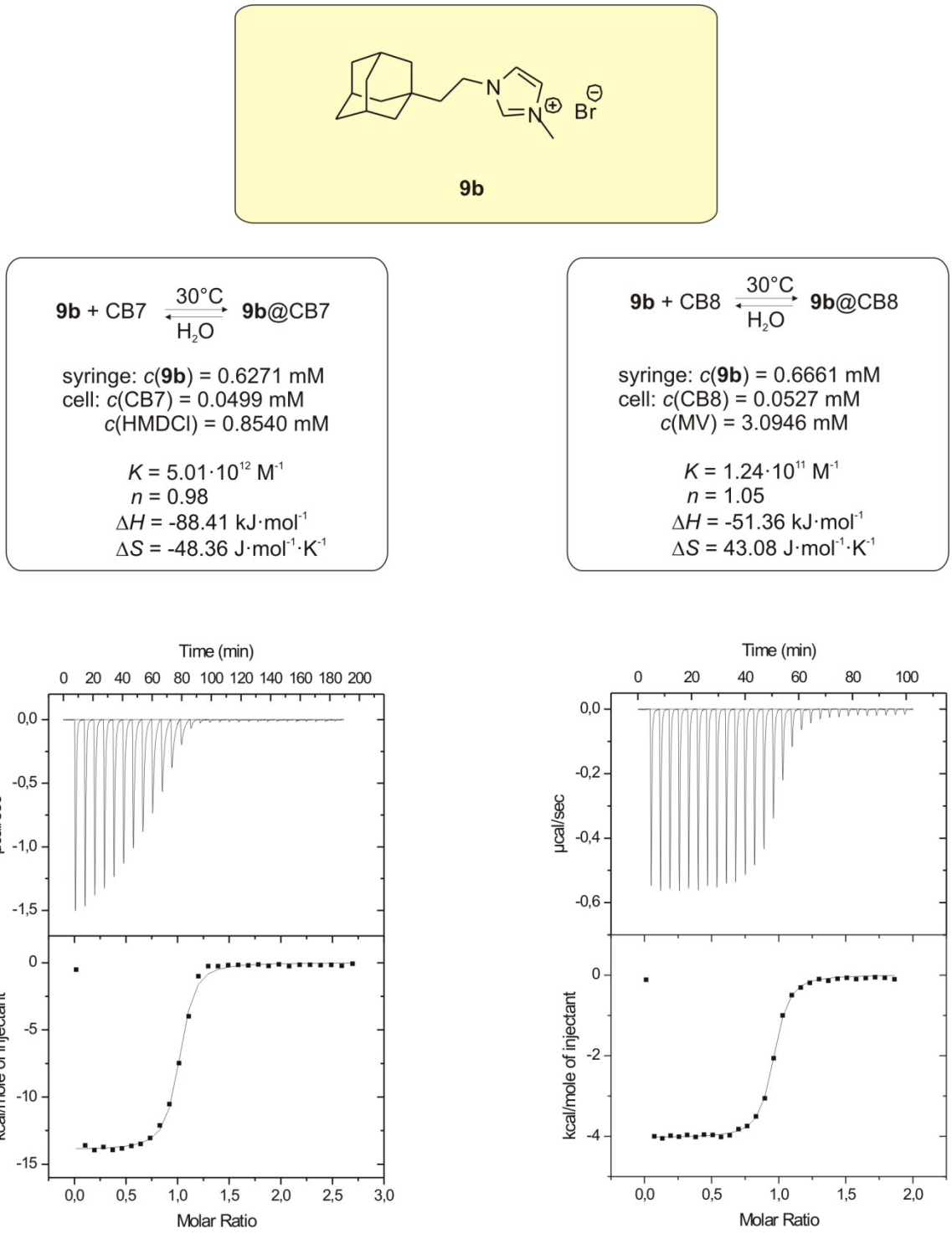

Figure S97: ITC experiments on complexation of **9b** with CB7 (left) and CB8 (right) in water and 50 mM NaCl at 30°C, respectively.

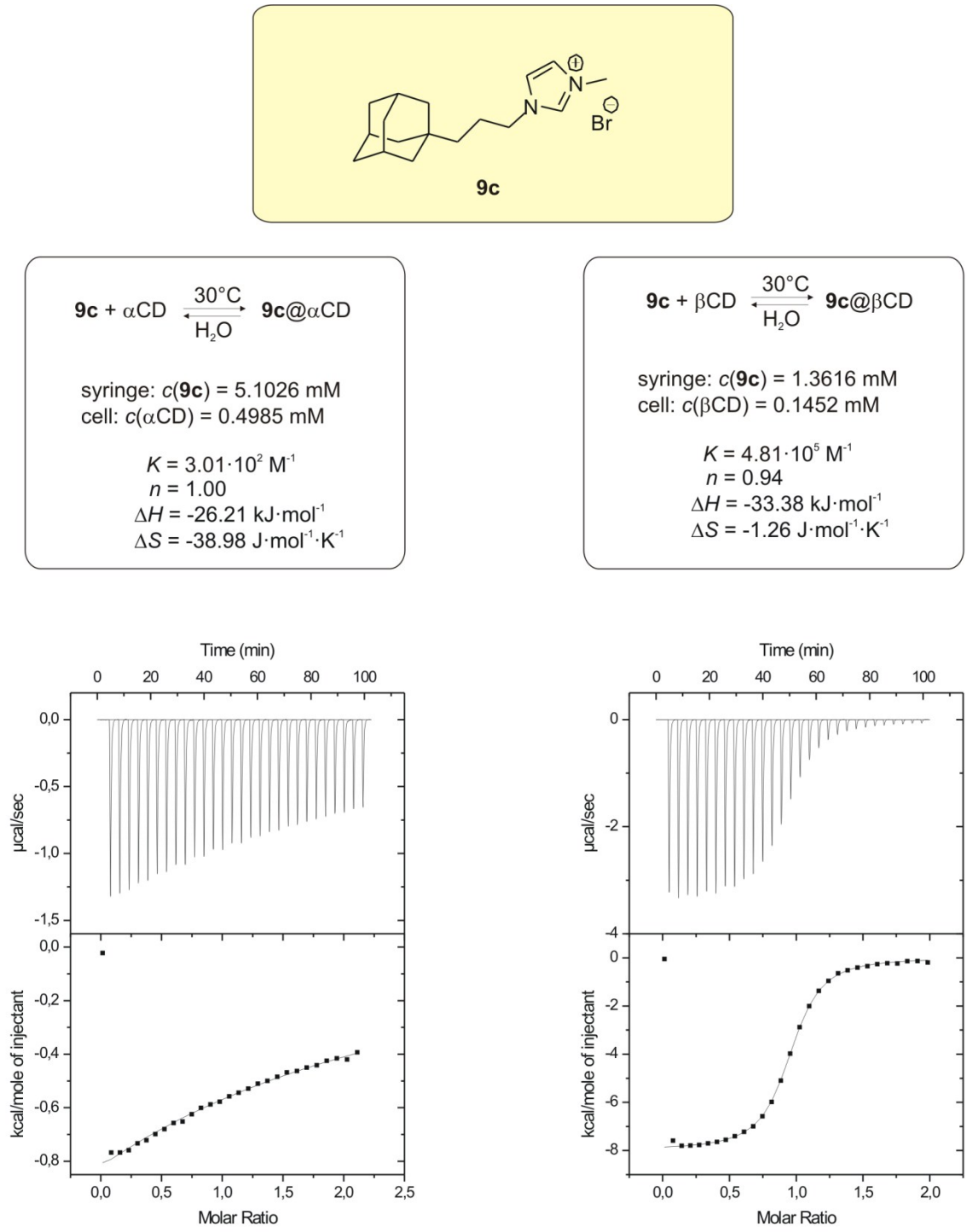

Figure S98: ITC experiments on complexation of **9c** with α-CD (left) and β-CD (right) in water at 30°C.

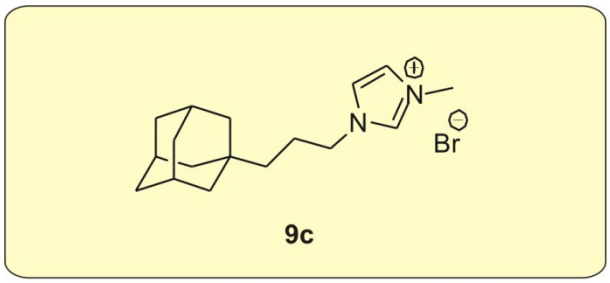

9c

9c + γCD $\underset{H_2O}{\overset{30°C}{\rightleftharpoons}}$ **9c**@γCD

syringe: c(**9c**) = 5.1015 mM
cell: c(γCD) = 0.5222 mM

$K = 1.22 \cdot 10^4\ M^{-1}$
$n = 0.95$
$\Delta H = 0.93\ kJ \cdot mol^{-1}$
$\Delta S = 81.23\ J \cdot mol^{-1} \cdot K^{-1}$

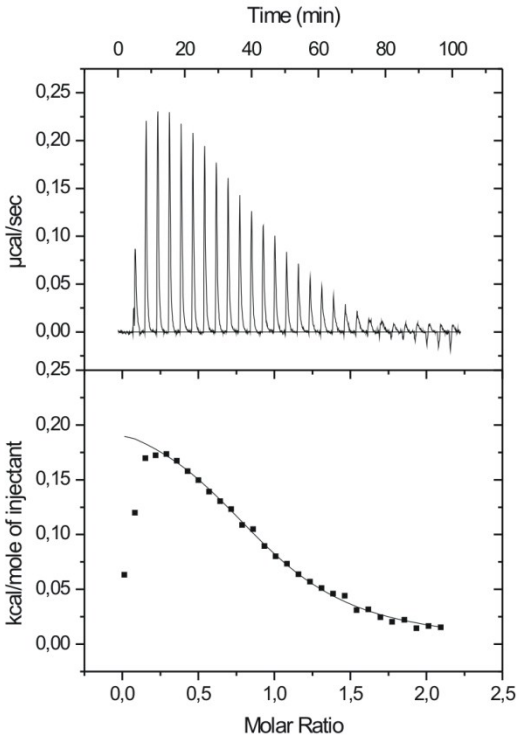

Figure S99: ITC experiment on complexation of **9c** with γ-CD in water at 30°C.

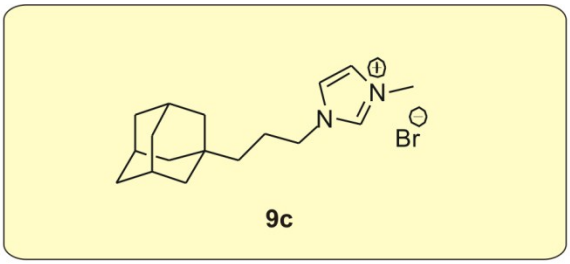

9c + CB7 $\underset{H_2O}{\overset{30°C}{\rightleftharpoons}}$ **9c**@CB7

syringe: c(**9c**) = 0.5364 mM
cell: c(CB7) = 0.0499 mM
c(HMDCl) = 0.5319 mM

$K = 7.96 \cdot 10^{12}$ M^{-1}
$n = 0.94$
$\Delta H = -84.31$ kJ·mol^{-1}
$\Delta S = -30.98$ J·mol^{-1}·K^{-1}

9c + CB8 $\underset{H_2O}{\overset{30°C}{\rightleftharpoons}}$ **9c**@CB8

syringe: c(**9c**) = 0.5305 mM
cell: c(CB8) = 0.0480 mM
c(MV) = 4.6539 mM

$K = 4.23 \cdot 10^{10}$ M^{-1}
$n = 0.97$
$\Delta H = -50.18$ kJ·mol^{-1}
$\Delta S = 38.04$ J·mol^{-1}·K^{-1}

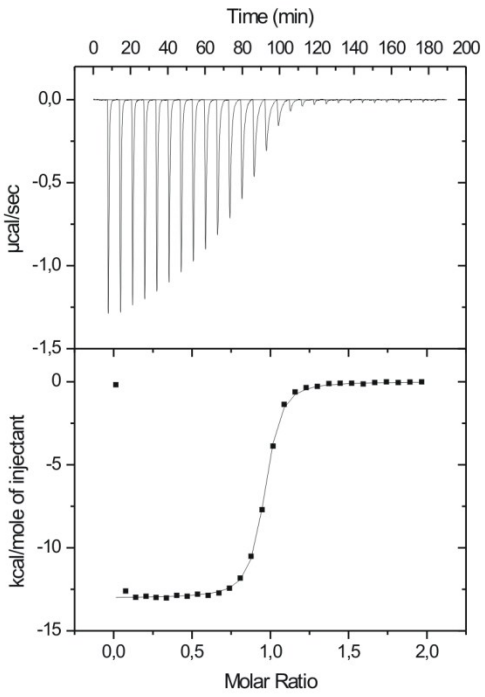

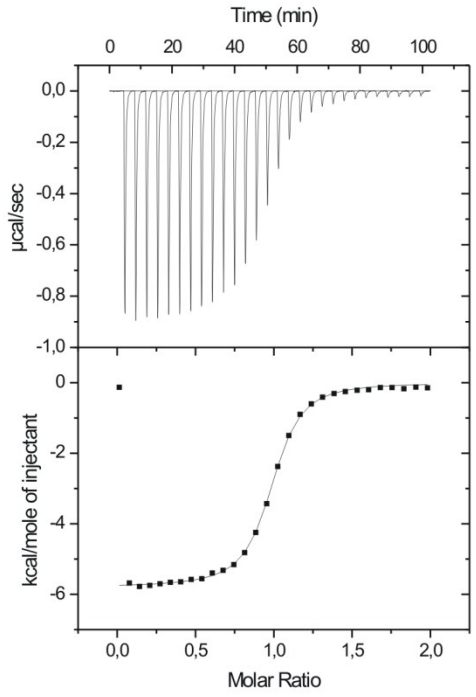

Figure S100:

ITC experiments on complexation of **9c** with CB7 (left) and CB8 (right) in water and 50 mM NaCl at 30°C, respectively.

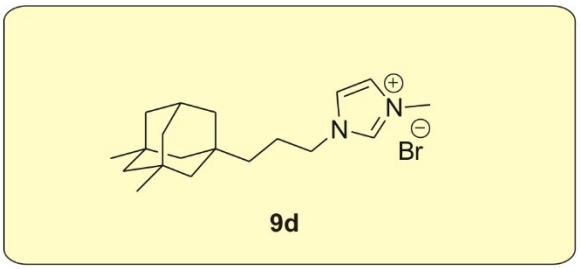

9d

9d + αCD $\underset{H_2O}{\overset{30°C}{\rightleftharpoons}}$ **9d**@αCD

syringe: *c*(**9d**) = 4.9244 mM
cell: *c*(αCD) = 0.5076 mM

$K = 7.65 \cdot 10^2\ M^{-1}$
$n = 1.00$
$\Delta H = -34.76\ kJ \cdot mol^{-1}$
$\Delta S = -59.46\ J \cdot mol^{-1} \cdot K^{-1}$

9d + βCD $\underset{H_2O}{\overset{30°C}{\rightleftharpoons}}$ **9d**@βCD

syringe: *c*(**9d**) = 1.5389 mM
cell: *c*(βCD) = 0.1432 mM

$K = 3.35 \cdot 10^5\ M^{-1}$
$n = 0.95$
$\Delta H = -39.35\ kJ \cdot mol^{-1}$
$\Delta S = -23.95\ J \cdot mol^{-1} \cdot K^{-1}$

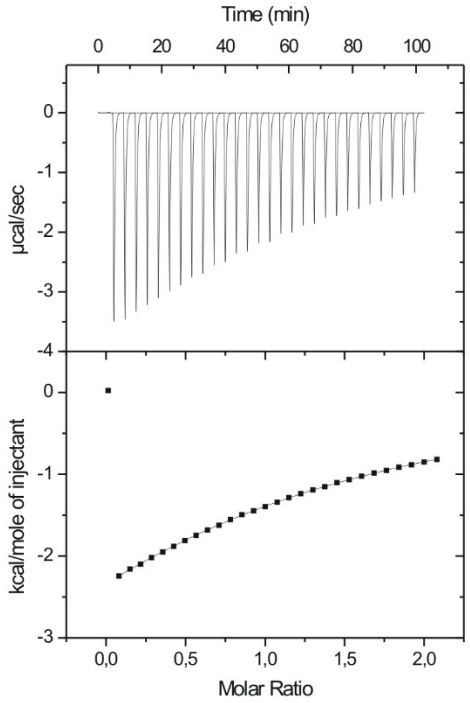

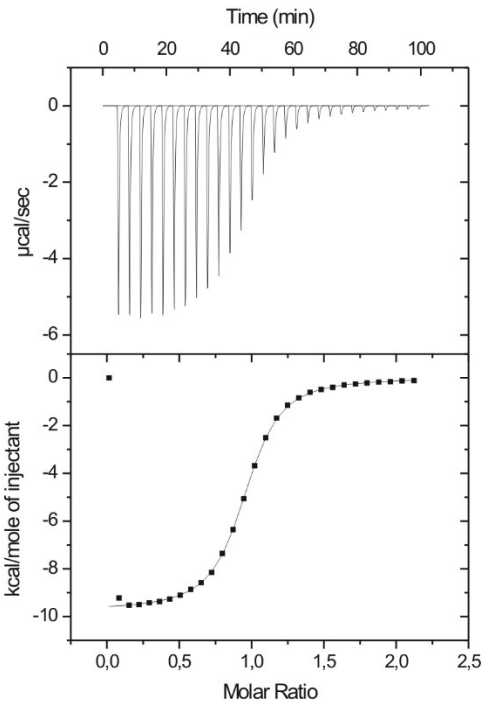

Figure S101: ITC experiments on complexation of **9d** with α-CD (left) and β-CD (right) in water at 30°C.

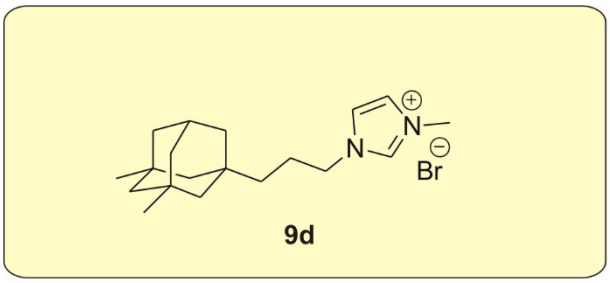

9d

9d + γCD $\underset{H_2O}{\overset{30°C}{\rightleftharpoons}}$ **9d**@γCD

syringe: c(**9d**) = 4.9265 mM
cell: c(γCD) = 0.4996 mM

$K = 8.41 \cdot 10^4\ M^{-1}$
$n = 0.93$
$\Delta H = -12.55\ kJ \cdot mol^{-1}$
$\Delta S = 52.76\ J \cdot mol^{-1} \cdot K^{-1}$

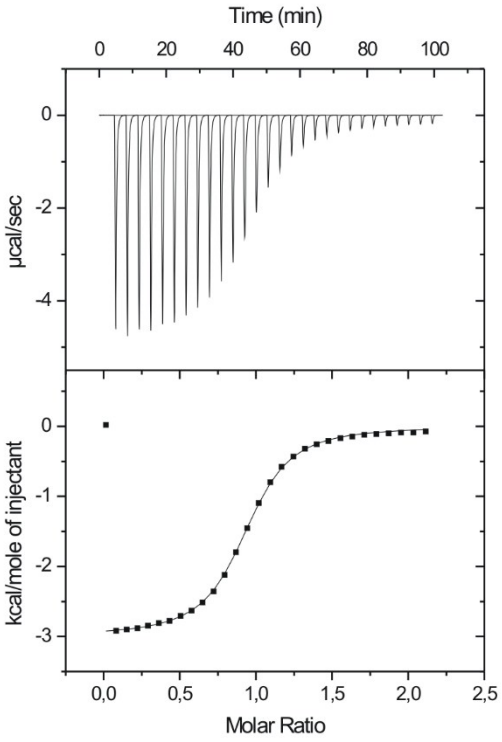

Figure S102: ITC experiment on complexation of **9d** with γ-CD in water at 30°C.

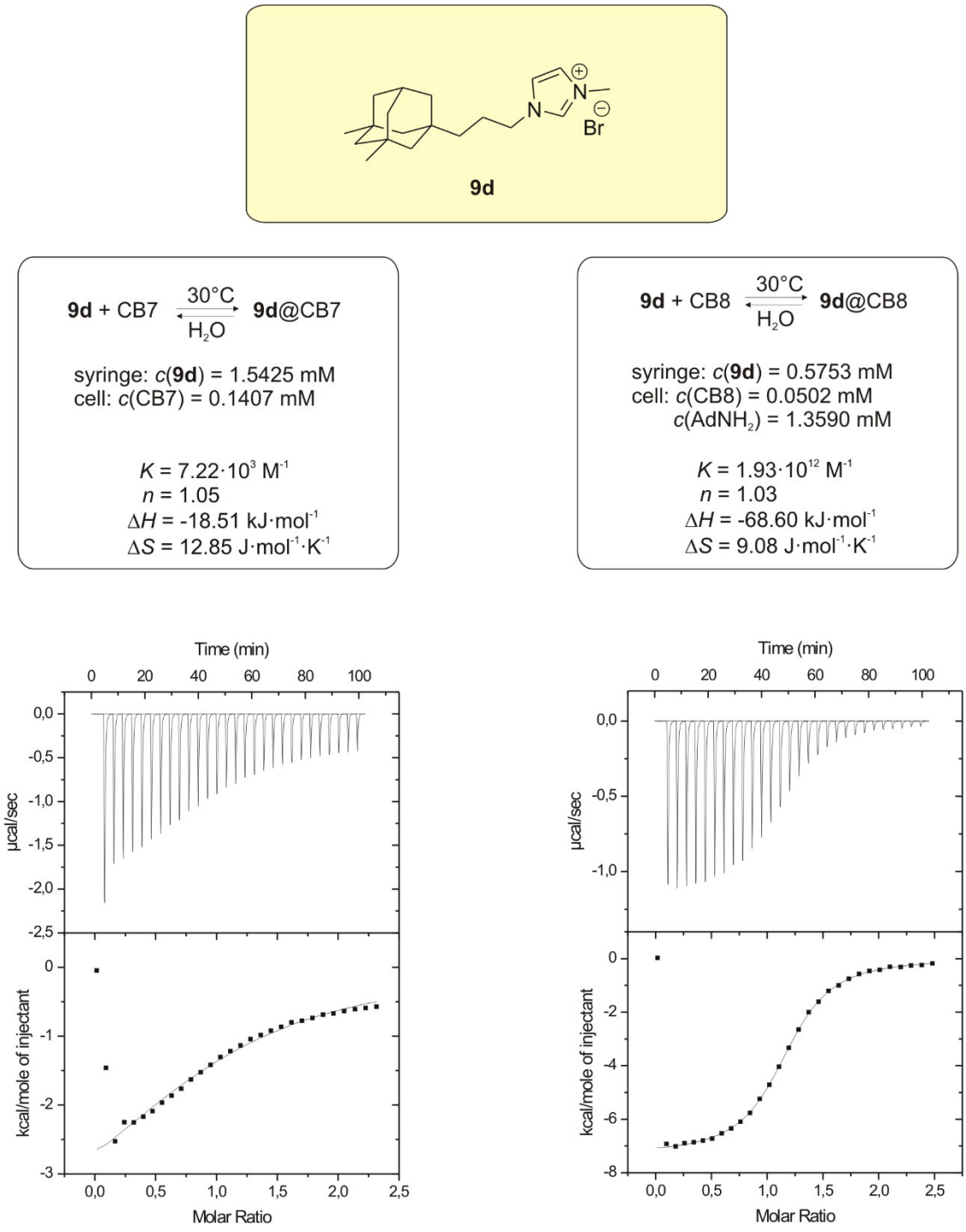

Figure S103: ITC experiments on complexation of **9d** with CB7 (left) and CB8 (right) in water and 50 mM NaCl at 30°C, respectively.

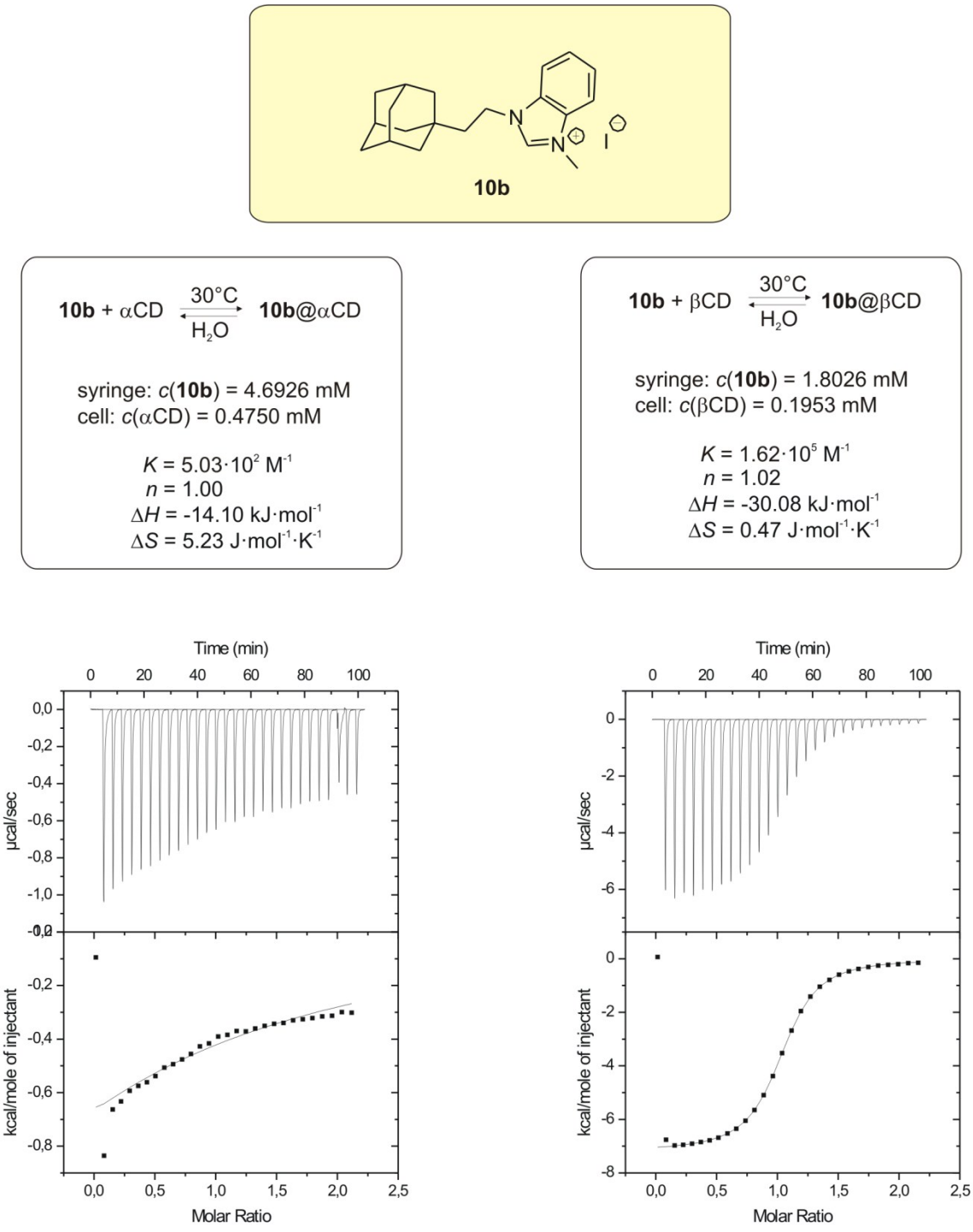

Figure S104: ITC experiments on complexation of **10b** with α-CD (left) and β-CD (right) in water at 30°C.

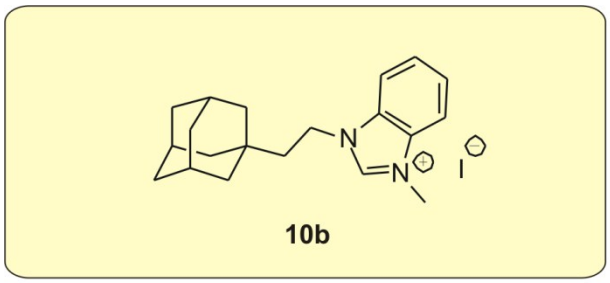

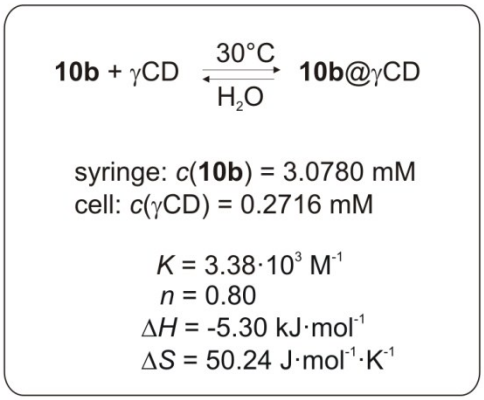

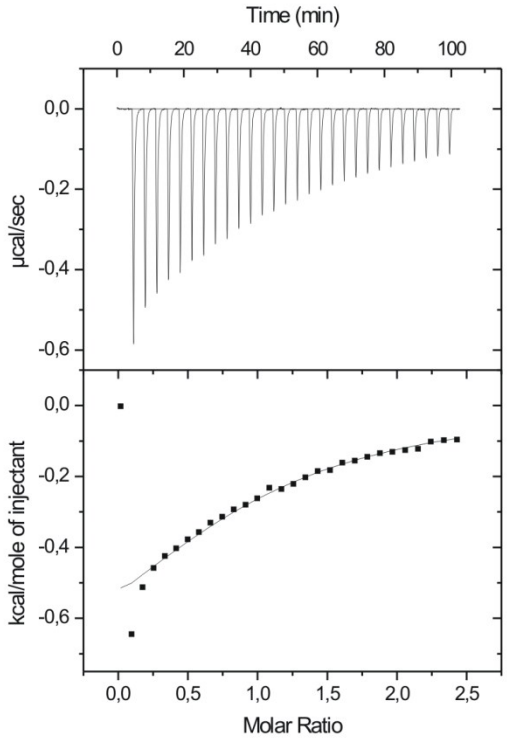

Figure S105: ITC experiment on complexation of **10b** with γ-CD in water at 30°C.

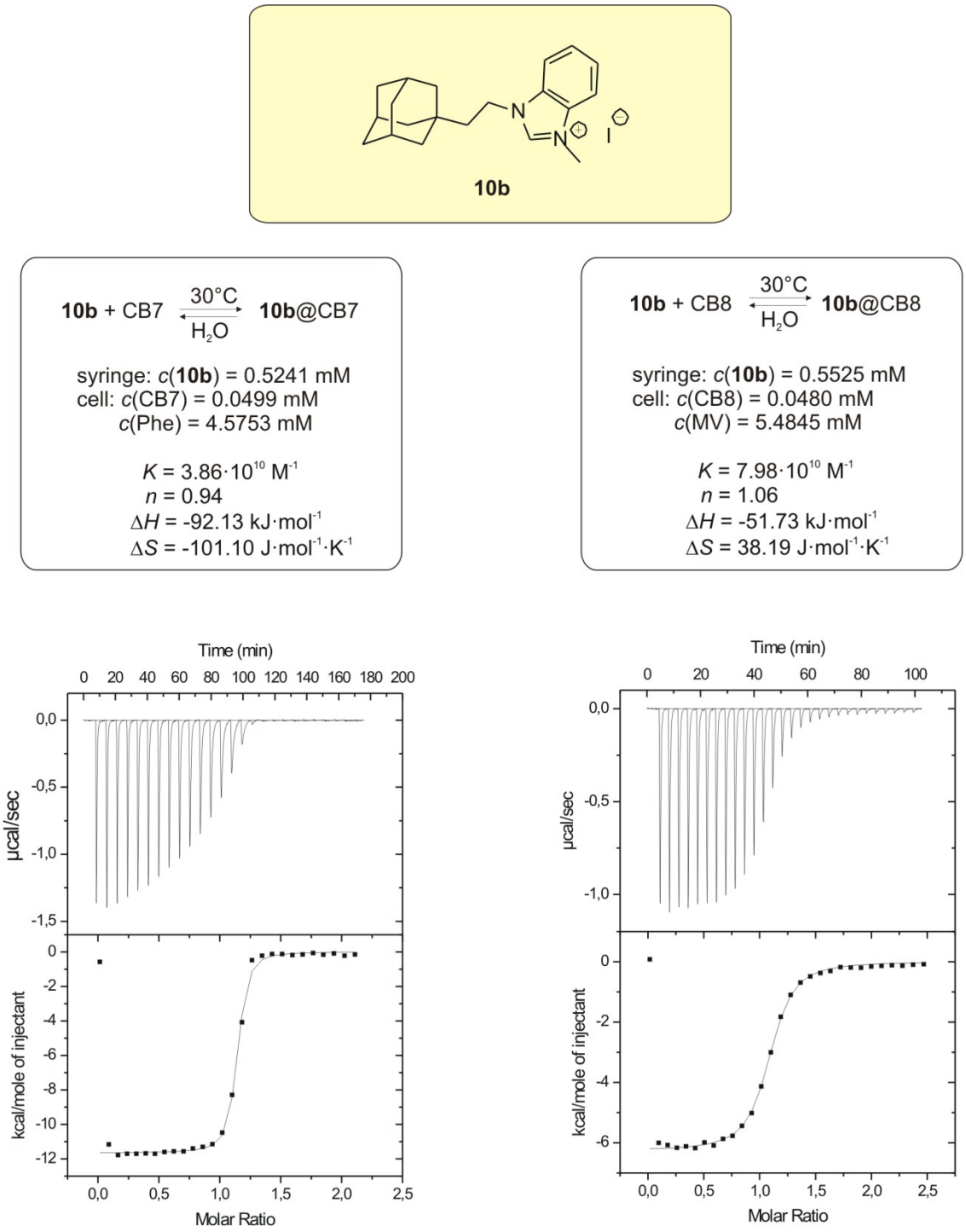

Figure S106: ITC experiments on complexation of **10b** with CB7 (left) and CB8 (right) in water and 50 mM NaCl at 30°C, respectively.

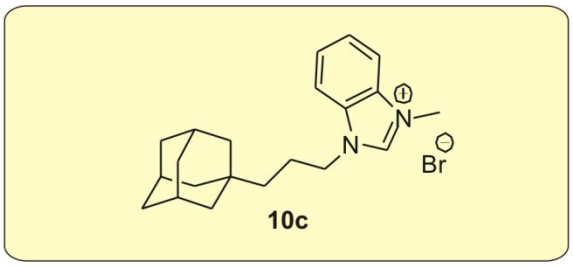

10c + αCD $\underset{H_2O}{\overset{30°C}{\rightleftharpoons}}$ **10c**@αCD

syringe: *c*(**10c**) = 5.0484 mM
cell: *c*(αCD) = 0.4701 mM

$K = 2.66 \cdot 10^2\ M^{-1}$
$n = 1.00$
$\Delta H = -28.08\ kJ \cdot mol^{-1}$
$\Delta S = -46.06\ J \cdot mol^{-1} \cdot K^{-1}$

10c + βCD $\underset{H_2O}{\overset{30°C}{\rightleftharpoons}}$ **10c**@βCD

syringe: *c*(**10c**) = 1.5085 mM
cell: *c*(βCD) = 0.1684 mM

$K = 4.91 \cdot 10^5\ M^{-1}$
$n = 0.97$
$\Delta H = -32.70\ kJ \cdot mol^{-1}$
$\Delta S = 1.15\ J \cdot mol^{-1} \cdot K^{-1}$

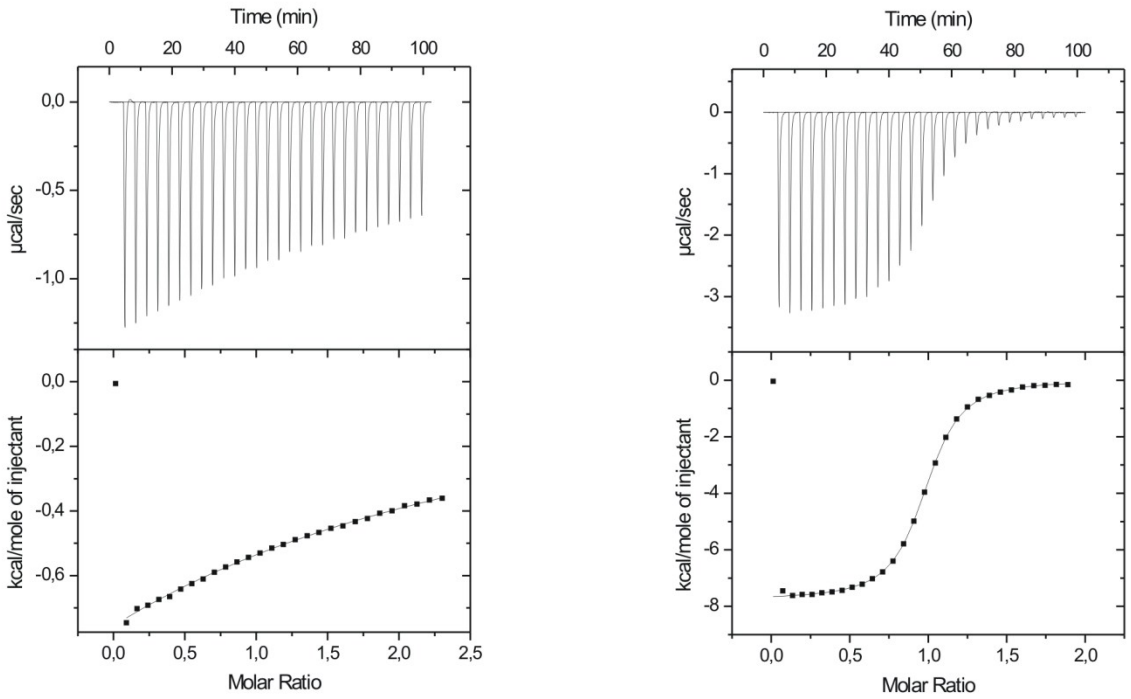

Figure S107: ITC experiments on complexation of **10c** with α-CD (left) and β-CD (right) in water at 30°C.

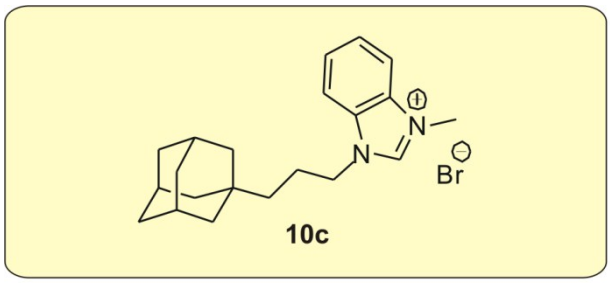

10c + γCD $\underset{H_2O}{\overset{30°C}{\rightleftharpoons}}$ **10c**@γCD

syringe: c(**10c**) = 5.0489 mM
cell: c(γCD) = 0.5039 mM

$K = 2.14 \cdot 10^4\ M^{-1}$
$n = 0.90$
$\Delta H = 1.19\ kJ \cdot mol^{-1}$
$\Delta S = 86.67\ J \cdot mol^{-1} \cdot K^{-1}$

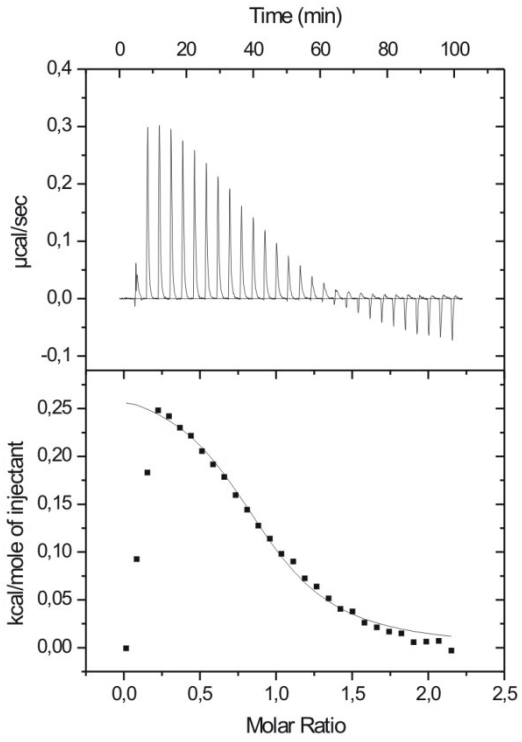

Figure S108: ITC experiment on complexation of **10c** with γ-CD in water at 30°C.

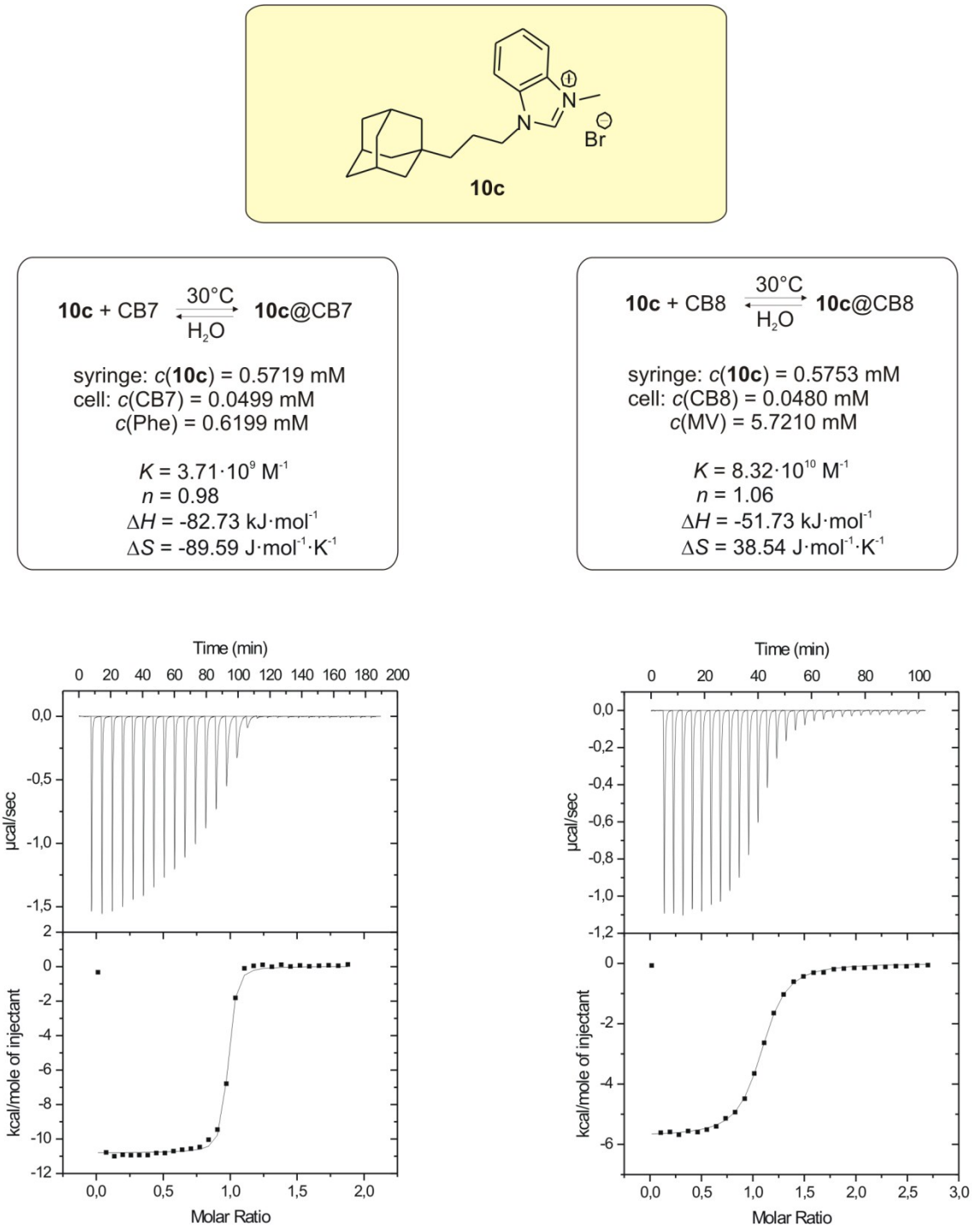

Figure S109: ITC experiments on complexation of **10c** with CB7 (left) and CB8 (right) in water and 50 mM NaCl at 30°C, respectively.

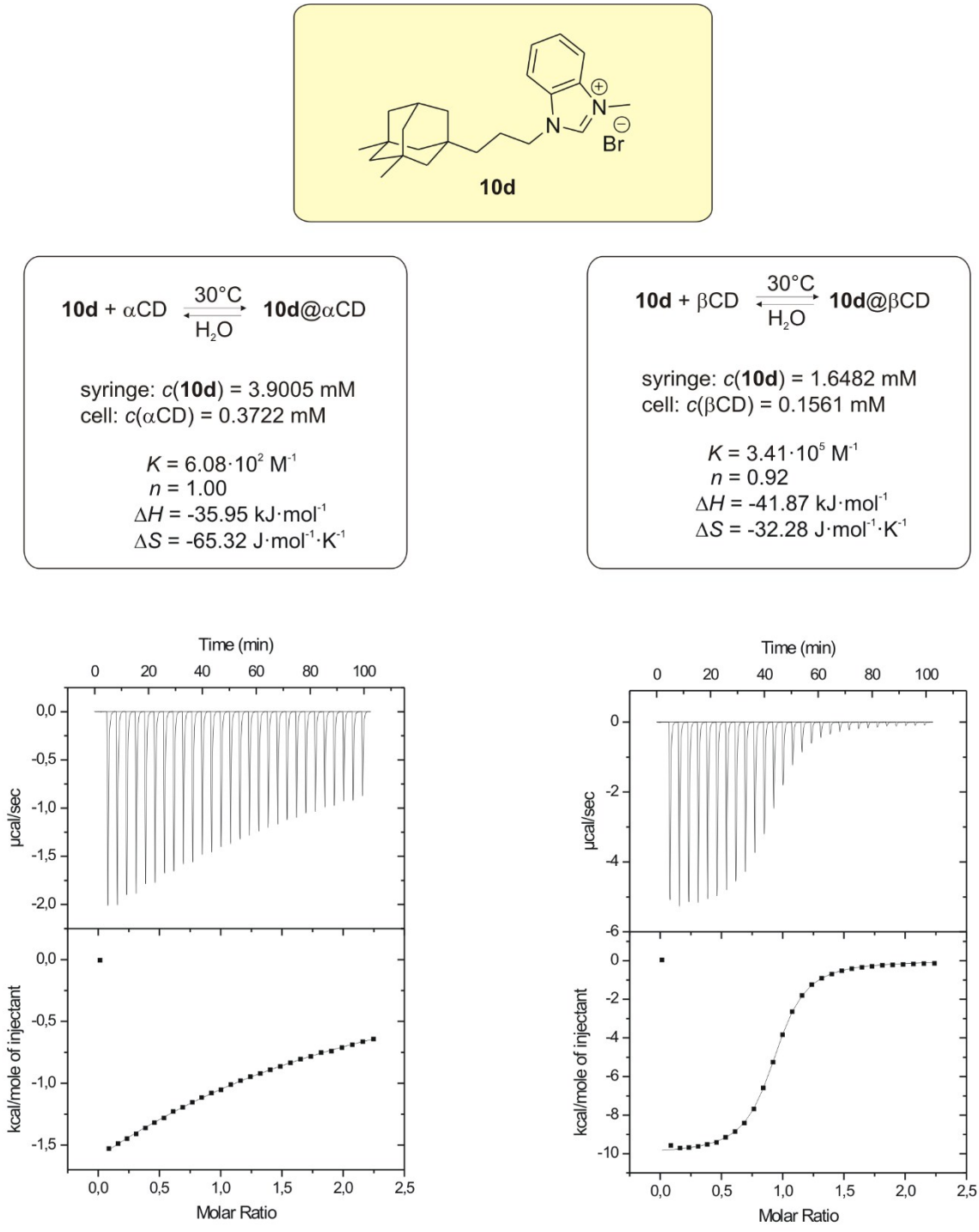

Figure S110: ITC experiments on complexation of **10d** with α-CD (left) and β-CD (right) in water at 30°C.

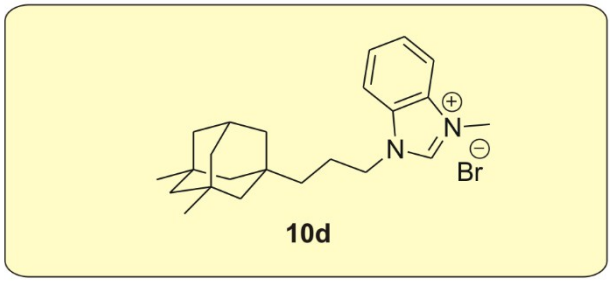

10d

10d + γCD $\underset{H_2O}{\overset{30°C}{\rightleftharpoons}}$ **10d**@γCD

syringe: c(**10d**) = 3.9025 mM
cell: c(γCD) = 0.3972 mM

$K = 7.87 \cdot 10^4\ M^{-1}$
$n = 1.02$
$\Delta H = -12.21\ kJ \cdot mol^{-1}$
$\Delta S = 53.59\ J \cdot mol^{-1} \cdot K^{-1}$

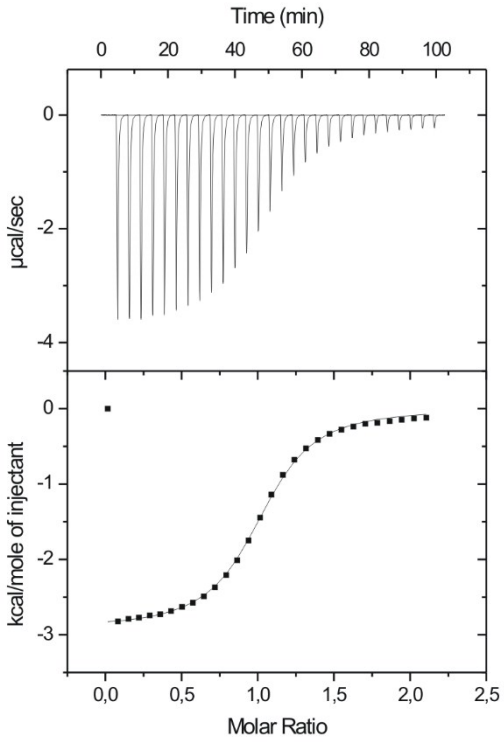

Figure S111: ITC experiment on complexation of **10d** with γ-CD in water at 30°C.

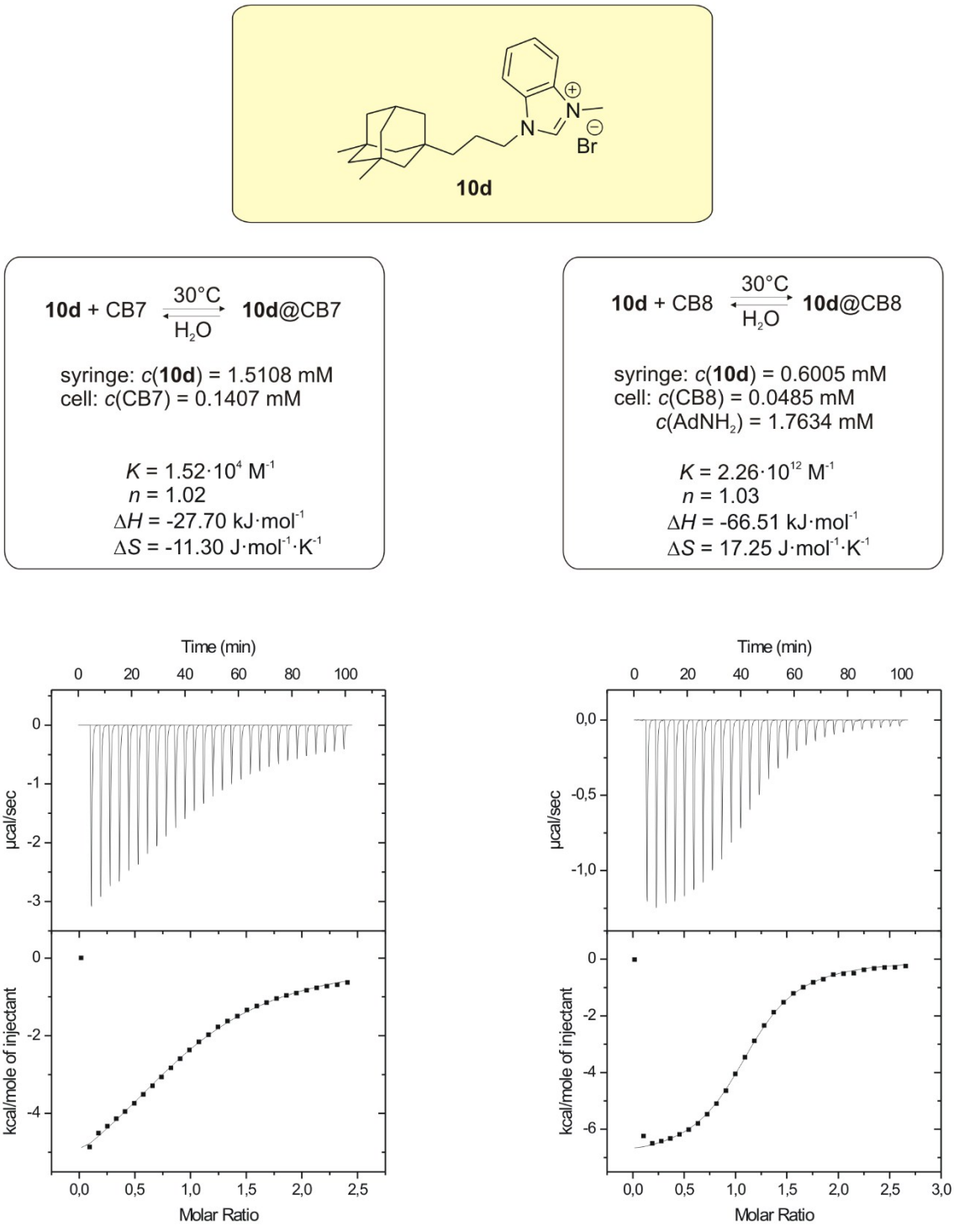

Figure S112: ITC experiments on complexation of **10d** with CB7 (left) and CB8 (right) in water and 50 mM NaCl at 30°C, respectively.